

Reply to Comments from Reviewer #1

Comments: The subject is appropriate to GMD. This manuscript presents results of a comprehensive comparative evaluation using the CAM5-chem within the CESM with two most commonly-used gas-phase chemical mechanisms: CB05_GE and MOZART-4x. The results showed that the two CAM5-chem simulations with CB05_GE and MOZART-4x predict similar chemical profiles for major gases compared to the aircraft measurements, with generally better agreement for NO_y profile by CB05_GE than MOZART-4x. They also found that the concentrations of SOA at four sites over continental US (CONUS) and organic carbon (OC) at the IMPROVE sites were well predicted by MOZART-4x but moderately underpredicted by CB05_GE. The results showed that the two simulations have similar cloud/radiative predictions, with slightly better performance of domain average cloud condensation nuclei (CCN) by CB05_GE, but slightly better agreement with observed CCN profile over Beijing by MOZART-4x. A lot of model evaluations have been done with tremendous observational data. Therefore I recommend clearly the acceptance for publication of this manuscript after minor revisions.

Reply:

We thank the reviewer for the positive comments. We have addressed all the comments, please see below our point-by-point reply.

Several editorial comments for improving the information content and presentation of the paper are listed as follows:

1. Abstract: Please use “continental US (CONUS)” instead of “CONUS” in the abstract.

Reply:

The suggested change has been made in the revised paper.

2. P3, L10-15: please add some references for these statements.

Reply:

A few references have been added in the Introduction section in the revised paper.

3. P4, L12-15: Regarding the possible effects of different chemical mechanisms on the performance of CMAQ, please add discussions about the recent work for the CMAQ (such as Yu, Shaocai, R. Mathur, G. Sarwar, D. Kang, D. Tong, G. Pouliot, and J. Pleim, 2010. Eta-CMAQ air quality forecasts for O₃ and related species using three different photochemical mechanisms (CB4, CB05, SAPRC-99): comparisons with measurements during the 2004 ICARTT study, Atmos. Chem. Phys., 10, 3001-3025.)

Reply:

The suggested discussions have been added along with the reference in the Introduction section in the revised paper.

4. P12, L24-26: Please cite the definitions of MB, NMB, RMSE etc for some references (such as Yu, Shaocai, Brian Eder, Robin Dennis, Shao-hang Chu, Stephen Schwartz, 2006. New unbiased symmetric metrics for evaluation of air quality models. Atmospheric Science Letter, 7, 26-34.).

Reply:

We have added the suggested references for this part in Section 3.3 in the revised paper.

5. P13, L1: CERES doesn't provide SWCF and LWCF. Please give more information about how to calculate them.

Reply:

The observed SWCF and LWCF data are from Clouds and Earth's Radiant Energy Systems (CERES) Energy Balanced and Filled (EBAF). We have included this information in Sections 3.2 and 3.3 in the revised paper.

6. P14-15, L25 (P14)-L1 (P15): The statement "The overpredictions of the NH₃ concentrations result in the overpredictions of the NH₄⁺ concentrations at the surface" is not necessary true. Please rewrite it. Regarding the bad performance of NH₃ and NO₃⁻, one of the reasons is because of partition of total (NH₃+NH₄⁺) (and total (HNO₃+NO₃⁻)) between gas and aerosol phases as discussed by Yu et al. (Yu, Shaocai, Robin Dennis, Shawn Roselle Athanasios Nenes, John Walker, Brian Eder, Kenneth Schere, Jenise Swall, Wayne Robarge, 2005. An assessment of the ability of 3-D air quality models with current thermodynamic equilibrium models to predict aerosol NO₃⁻. Journal of Geophysical Research, 110, D07S13, doi:10.1029/2004JD004718.). Please add this discussion.

Reply:

We have added additional discussion along with the suggested reference for this part in Section 4.1.1.

7. Regarding Figures 1, 4 and 9: They are too small to be seen clearly. Please enlarge them.

Reply:

We have enlarged the plots in Figures 1, 4, and 7 (original Figure 9).

Reply to Comments by Reviewer #2

General comments:

The authors implemented two different gas-phase chemical mechanisms (CB05_GE and MOZART-4x) into the CESM/CAM5 model and performed model simulations for three years. Model predictions obtained with one mechanism are compared to those obtained with the other mechanism and also to measurements from a large number of observational datasets. The article will be useful to air quality scientists and merits publication. However, several issues need to be addressed. Specific comments are provided below:

Reply:

We thank the reviewer for the positive review. We have addressed all the comments, please see below our point-by-point reply. The page and section numbers correspond to those in the manuscript with revision in track mode.

Specific comments:

Grid issue

Large horizontal grids are employed in the simulation since a global model is used in the study. Surface measurements are generally done at fixed locations. Large spatial variations exist in pollutant concentrations (especially between urban, semi-urban and rural areas). A global model utilizing coarse horizontal grids is unable to capture such spatial variation. Presumably model comparisons with observed data from the Air Quality System (AQS) in the US are not performed for such reason. Comparison of model predictions employing large grids to observed data from fixed surface monitors contain inherent uncertainty. The readers will benefit from a general discussion on the ability of such models to capture spatial gradients of pollutants (especially near urban areas) and comparison with observed data.

Reply:

We agree with the reviewer that there may be large uncertainties associated with comparison of grid averaged model output with pointwise observations. The horizontal grid used in this work is $0.9^{\circ} \times 1.25^{\circ}$. For model evaluation, there may be multiple observational sites located in one grid cell, so all the observations within one grid cell are averaged and compared to the simulated results in that grid cell. While using grid averaged observations helps reduce the uncertainties to some extent, this approach cannot address the inherent uncertainties associated with the evaluation of the model results obtained at a coarse grid resolution.

To address the reviewer's comments, we have provided more information regarding the evaluation and also indicated the inherent uncertainties associated with the approach we used in Section 3.3.

NO_x issue

Column (Table 3) and zonal NO_x (Figure 3) are over-predicted. In contrast, NO_x from surface-based monitors (Table 3) and aircraft based monitors (Figure 4) are under-predicted. Despite under-prediction of NO_x compared to observations from surface-based and aircraft based monitors, model over-predicts NO_x compared to satellite data. Can the authors discuss some reasons for such behavior?

A presentation on the comparison of model and satellite NO₂ is available at:

(https://www.cmascenter.org/conference/2012/slides/yarwood_evaluating_nox_2012.pdf)

Reply:

The underpredictions of NO_x against surface-based observations can be attributed to the uncertainties in the anthropogenic NO_x emissions as well as vertical transport. It is likely that more NO_x are transported into upper layers, resulting in the underpredictions in surface NO_x predictions. The underpredictions of NO_x against aircraft based observations may be due in part to the uncertainties in the measurements. Some field campaigns (e.g., ARCPAC) focused on the polluted regions with a significant contribution from biomass burning and local sources (Tilmes et al., 2015). The underestimations of emissions from these sources and uncertainties in the vertical mixing scheme can result in the underpredictions of their profiles.

The comparison of tropospheric NO₂ column against satellite data (e.g., SCIAMACHY) can be attributed to the uncertainties in NO_x emissions and the satellite retrievals. As indicated in Yarwood et al. (2012), errors in satellite NO₂ retrievals are dominated by atmospheric mass factor, which has a large uncertainty due to errors in specification of clouds, surface albedo, a priori NO₂ profile shape, and aerosols. Boersma et al. (2004) found there is an error of 35-60% in the tropospheric NO₂ retrievals, especially over polluted areas.

To address the reviewer's comments, we have included the above points along with relevant references in the revised paper, Section 4.2.

Ozone issue

The model over-predicts ozone for both mechanisms compared to the observed data (Table 3). The over-predictions has been linked to less titration resulting from the under-prediction of NO_x, coarse resolution, as well as dilution of NO_x. It is well-known that the addition of more NO_x reduces ozone only in NO_x rich areas. As the additional NO_x is transported to outside the NO_x rich areas, it increases ozone in those areas. Thus, the addition of NO_x may not necessarily reduce overall ozone. I think the use of coarse resolution is diluting NO_x; thus coarse resolution and dilution of NO_x are not independent reasons. In addition, model under-predicts VOC. If the model is revised to add corrected amount of VOC emissions, then it will produce more ozone which will further deteriorate the model performance.

Reply:

We agree with the reviewer that O₃ titration is more important over NO_x rich areas and diluting NO_x associated with coarse resolution can be one of the reasons for O₃ overpredictions. VOCs are underpredicted in the current model, so it cannot explain the O₃ overpredictions. Another possible reason for O₃ overpredictions may be underestimation in dry deposition. For example, Martin et al. (2014) reported the uncertainties in O₃ dry deposition associated with vegetation phenology in CAM-chem, which were responsible for the mean positive biases of 16 ppb in summertime surface O₃ mixing ratios over eastern U.S. and 8 ppb over Europe, respectively. Therefore, uncertainties in O₃ dry deposition can also partly explain the O₃ overpredictions.

To address the reviewer's comments, we have included the above discussion in the revised paper.

While the model under-predicts NO_x, its NO_y predictions agree closer to observed data (Figure 4). If the model is revised to use corrected NO_x, then it is likely to over-predict NO_y. Predictions with the CB05-GE mechanism agree better with observed NO_y. Column NO_y obtained with MOZART-4x is 46% lower than that that with CB05-GE (section 4.2) which suggests that NO_x is processed quite differently in the two mechanisms. Which specific chemical reactions are causing such a large difference in NO_y predictions and how are they different in the two mechanisms? What are the largest 2 chemical species in NO_y and how they differ between the two mechanisms?

Reply:

To address the reviewer's comments, we have performed additional analyses and added a new Table (Table S2) and two new figures, i.e., Figure S1, to show the dominant species in NO_y for both MOZART-4x and CB05_GE, and Figure S2 to show the absolute and relative differences for major NO_y species between MOZART-4x and CB05_GE. As shown in Figure S1, NO_x, HNO₃, and TPAN (PAN+PANX for CB05_GE and PAN+MPAN for MOZART-4x) are the major components for NO_y concentrations, with ratios of 90.5% and 91.7%, respectively, for the sum of the mixing ratios of the top three species to that of NO_y. NO_x dominates over East Asia, eastern U.S., and western Europe, whereas TPAN dominates over most oceanic area. As shown in Figure S2, MOZART-4x predicts lower TPAN by 2.9×10^{19} molecules m⁻² (or by 63.4%), which dominates the differences in NO_y predictions between the two simulations. The differences in TPAN predictions can be attributed to the differences in the kinetic reactions. Table S2 lists the reactions involving TPAN. As shown in Table S2, besides the differences in the reaction rate calculation, MOZART-4x includes one additional reaction for PAN destruction by OH, which is not included in CB05_GE. In addition, OH levels are higher in MOZART-4x than CB05_GE, which could result in more TPAN loss through oxidation by OH. These differences can explain the lower TPAN in MOZART-4x than in CB05_GE. We have included the above information in the revised paper, see pages 35-36.

Some of the nitrogen species partition into aerosol nitrate. Does the difference in NO_y between two mechanisms decrease if aerosol nitrate is accounted in the NO_y definition? How does the

model predictions compare to observed data (Figure 4) if aerosol nitrate is accounted in the NO_y definition?

Reply:

Table S3 lists the NO_y species used in the calculation for Figure 4 and other NO_y related comparisons. Note that Figure 8b includes the column comparison of aerosol nitrate. To address the reviewer's questions, we have included aerosol nitrate in the NO_y calculation and replace the NO_y plots in Figures 4 and 8a by those plots accounting for aerosol nitrate in NO_y. Figure S3 shows the absolute differences in NO_y (with and without inclusion of aerosol nitrate) between MOZART-4x and CB05_GE. If aerosol nitrate is accounted for in the NO_y definition, the differences in NO_y between two mechanisms decrease over East Asia, eastern U.S., Europe, and middle Africa as aerosol nitrate is higher in MOZART-4x over these regions (see Figure 6b). For the rest of areas, the differences in NO_y between two mechanisms increase if aerosol nitrate is accounted for in the NO_y definition.

To address the reviewer's comments, we added the above discussions in page 36.

NO_y definition includes BrONO₂ which suggests bromine chemistry is being used in the model. Which bromine emissions are used in the model?

Reply:

We have bromine chemistry included in both MOZART-4x and CB05_GE. For bromine/chlorine species (e.g., CF₂CLBR, CF₃BR, CFC11, CFC12, CH₃BR, and CH₃CL), their surface concentrations are specified using the historical reconstruction from Meinshausen et al. (2011). No bromine emissions were included.

The above point was added in Section 3.1.

Also, need to clarify that section 4.2 contains only model-to-model comparison.

Reply:

This has been clarified in Section 4.2.

HNO₃ issue

The model over-predicts HNO₃ over CONUS while under-predicting it over Europe. Under-prediction of HNO₃ over Europe is linked to under-prediction on NO_x. Surface NO₂ comparison for CONUS is not shown in Table 3. Does the over-prediction of HNO₃ over CONUS occur due to over-prediction on NO_x?

Reply:

To address the reviewer's comment, we have included NO₂ evaluation against AQS sites over CONUS. The results show that both CB05_GE and MOZART-4x underpredict surface NO₂ concentrations, with NMBs of -52.2% and -51.4%, respectively. The overpredictions of HNO₃ over CONUS are mainly due to more total nitrate partitioned into HNO₃ (which is reflected by the underpredictions of NO₃⁻ over CONUS) resulted from the overpredictions of SO₄²⁻ over CONUS. Compared to NO₃⁻, SO₄²⁻ can more easily combine with NH₄⁺ to stay in aerosol phase. There are not enough NH₄⁺ to neutralize NO₃⁻, driving NO₃⁻ to HNO₃ in the gas-phase resulting in overpredictions of HNO₃ over CONUS. We have included this explanation in the revised paper, Section 4.1.1.

Cl⁻ issue

The model under-predicts Cl⁻ over CONUS while over-predicting it over Europe. Over-prediction of Cl⁻ over Europe has been linked to gas/particle partitioning. Can the authors suggest any reasons for under-prediction of Cl⁻ over CONUS? Reff et al. (2009) suggest many sources can emit Cl⁻; are emissions from these sources included in the study?

Reff, et al.: Emissions inventory of PM_{2.5} trace elements across the United States, Environmental Science & Technology, 43, 5790–5796, 2009.

Reply:

We did not include any anthropogenic Cl⁻ emissions in the model except from sea-salt emissions, which is calculated online in CESM/CAM5. The missing sources can contribute to the underpredictions of Cl⁻. On the other hand, due to the overpredictions of SO₄²⁻, there are less NH₄⁺ available to neutralize Cl⁻, driving Cl⁻ to HCl in the gas-phase, resulting in underpredictions of Cl⁻. In addition, the performance of Cl⁻ over CONUS is only for fine Cl⁻ (Aitken, accumulation, fine sea-salt, and fine dust modes), whereas the performance of Cl⁻ over Europe is for fine and coarse Cl⁻ (all seven modes). As the thermodynamic equilibrium is not treated for coarse particles (the irreversible condensation of HCl is assumed to occur on the surface of coarse particles), it is likely that the model overpredicts coarse Cl⁻, but underpredicts fine Cl⁻ due to the missing sources.

To address the reviewer's comments, we have clarified the above issues in page 23, Section 4.1.1.

SO₂/SO₄²⁻ issue

The model over-predicts surface SO₂/SO₄²⁻ compared to the observed data (Table 3). The over-estimation of SO₂ has been explained with SO₂ emissions, injection height uncertainty, and vertical mixing issue while the over-prediction of SO₂ has been suggested to be the reason for over-prediction of SO₄²⁻. Most models over-predict surface SO₂ and tend to under-predict surface SO₄²⁻ compared to observed data. Here, the model over-predicts both surface SO₂/SO₄²⁻. Interestingly column SO₂ is underpredicted which suggests possible problem with vertical mixing in the model that may have contributed to the over-prediction of surface SO₂.

Reply:

As we explained, the overpredictions of surface SO₂ concentrations may be due to the uncertainties in the SO₂ emissions, injection height uncertainty, and vertical mixing. The underpredictions of column SO₂ can also be attributed to the uncertainties in the vertical mixing as well as uncertainties in the satellite retrievals. For example, Lee et al. (2009) found that there is an overall error in the annual SO₂ retrievals of 45-80% over polluted regions, especially over eastern China. Therefore, the uncertainties in the satellite SO₂ retrievals can affect the model evaluation. The overpredictions of SO₄²⁻ can be due to the overpredictions of SO₂ as well as uncertainties in the SO₄²⁻ emissions. CESM/CAM5 also reads the default vertical SO₄²⁻ emission profiles for the simulations. The uncertainties in the SO₄²⁻ emissions can contribute to the inaccurate predictions of SO₄²⁻ as well.

To address the reviewer's comments, we have included the above explanation in the revised paper in Section 6.

Other factors may also affect SO₄²⁻ predictions. Aqueous-phase reaction with H₂O₂ and gas-phase reaction with OH tend to be the most important pathways for the conversion into SO₄²⁻. The article does contain any discussion of predicted oxidant levels (H₂O₂ and OH). If the predicted oxidant levels are too high, SO₄²⁻ predictions will also be high. I am not suggesting to perform any detailed comparison of predicted H₂O₂ and OH with observed data but some discussion of predicted oxidants levels and typical observed values will be helpful to readers.

Reply:

We agree with the reviewer that aqueous phase reaction with H₂O₂ and gas-phase reaction with OH are important pathways for SO₄²⁻ formation. We have added the comparisons of OH and H₂O₂ profiles with aircraft measurements in Figure 4 in the revised paper. As shown in Figure 4, both OH and H₂O₂ are underpredicted, but MOZART-4x predicts slightly higher H₂O₂ within 4-km above the surface compared to CB05_GE. However, the performance here only represents the local condition, instead of global condition.

To address the reviewer's comment, we also compared the global mean tropospheric OH concentrations with other studies. The simulated air-mass weighted tropospheric mean OH concentrations predicted by MOZART-4x and CB05_GE are both 13.1×10^5 molec cm⁻³, which is slightly higher than Naik et al. (2013) with present-day tropospheric mean OH levels of 11.1 ± 1.6 molec cm⁻³. So both CB05_GE and MOZART-4x tend to predict higher OH levels, which may partly explain the overpredictions of SO₄²⁻. We have included this explanation in the revised paper, Section 4.1.1.

The model under-predicts cloud liquid water path compared to MODIS data (Table 5). If the model is revised to include the correct amount of cloud liquid water, then it will produce more SO₄²⁻ and the model performance for SO₄²⁻ will further deteriorate and the model performance for SO₂ will improve. It is also possible that the model produces more SO₄²⁻ by placing clouds in incorrect vertical layers. Inadequate precipitation in the model may also lead to higher than observed SO₄²⁻ in the model.

Reply:

Cloud liquid water path (LWP) is moderately underpredicted by both MOZART-4x and CB05_GE against MODIS data, but it is relatively well predicted against Bennartz (2007), which filtered out large uncertainties associated with MODIS retrievals. Therefore, the model predicts LWP relatively well against Bennartz (2007). But we agree with the reviewer that the model may inaccurately predict clouds vertically as the simulations with both MOZART-4x and CB05_GE show moderate biases for COT and CDNC.

We also agree with the reviewer that inadequate precipitation can contribute to the overpredictions of SO_4^{2-} . Both simulations are driven by prescribed meteorology, so we did not compare meteorology from the two simulations. To address the reviewer's comment, we evaluated precipitation and the results show that precipitation is well predicted by both MOZART-4x and CB05_GE, with NMBs of 1.9% and 1.6%, respectively. Therefore, the overpredictions of SO_4^{2-} are not due to the insufficient precipitation.

SOA issue

The model is able to capture observed SOA (Table 3 and Figure 2). However, VOCs are under-predicted. If the model is revised to use corrected amount of VOC emissions, then SOA predictions will be higher. Does the model capture SOA for the correct reason? Again, discussion of predicted oxidant levels with typical observed values will also be helpful for discussing SOA predictions?

Reply:

We agree with the reviewer that using correct VOCs emissions can increase the SOA concentrations. As we discussed above, our model tends to predict higher OH levels on a global scale, which can partly explain the well predicted SOA despite the underpredictions of VOCs. Also, the SOA statistics are calculated using only four pairs of seasonal mean values at four sites in the U.S. where the observed SOA data are available during 2008-2010; they, therefore, are not be representative of the entire CONUS because of limited data used for calculation. We have indicated this limitation in the paper.

Minor editorial suggestions

The objectives of the study are to examine the differences in the SOA predictions, and study the sensitivity of air quality and climate predictions to different gas-phase chemical mechanisms (introduction section). However, the title does not reflect that SOA predictions are being examined. Perhaps the authors can reconcile the apparent difference.

Reply:

SOA is part of the global air quality, so the title does include examination of SOA predictions from both simulations.

Most chemical species in the article have been defined. However, some have not been defined. For example, CO, HOx, and NOx in line 24 (page 7191) are not defined. I suggest that the authors check the entire article and define the chemical species when it is used first time.

In the description, two names for α -pinene (alpha-pinene and α -pinene) and β -pinene are used. One name should be used throughout the article (Chemical mechanism - 2.1)

Reply:

We have checked the paper thoroughly and defined all the species and we also use consistent names for the species in the revised paper.

Figure 1 also contains a comparison of SOA which is not mentioned in the caption

Reply:

SOA has been added in the Figure 1 caption in the revised paper.

Conclusion section is long and can be shortened

Reply:

Conclusion has been shortened in the revised paper.

References cited in this reply

- Boersma, K. F., Eskes, H. J., and Brinksma E. J.: Error analysis for tropospheric NO₂ retrieval from space, *J. Geophys. Res.*, 109, D04311, doi:10.1029/2003JD003962, 2004.
- Lee, C., Martin, R. V., Donkelaar, A. van, O'Byrne, G., Krotkov, N., Richter, A., Huey, L. G., and Holloway, J. S.: Retrieval of vertical columns of sulfur dioxide from SCIAMACHY and OMI: Air mass factor algorithm development, validation, and error analysis, *J. Geophys. Res.*, 114, D22303, doi:10.1029/2009JD012123, 2009.
- Martin, M. V., Heald, C. L., and Arnold, S. R.: Coupling dry deposition to vegetation phenology in the Community Earth System Model: Implications for the simulation of surface O₃, *Geophys. Res. Lett.*, 41, 2988-2996, doi:10.1002/2014GL059651, 2014.
- Meinshausen, M., Smith, S. J., Calvin, K., Daniel, J. S., Kainuma, M. L. T., Lamarque, J.-F., Matsumoto, K., Montzka, S., Raper, S., Riahi, K., Thomson, A., Velders, G. J. M., and van Vuuren, D. P.: The RCP Greenhouse Gas Concentrations and their Extensions from 1765 to 2300, *Climatic Change*, 109, 213-241, 2011.
- Naik, V., Voulgarakis, A., Fiore, A. M., Horowitz, L. W., Lamarque, J.-F., Lin, M., Prather, M. J., Young, P. J., Bergmann, D., Cameron-Smith, P. J., Cionni, I., Collins, W. J., Dalsøren, S. B., Doherty, R., Eyring, V., Faluvegi, G., Folberth, G. A., Josse, B., Lee, Y. H., MacKenzie, I. A., Nagashima, T., van Noije, T. P. C., Plummer, D. A., Righi, M., Rumbold, S. T., Skeie, R., Shindell, D. T., Stevenson, D. S., Strode, S., Sudo, K., Szopa, S., and Zeng, G.: Preindustrial to present-day changes in tropospheric hydroxyl radical and methane lifetime from the Atmospheric Chemistry and Climate Model Intercomparison Project (ACCMIP), *Atmos. Chem. Phys.*, 13, 5277-5298, doi:10.5194/acp-13-5277-2013, 2013.
- Tilmes, S., Lamarque, J.-F., Emmons, L. K., Kinnison, D. E., Ma, P.-L., Liu, X., Ghan, S., Bardeen, C., Arnold, S., Deeter, M., Vitt, F., Ryerson, T., Elkins, J. W., Moore, F., Spackman, R., and Martin, M. V.: Description and evaluation of tropospheric chemistry and aerosols in the Community Earth System Model (CESM1.2), *Geosci. Model Dev.*, 8, 1395-1426, doi:10.5194/gmd-8-1395-2015, 2015.
- Yarwood, G., Kemball-Cook, S., Johnson, J, Wilson, G, Dornblaser, B, and Estes, M: Evaluating NO_x Emission Inventories for Air Quality Modeling Using Satellite, Model and SEARCH NO₂ Data, 11th Annual CMAS Conference, Chapel Hill, NC, October 16, 2012.

Reply to Comments by Reviewer #3

This manuscript documents the comprehensive evaluations and comparisons of two chemistry mechanisms (CB05-GE and MOZART-4) in CESM/CAM5. The topics are well within the scope of GMD. I recommend the acceptance for the publication after following comments are addressed.

Reply:

We thank the reviewer for the positive comments. We have addressed all the comments, please see below our point-by-point reply.

1. Many fields related to chemical species, aerosol species, CCN, clouds are discussed and evaluated in the study. To improve the clarity and readability, the authors may consider to use another way of presentation in section 4. For example, you may consider to add subtitle for different types of gas and aerosol species, e.g., NO_x, NO_y, O₃, HNO₃, aerosols (BC, OC, SOA, SO₄ and associated precursors), CCN, cloud, radiation.

Reply:

To improve the readability, we added subtitles for evaluation of different types of species and variables in the revised paper.

2. The organization of section 4 is somehow confusing. How about putting all the evaluations in one subsection 4.1 and all the comparisons in the other subsection 4.2. Within each subsection there are different components (e.g., surface, vertical profile, column evaluations..).

Reply:

To avoid confusion, we have split the original Section 4 into Sections 4 and 5 in the revised paper.

Specific comments:

1. Abstract. Line 19, what is CONUS?

Reply:

CONUS is continental U.S. We have added the full name in the Abstract in the revised paper.

2. Abstract. Line 23, why the biogenic emissions are different between the two mechanisms.

Reply:

The different biogenic emissions are mainly due to the different BVOCs mapping for MOZART-4x and CB05_GE. As discussed in Section 2.1 in the paper, both MOZART-4x and CB05_GE include α -pinene (APIN), β -pinene (BPIN), limonene, and ISOP as precursors for biogenic SOA. CB05_GE also includes additional biogenic precursors such as speciated ocimene (OCI), humulene (HUM) and terpinene (TER). However, in MOZART-4x, the species mapping for MEGAN emission calculation is slightly different. For example, α -pinene and other compounds (e.g., α -thujene, p-cymene, and o-cymene) are mapped into APIN; β -pinene and other compounds (e.g., sabinene and camphene) are mapped into BPIN; limonene and other compounds (e.g., phellandrene and terpinene) are mapped into LIMON; myrcene and other compounds (e.g., ocimene) are mapped into MYRC; and beta-caryophyllene and other sesquiterpenes (e.g., humulene and α -bergamotene) are mapped into BCARY. Due to the different mapping for MEGAN species, biogenic emissions between MOZART-4x and CB05_GE are different.

To address the reviewer's comments, we have provided an explanation for different biogenic emissions between MOZART-4x and CB05_GE in the revised paper, see Section 2.1.

3. Page 7198. Line 12, which analysis fields are nudged?

Reply:

The nudged meteorological fields include surface pressure, meridional wind, zonal wind, zonal surface stress, meridional surface stress, snow height, solar flux at surface, soil moisture fraction, surface temperature, temperature, specific humidity, surface geopotential, orography flag, surface water flux, and surface sensible flux. We have included this info in the revised paper, Section 3.1.

4. Page 7201. Line 13-14, please compute PM_{2.5} accurately since the MAM aerosol scheme predicts the aerosol size distributions for different aerosol modes.

Reply:

In this work, lognormal size distribution is used for each mode, with prognostic mode dry and wet radius based on number and total dry and wet volume change. The geometric standard deviation (σ_g) of each mode is prescribed and given in Table S1 in the supplementary material, along with the size range of each mode used in this work.

To address the reviewer's comments, we have calculated PM_{2.5} concentrations based on prescribed mode dry radius and geometric standard deviation for mode 6 (coarse sea-salt mode) as all other modes are within the diameter $\leq 2.5 \mu\text{m}$. We have updated results in the revised paper.

5. Page 7203 and follow many pages. There are many "likely". I would like to have more certain assessments.

Reply:

We were trying to include all likely causes for the model performance. However, it is not possible to pin-point exact causes without carrying out a large number of sensitivity simulations, which is beyond the scope of current work and may be a subject of future work. To address the reviewer's comment, we have included some references to support our explanations and speculations in the revised paper.

6. Page 7208. Line 26, change “include” to “included”

Reply:

The suggested change has been made in the revised paper.

7. Page 7211. Please compare your SOA treatment with the Shrivastava et al. (2014) “Global transformation and fate of SOA: Implications of lowvolatility SOA and gas-phase fragmentation reactions” in JGR for treatment of SOA in CAM5 and simulation results if possible.

Reply:

Our SOA treatments include volatile SOA formation from anthropogenic VOCs (AVOCs) and biogenic VOCs (BVOCs) and semi volatile SOA from primary organic aerosol (POA). We also implemented functionalization and fragmentation treatments based on Shrivastava et al. (2013). We still use nine volatility bins to represent the aging and gas-particle partitioning of SOA, instead of five volatility bins used in Shrivastava et al. (2015). In addition, compared to the reaction (3) in Shrivastava et al. (2015), we do not have the third term, which denotes additional fragmentation where 10% of the mass results in low carbon number species with very high volatility that is eventually oxidized to CO/CO₂ and/or removed by dry deposition. In our model treatment, the remaining mass is assumed to be lost to species with a volatility higher than the volatility values in the VBS structure.

Our model (i.e., MOZART-4x) predicts POA burden of 0.36 Tg, which is about 0.1 Tg lower than Shrivastava et al. (2015), indicating that POA may be too volatile with the current implementation in our model and uncertainties in POA emissions used in our simulations. Our model (i.e., MOZART-4x) predicts SOA burden of 1.82 Tg, which is slightly higher (by 0.05 Tg) than the FragSVSOA case in Shrivastava et al. (2015). This can be attributed to the different emissions used in both work and the fact that more POA is allowed to age to SOA in our model comparing to the FragSVSOA case in Shrivastava et al. (2015).

To address the reviewer's comment, we have provided a description on the SOA treatment in Section 2.2 in the paper. We also compared our POA and SOA burdens with those of Shrivastava et al. (2015).

Reference cited in this reply

Shrivastava, M., Easter, R., Liu, X., Zelenyuk, A., Singh, B., Zhang, K., Ma, P-L, Chand, D., Ghan, S., Jimenez, J.L., Zhang, Q., Fast, J., Rasch, P. and Tiitta, P.: Global transformation and fate of SOA: Implications of low volatility SOA and gas-phase fragmentation reactions, *J. Geophys. Res. Atmos.*, 120, 4169-4195, doi:10.1002/2014JD022563, 2015.

1 CESM/CAM5 Improvement and Application: Comparison and Evaluation of Updated
2 CB05_GE and MOZART-4 Gas-Phase Mechanisms and Associated Impacts on Global
3 Air Quality and Climate

4 Jian He¹, Yang Zhang^{1*}, Simone Tilmes², Louisa Emmons², Jean-Francois Lamarque²,
5 Tim Glotfelty¹, Alma Hodzic², and Francis Vitt²

6 ¹ Department of Marine, Earth, and Atmospheric Science, North Carolina State
7 University, Raleigh, NC

8 ² National Center for Atmospheric Research, Boulder, CO
9

10 **Abstract:** Atmospheric chemistry plays a key role in determining the amounts and
11 distributions of oxidants and gaseous precursors that control the formation of secondary
12 gaseous and aerosol pollutants; all of those species can interact with the climate system.
13 To understand the impacts of different gas-phase mechanisms on global air quality and
14 climate predictions, in this work, a comprehensive comparative evaluation is performed
15 using the Community Atmosphere Model (CAM) Version 5 with comprehensive
16 tropospheric and stratospheric chemistry (CAM5-chem) within the Community Earth
17 System Model (CESM) with two most commonly-used gas-phase chemical mechanisms:
18 the 2005 Carbon Bond mechanism with Global Extension (CB05_GE) and the Model of
19 OZone and Related chemical Tracers version 4 (MOZART-4) mechanism with additional
20 updates (MOZART-4x). MOZART-4x and CB05_GE use different approaches to
21 represent volatile organic compounds (VOCs) and different surrogates for secondary
22 organic aerosol (SOA) precursors. MOZART-4x includes a more detailed representation
23 of isoprene chemistry compared to CB05_GE. CB05_GE includes additional oxidation of

* Corresponding author: Yang Zhang, Email: yang_zhang@ncsu.edu, Phone: (919)-515-9688

24 SO₂ by O₃ over the surface of dust particles, which is not included in MOZART-4x. The
25 results show that the two CAM5-chem simulations with CB05_GE and MOZART-4x
26 predict similar chemical profiles for major gases (e.g., O₃, CO, and NO_x) compared to the
27 aircraft measurements, with generally better agreement for NO_y profile by CB05_GE
28 than MOZART-4x. The concentrations of SOA at four sites in [continental U.S.](#)
29 [\(CONUS\)](#) and organic carbon (OC) over the IMPROVE sites are well predicted
30 by MOZART-4x (with NMBs of -1.9% and 2.1%, respectively) but moderately
31 underpredicted by CB05_GE (with NMBs of -23.1% and -20.7%, respectively). This is
32 mainly due to the higher biogenic emissions and OH levels simulated with MOZART-4x
33 than with CB05_GE. The concentrations of OC over Europe are largely underpredicted
34 by both MOZART-4x and CB05_GE, with NMBs of -73.0% and -75.1%, respectively,
35 indicating the uncertainties in the emissions of precursors and primary OC and relevant
36 model treatments such as the oxidations of VOCs and SOA formation. Uncertainties in
37 the emissions and convection scheme can contribute to the large bias in the model
38 predictions (e.g., SO₂, CO, black carbon, and aerosol optical depth). The two simulations
39 also have similar cloud/radiative predictions, with slightly better performance of domain
40 average cloud condensation nuclei (CCN) at supersaturation of 0.5% by CB05_GE, but
41 slightly better agreement with observed CCN (at supersaturation of 0.2%) profile over
42 Beijing by MOZART-4x. The two gas-phase mechanisms result in a global average
43 difference of 0.5 W m⁻² in simulated shortwave cloud radiative forcing, with significant

44 differences (e.g., up to 13.6 W m^{-2}) over subtropical regions.

45 **Keywords:** CB05_GE, MOZART-4, CAM5-chem, atmospheric gas-phase chemistry,

46 secondary organic aerosol, model evaluation

47

48 **1. Introduction**

49 Atmospheric chemistry plays an important role in the perturbation of climate

50 system by determining the amounts and distributions of important oxidants and gaseous

51 precursors for secondary air pollutants such as ozone (O_3) and aerosols ([IPCC, 2013](#)).

52 Aerosols can influence the Earth's radiative balance by directly scattering and absorbing

53 radiation and indirectly affecting cloud properties through acting as cloud condensation

54 nuclei (CCN) and ice nuclei ([IPCC, 2013](#)). The aerosol effects on radiation depend

55 critically on their chemical composition and physical properties. Therefore, atmospheric

56 chemistry is an important component for atmospheric and Earth system models. Different

57 chemical mechanisms (e.g., different chemical reactions and kinetic parameters) can lead

58 to differences in the predictions of gases, secondary aerosols, as well as climatic variables

59 such as CCN, cloud droplet number concentration (CDNC), and radiative forcings

60 (Luecken et al., 2008; Sarwar et al., 2008; Zhang et al., 2012a; Lamarque et al., 2013).

61 There are generally two types of species in the gas-phase mechanisms: inorganic

62 and organic. Although most mechanisms include the same important inorganic species

63 (e.g., O_3 , [carbon monoxide \(CO\)](#), HO_x ([odd hydrogen = hydroxyl radical \(\$\cdot\text{OH}\$ \) +](#)

64 [hydroperoxyl radical \(\$\text{-HO}_2\$ \)](#), and [nitrogen oxides \(\$\text{NO}_x\$ \)](#), the predicted amounts can
65 vary greatly among different mechanisms (Knote et al., 2014a). Some mechanisms ignore
66 reactions with very low reaction rates since they do not affect results significantly. Also,
67 some reactions may use different rate coefficients with different dependence on
68 atmospheric temperature and pressure due to the uncertainties in the laboratory
69 measurements or the use of mechanisms that have not been updated in time. Unlike
70 inorganic species, there are more significant differences in the representation of organic
71 species. Light organic species with low molecular weight are often explicitly treated (e.g.,
72 methane, formaldehyde (HCHO)), whereas lumped or surrogate species are used to
73 represent more complex mixtures of heavy organic compounds with high molecular
74 weight (e.g., aromatics, organic nitrates). There are three most common representations
75 of organic chemistry, including the lumped structure technique, the surrogate species
76 approach, and the lumped species method (Zhang et al., 2004). For example, the Carbon
77 Bond mechanism version IV (CB-IV, Gery et al., 1989), which uses the lumped structure
78 approach for volatile organic compounds (VOCs), has been widely used in air quality
79 modeling systems through urban to regional scales for many years. This mechanism has
80 later been extensively updated in 2005 (CB05, Yarwood et al., 2005), and has been
81 implemented into the Community Multiscale Air Quality model (CMAQ, Sarwar et al.,
82 2008) and the Weather Research and Forecasting model with Chemistry (WRF-Chem,
83 Wang et al., 2014). CB05 has been further expanded to include more than 120 reactions

84 that are important on global scale (CB05 with global extension (CB05_GE),
85 Karamchandani et al., 2012) and implemented into global models, such as the
86 Global-through-Urban WRF/Chem (GU-WRF/Chem, Zhang et al., 2012a) and the
87 Community Atmosphere Model version 5 (CAM5), the atmospheric component of the
88 Community Earth System Model (CESM/CAM5, He and Zhang, 2014). The Model of
89 OZone and Related chemical Tracers version 4 (MOZART-4, Emmons et al., 2010)
90 mechanism, which uses the lumped species approach for VOCs, has also been used in
91 WRF-Chem (Knote et al., 2014b), and CAM with extensive tropospheric and
92 stratospheric chemistry (CAM-chem) Versions 4 and 5 (Lamarque et al., 2012; Tilmes et
93 al., 2015). Different gas-phase mechanisms have also been compared in several studies,
94 however, most of which are conducted in box models or using regional models (Kim et
95 al., 2009; Kim et al., 2011a, b; [Yu et al., 2010](#)). For example, using WRF-Chem, Zhang et
96 al. (2012b) found that three different mechanisms (i.e., the Carbon Bond Mechanism-Z
97 (CBM-Z), the 1999 Statewide Air Pollution Research Center Mechanism (SAPRC99),
98 and the CB05) can predict different O₃ concentrations up to 5 ppb at surface in July, 2001.
99 [Yu et al. \(2010\) compared the O₃ predictions from three different mechanisms \(i.e., CB4,
100 CB05, and SAPRC99\) using Eta-CMAQ and found that at the AIRNow surface sites,
101 CB05 gives the best O₃ performance followed by CB4 and SAPRC-99 for observed O₃ ≥
102 75 ppb, whereas CB4 gives the best O₃ performance for observed O₃ < 75 ppb.](#) Knote et
103 al. (2014a) also compared seven chemical mechanisms using a box model and found that

104 the differences in daytime OH radical concentrations can be up to 40%.

105 Climate change can also strongly influence atmospheric chemistry and aerosols
106 and therefore air quality. For example, photolysis and temperature-dependent reactions
107 can be directly impacted by climate change (Jacob and Winner, 2009). Due to the
108 nonlinear relationships between chemistry, aerosols, and climate, it is important to
109 accurately represent their interactions in a three-dimensional global model. Several
110 studies have demonstrated the capability of CAM-chem to represent tropospheric
111 (Aghedo et al., 2011; Lamarque et al., 2010, 2011a, b; Tilmes et al., 2015) and
112 stratospheric (Lamarque et al., 2008; Lamarque and Solomon, 2010) conditions. The
113 chemical mechanism used in CAM-chem is based on MOZART-4, with detailed
114 stratospheric chemistry of Kinnison et al. (2007). In this work, two most commonly used
115 gas-phase mechanisms: the extended MOZART-4 (with updates as described by Knote et
116 al. (2014b) and additional updates in this work) (referred to as MOZART-4x) and the
117 CB05_GE chemical mechanisms are compared using the latest CESM/CAM5. The
118 objectives are to examine the differences in the secondary organic aerosols (SOA)
119 predictions resulted from the two gas-phase chemical mechanisms and study the
120 sensitivity of air quality and climate predictions to different gas-phase chemical
121 mechanisms.

122

123 **2. Model Descriptions**

124 The CESM/CAM5 used in this work is based on CAM version 5.3 of CESM
125 version 1.2.2, coupled to comprehensive tropospheric and stratospheric chemistry
126 (CAM5-chem, Tilmes et al., 2015) using the 7-mode Modal Aerosol Model (MAM7)
127 (Liu et al., 2012). This version of CAM5-chem was further developed and improved at
128 North Carolina State University (NCSU) in collaboration with NCAR, as described below.
129 A more detailed description of this version of CESM CAM5-chem (referred to as
130 CAM5-NCSU hereafter) used in this study can be found in He and Zhang (2014) and He
131 et al. (2015).

132

133 2.1 Chemical Mechanisms

134 In this study, CB05_GE has been updated to include additional kinetic reactions
135 describing interactions between functionalization and fragmentation processes during
136 gas-phase oxidation of anthropogenic and biogenic VOCs by OH (Glotfelty et al., 2015).
137 The products of those reactions are linked with the organic gas/particle partitioning for
138 SOA formation. Heterogeneous reactions on tropospheric aerosols and stratospheric
139 clouds are also added as same as those in MOZART-4x (Tilmes et al., 2015) with one
140 additional pathway in CB05_GE to simulate sulfate formation through oxidation of sulfur
141 dioxide (SO₂) by O₃ on the surface of dust particles.

142 MOZART-4x used in this work extends the MOZART chemical mechanism used
143 in Lamarque et al. (2012) and Tilmes et al. (2015) to include several updates as described

144 in Knote et al. (2014b). These updates include (1) detailed treatments of monoterpenes
145 (α -pinene, β -pinene, and limonene) and 2-methyl-3-buten-2-ol (MBO); (2) detailed
146 treatments of aromatics (e.g., benzene, toluene, and xylenes); (3) additional glyoxal
147 ($C_2H_2O_2$) production from oxidized VOCs products; and (4) an updated isoprene (ISOP)
148 oxidation scheme. In this work, the oxidation of anthropogenic and biogenic VOCs and
149 subsequent aging processes are also included in MOZART-4x, and the products of those
150 reactions are linked with the organic gas/particle partitioning for SOA formation.

151 Table 1 shows the gas-phase organic precursors for SOA formation treated in
152 MOZART-4x and CB05_GE. For aromatic precursors of SOA, MOZART-4x includes
153 benzene, toluene (TOL), xylenes, and cresol. Although CB05_GE does not include
154 benzene, it includes polycyclic aromatic hydrocarbons (PAH) as a SOA precursor. For
155 alkane precursors of SOA, MOZART-4x includes BIGALK (lumped alkanes with carbon
156 (C) number > 3), whereas CB05_GE includes ALKH (long-chain alkanes, with C > 6).
157 For anthropogenic alkene precursors of SOA, MOZART-4x includes propene (C_3H_6) and
158 BIGENE (lumped alkenes with C >3), whereas CB05_GE includes terminal olefin (OLE)
159 and internal olefin (IOLE). The emissions for biogenic alkene precursors are from the
160 Model of Emissions of Gases and Aerosols from Nature version 2.1 (MEGAN2.1,
161 Guenther et al., 2012). Both MOZART-4x and CB05_GE include α -pinene (APIN),
162 β -pinene (BPIN), limonene, and ISOP as precursors for biogenic SOA. CB05_GE also
163 includes additional biogenic precursors such as speciated ocimene (OCI), humulene

164 (HUM) and terpinene (TER). However, in MOZART-4x, the species mapping for
165 MEGAN emission calculation is slightly different. For example, α -pinene and other
166 compounds (e.g., α -thujene, p-cymene, and o-cymene) are mapped into APIN, β -pinene
167 and other compounds (e.g., sabinene and camphene) are mapped into BPIN, limonene
168 and other compounds (e.g.; phellandrene and terpinene) are mapped into LIMON,
169 myrcene and other compounds (e.g., ocimene) are mapped into MYRC, and
170 beta-caryophyllene and other sesquiterpenes (e.g., humulene and α -bergamotene) are
171 mapped into BCARY. Due to the different mapping for MEGAN species, biogenic
172 emissions between MOZART-4x and CB05_GE are different, which can result in
173 different biogenic SOA predictions. On the other hand, the rate coefficients for the
174 oxidations of biogenic VOCs (e.g., APIN, BPIN, and limonene) are constant in
175 CB05_GE, whereas they are temperature dependent in MOZART-4x, such a difference
176 can result in different SOA predictions as well. In addition, there are uncertainties in the
177 HO_x recycling associated with isoprene chemistry in CB05_GE (Karamchandani et al.,
178 2012), whereas MOZART-4x used in this work includes OH recycling from improved
179 isoprene chemistry. For example, in CB05_GE, ISOP is oxidized by OH to generate 91.2%
180 molar yield of HO₂. In MOZART-4x, the isoprene peroxy radical from the oxidation
181 ISOP by OH (i.e., ISOPO₂) has different yields of HO₂ through reactions with [nitrogen](#)
182 [monoxide \(NO\)](#), [nitrate radical \(NO₃\)](#), methylperoxy radical (CH₃O₂), and acetylperoxy
183 radical (CH₃CO₃), and it can also consume HO₂ itself. These reactions have different

184 reaction rate coefficients. These differences can affect O₃, OH, and NO_x predictions, and
185 thus the oxidation of VOCs.

186

187 2.2 Aerosol/Cloud Treatments

188 In CAM5-NCSU, the aerosol module is based on MAM7 of Liu et al. (2012),
189 with improvements in terms of condensation, nucleation, aerosol thermodynamics, and
190 aerosol activation (He and Zhang, 2014; Gantt et al., 2014). The major updates include:
191 (1) the new particle formation treatments with a combination of the default nucleation
192 parameterizations of Vehkamäki et al. (2002), Merikanto et al. (2007), and a newly added
193 ion-mediated aerosol nucleation (Yu, 2010) above the planetary boundary layer (PBL),
194 and a combination of the three and an additional parameterization of Wang and Penner
195 (2009) in the PBL; (2) the inorganic aerosol thermodynamics based on ISORROPIA II of
196 Fountoukis and Nenes (2007), which explicitly simulates the thermodynamics of sulfate
197 (SO₄²⁻), ammonium (NH₄⁺), nitrate (NO₃⁻), sodium (Na⁺), and chloride (Cl⁻) in the Aitken,
198 accumulation, and fine sea-salt modes, as well as the impact of crustal species associated
199 with the fine dust mode; (3) an advanced aerosol activation scheme based on Fountoukis
200 and Nenes (2005) with additional updates based on Kumar et al. (2009) and Barahona et
201 al. (2010), which accounts for adsorption activation from insoluble CCN and giant CCN
202 equilibrium timescale on aerosol activation.

203 CAM5-NCSU also includes an advanced treatment for SOA formation based on a

204 volatility-basis-set (VBS) approach that has been coupled with CB05_GE by Glotfelty et
205 al. (2015) and is also coupled with MOZART-4x in this work. This approach consists of
206 two primary components: (1) volatile SOA (VSOA) formation from anthropogenic VOCs
207 (AVOCs) and biogenic VOCs (BVOCs) and (2) the volatility and aging of primary
208 organic aerosol (POA) and the repartitioning of the semi/intermediate volatility
209 compounds (S/IVOC) into SOA. The VSOA treatment is based on the treatment of
210 Tsimpidi et al. (2010). The products of VOC oxidation are mapped onto the volatility
211 distribution using the aerosol mass yields listed in Tsimpidi et al. (2010) using the
212 CB05_GE species that represent those precursor VOCs. An additional pathway for the
213 formation of SOA from PAH is also added in CB05_GE. The SOA mass yields for PAHs
214 are derived from the laboratory measurements of Chan et al. (2009) following the
215 approach of Stainer et al. (2008), where the SOA mass yields for naphthalene,
216 1-methylnaphthalene, and 2-methylnaphthalene are averaged as surrogates for PAHs. The
217 volatility of POA and the subsequent formation of SOA from POA vapors are based on
218 the work of Robinson et al. (2007) and Shrivastava et al. (2008). POA emissions are
219 distributed into nine logarithmically-spaced volatility bins with effective saturation (C^*)
220 values ranging from 10^{-2} to $10^6 \mu\text{g m}^{-3}$. An updated emission spectrum is used to
221 distribute the POA emissions into the volatility bins as the emission spectrum used in
222 Robinson et al. (2007) has been shown to be too volatile (Cappa and Jimenez, 2010;
223 Hodzic et al., 2010; Jathar et al., 2011). This new emission spectrum maps the

224 anthropogenic POA emissions onto the volatility distribution based on thermodynamic
225 measurements of gasoline exhaust and also contains separate emissions fractions for
226 biomass burning aerosol which is less volatile than anthropogenic POA (May et al.,
227 2013a, b). The emission spectrum of Robinson et al. (2007), also assumes that the
228 emissions of SVOCs are fully captured by the original POA emissions and missing
229 IVOCs are assumed to be equivalent to 1.5 times the POA emissions inventory with these
230 additional emissions placed in the three highest volatility bins. However, because the
231 estimations of the missing IVOC emissions are poorly constrained, the 1.5 times the POA
232 mass for IVOCs is not included in this study.

233 In addition to the classic 1-D VBS treatment as described above,
234 functionalization and fragmentation treatment described in Shrivastava et al. (2013) are
235 included in this version of VBS for both VSOA and S/IVOCs (referred to as 1.5 D VBS).
236 In this treatment, the VSOA and S/IVOCs in each volatility bin are split into three
237 different species representing three generations of oxidation. During the first two
238 generations of oxidation the mass of the VSOA and S/IVOCs grows by 15%, reflecting
239 the addition of oxygen atoms. In this aging scheme not only do the masses of VSOA and
240 S/IVOCs increase in generation when oxidized by OH (at a rate of 1.0×10^{-11} and
241 $4.0 \times 10^{-11} \text{ cm}^3 \text{ molecule}^{-1} \text{ s}^{-1}$, respectively) but also their volatility decrease as they are
242 moved into smaller volatility bins. Fragmentation occurs once the VSOA and S/IVOCs
243 have aged to the third generation. This represents the breaking of carbon bonds, which

244 can increase volatility of the organic species thus reducing SOA formation. This is
245 parameterized by allowing 17.25% of the organic mass to pass to the next lowest
246 volatility bin but passing 75% of the VSOA and S/IVOC to the highest volatility bin in
247 the VBS structure. The remaining mass is assumed to be lost to species of higher
248 volatility than the VBS structure. There are several differences between the VBS used in
249 this work and Shrivastava et al. (2015). For example, nine volatility bins are used in this
250 work to represent the aging and gas-particle partitioning of POA, instead of five volatility
251 bins used in Shrivastava et al. (2015). In addition, compared to the reaction (3) in
252 Shrivastava et al. (2015), we do not have the third term, which denotes additional
253 fragmentation where 10% of the mass results in low carbon number species with very
254 high volatility that is eventually oxidized to CO/CO₂ and/or removed by dry deposition.
255 In ~~our~~ the model treatment used in this work, the remaining mass is assumed to be lost to
256 species with a volatility higher than the volatility values in the VBS structure. A more
257 detailed description of SOA formation from the VBS approach is summarized in
258 Glotfelty et al. (2015).

259

260 **3. Model Configurations and Evaluation Protocols**

261 3.1 Model Setup and Inputs

262 The simulations are performed with specified dynamics configuration, of which
263 winds and temperature are driven by the Goddard Earth Observing System Model,

264 Version 5 (GEOS-5) meteorology. The internally-derived meteorological fields are
265 nudged every time step (30 min) by 10% towards analysis fields from GEOS-5. [The](#)
266 [nudged meteorological fields include surface pressure, meridional wind, zonal wind,](#)
267 [zonal surface stress, meridional surface stress, snow height, solar flux at surface, soil](#)
268 [moisture fraction, surface temperature, temperature, specific humidity, surface](#)
269 [geopotential, orography flag, surface water flux, and surface sensible flux.](#) The
270 simulations are conducted for a 3-year period of 2008-2010 at a horizontal resolution of
271 $0.9^\circ \times 1.25^\circ$ and a vertical resolution of 56 layers for CAM5. The initial chemical
272 conditions are generated with same configurations with 1-year spinup.
273 The offline emissions used in this work are based on those used in Tilmes et al. (2015), of
274 which the anthropogenic and biofuel emissions are from the Monitoring Atmospheric
275 Composition and Climate/CityZen (MACCity) emission data set (Granier et al., 2011),
276 and biomass burning emissions are taken from the Atmospheric Chemistry and Climate
277 Model Intercomparison Project (ACCMIP) historical emissions dataset (Lamarque et al.,
278 2010). The ACCMIP emissions are extrapolated for 2008-2010 with the Representative
279 Concentration Pathway (RCP) 8.5 scenario and extended for VOCs and several other
280 species for MOZART-4x species. MOZART-4x species are then mapped into CB05_GE
281 species to generate emissions for CB05_GE species. [Although both MOZART-4x and](#)
282 [CB05_GE simulates bromine chemistry, no bromine emissions are included. For](#)
283 [bromine/chlorine species \(e.g., CF2CLBR, CF3BR, CFC11, CFC12, CH3BR, and](#)

284 [CH₃CL](#)), their surface concentrations are specified using the historical reconstruction
285 [from Meinshausen et al. \(2011\)](#). No bromine emissions were included.

286 The online emissions include biogenic VOCs from MEGAN2.1 (Guenther et al.,
287 2012), lightning NO_x (Price and Rind, 1992; Price et al., 1997), mineral dust (Zender et
288 al., 2003), and sea-salt (Martensson et al., 2003).

289

290 3.2 Available Measurements for Model Evaluation

291 A number of observational datasets from surface networks and satellites are used
292 for model evaluation. They are summarized along with the variables to be evaluated in
293 Table 2. The global surface network includes data sets from the National Oceanic and
294 Atmospheric Administration Climate Diagnostics Center (NOAA/CDC). The satellite
295 datasets include the Moderate Resolution Imaging Spectroradiometer (MODIS) for the
296 retrievals of cloud properties, the Clouds and Earth's Radiant Energy System (CERES)
297 [Energy Balanced and Filled \(EBAF\)](#) for the retrievals of radiation fluxes at surface and
298 top of atmosphere, the Aura Ozone Monitoring Instrument in combination with Aura
299 Microwave Limb Sounder (OMI/MLS) for the tropospheric ozone retrieval, the
300 Measurements Of Pollution In The Troposphere (MOPITT) for tropospheric carbon
301 monoxide (CO) retrieval, and the SCanning Imaging Absorption spectroMeter for
302 Atmospheric CHartographY (SCIAMACHY) for the retrievals of tropospheric nitrogen
303 dioxide (NO₂), HCHO, and C₂H₂O₂. Other satellite-based data include the

304 MODIS-derived CDNC and cloud liquid water path (LWP) by Bennartz (2007).
305 Regional observational networks include the Clean Air Status and Trends
306 Network (CASTNET), the Interagency Monitoring of Protected Visual Environments
307 (IMPROVE), the Speciation Trends Network (STN), and the Air Quality System (AQS)
308 over CONUS; the European Monitoring and Evaluation Program (EMEP), the Base de
309 Données sur la Qualité de l'Air (BDQA, France), and the European air quality database
310 (AirBase) over Europe; the Ministry of Environmental Protection of China (MEPC), the
311 National Institute for Environmental Studies of Japan (NIESJ), the Korean Ministry Of
312 Environment (KMOE), and Taiwan Air Quality Monitoring Network (TAQMN) over
313 East Asia. In addition to the data from the above networks, SOA measurements collected
314 by Lewandowski et al. (2013) at four field study sites including Cleveland and Medina,
315 OH (July-August, 2009), and Bakersfield and Pasadena, CA (May-June, 2010) are used
316 to evaluate SOA predictions.

317 Aircraft measurements include aircraft campaigns from Aerosol, Radiation, and
318 Cloud Processes affecting Arctic Climate (ARCPAC), Stratosphere-Troposphere
319 Analyses of Regional Transport in 2008 (START08), California Nexus 2010 (CalNex),
320 Arctic Research of the Composition of the Troposphere from Aircraft and Satellites
321 (ARCTAS), and CCN measurements in China (CCN_China). ARCPAC (Brock et al.,
322 2011) was conducted during March-April 2008 in the troposphere of the Alaskan Arctic,
323 including particle size distributions, composition, and optical properties. START08 (Pan

324 et al., 2010) was conducted during April-June 2008 to study the chemical and transport
325 characteristics of the extratropical upper tropospheric and lower stratospheric region over
326 central North America. CalNex (Ryerson et al., 2013) was conducted during May-July
327 2010 to provide improved scientific knowledge for emission control strategies to
328 simultaneously address the interrelated issues of air quality and climate change. ARCTAS
329 (Jacob et al., 2010) was conducted during April-June 2008 to investigate the chemistry of
330 the Arctic's lower atmosphere. CCN_China (Zhang et al., 2011) was conducted over
331 Beijing during July-September 2008, to investigate the impacts of aerosols on cloud
332 formation.

333

334 3.3 Evaluation Protocol

335 The protocols for performance evaluation include spatial distributions and
336 statistics, following the approach of Zhang et al. (2012b). The aircraft profile evaluation
337 is based on the Atmospheric Model Working Group (AMWG) diagnostics package
338 (Tilmes et al., 2015). Monthly-mean model results are compared for corresponding
339 regions and seasons of the field campaign. The analysis of the performance statistics will
340 focus on mean bias (MB), normalized mean bias (NMB), normalized mean error (NME),
341 and root mean square error (RMSE) [defined by Yu et al. \(2006\) and Zhang et al. \(2006\)](#).

342 The radiative/cloud variables are evaluated annually, including outgoing longwave
343 radiation (OLR) from NOAA/CDC; downwelling shortwave radiation (FSDS),

344 downwelling longwave radiation (FLDS), shortwave cloud forcing (SWCF), and
345 longwave cloud forcing (LWCF) from CERES-[EBAF](#); cloud fraction (CF), aerosol
346 optical depth (AOD), cloud optical thickness (COT), precipitating water vapor (PWV),
347 and CCN from MODIS, as well as CDNC and LWP from Bennartz (2007). CDNC is
348 calculated as an average value of layers between 850 and 960 hPa for comparison with
349 the satellite-derived values. Chemical concentrations evaluated include CO, O₃, SO₂,
350 ammonia (NH₃), NO₂, nitric acid (HNO₃), VOCs (i.e., formaldehyde, isoprene, and
351 toluene), particulate matter (PM) with diameter less than and equal to 10 μm (PM₁₀) and
352 2.5 μm (PM_{2.5}), and PM_{2.5} major components (e.g., SO₄²⁻, NH₄⁺, NO₃⁻, black carbon (BC),
353 organic carbon (OC), and total carbon (TC)) for CONUS and Europe. The chemical
354 observations over East Asia are very limited, which only include surface observations of
355 CO, SO₂, NO₂, and O₃ from Hong Kong, South Korea, and Japan, and PM₁₀ over
356 mainland China (derived from air pollution index), Hong Kong, South Korea, and Japan.
357 Since PM_{2.5} and PM₁₀ are not explicit species simulated in MAM7, their concentrations
358 are estimated based on prescribed-size distributions of dry particles predicted by used in
359 MAM7 simply assumed to be the particles in the first 5 modes (i.e., Aitken, accumulation,
360 primary carbon, fine sea salt, and fine dust modes) and the total 7 modes (i.e., Aitken,
361 accumulation, primary carbon, fine sea salt, fine dust, coarse sea salt, and coarse dust
362 modes), respectively. The properties of the particle size distribution for MAM7 are
363 summarized in Table S1 in the supplementary material.

364 Column concentrations of tropospheric CO, NO₂, HCHO, C₂H₂O₂, and
365 tropospheric O₃ residual (TOR) are evaluated for globe. The CO column evaluation
366 follows the AMWG diagnostics approach, which applies 1° × 1° monthly mean Level 3
367 MOPITT a priori and averaging kernels to monthly mean model results to account for the
368 a priori dependence and vertical resolution of the MOPITT data. The measured NO₂ and
369 HCHO columns are derived from the satellite retrievals from SCIAMCHY, which are
370 monthly mean gridded data on a 0.25° × 0.25° horizontal grid resolution for the period of
371 2008-2010. The measured glyoxal column is derived from the satellite retrievals from
372 SCIAMCHY, which are monthly mean gridded data on a 0.125° × 0.125° horizontal grid
373 resolution for the period of 2008. The measured O₃ is derived from the combining retrievals
374 from the Aura Ozone Monitoring Instrument and Microwave Limb Sounder observations,
375 which are monthly mean gridded data on a 1.25° × 1.25° horizontal grid resolution for the
376 period of 2008-2010.

377 All surface observational data used for evaluating 2008-2010 simulations are
378 available throughout 2008-2010 except for several variables with data during a limited
379 time period of 2001-2010 including OC from EMEP, SOA from Lewandowski et al.
380 (2013), and OA from Zhang et al. (2007) and Jimenez et al. (2009). For one grid cell
381 containing multiple observational sites, all the observations within the grid cell are
382 averaged and compared to the simulated results in that grid cell. While using grid
383 averaged observations helps reduce, to some extent, the uncertainties in comparing grid

384 averaged model output with pointwise observations, this approach cannot address the
385 inherent uncertainties associated with the evaluation of the model results obtained at a
386 coarse grid resolution.

387

388 **4 Model Evaluations**

389 **4.1 Surface Evaluation**

390 **4.1.1 Inorganic gGases and aAerosols**

391 Table 3 summarizes the performance statistics for major chemical species for
392 CAM5-NCSU simulations with MOZART-4x and CB05_GE. Figure 1 shows the scatter
393 plots between observations and model results. The statistical performance of
394 MOZART-4x and CB05_GE are similar for most chemical species. As shown in Table 3,
395 CO is underpredicted over East Asia by both MOZART-4x and CB05_GE, with NMBs of
396 -65.6% and -65.7%, respectively. The underprediction of CO is mainly due to the
397 underestimation of CO emissions from biomass burning (Tilmes et al., 2015). The
398 underestimations in CO emissions lead to underpredictions of column CO concentrations,
399 with NMBs of -25.8% and -24.4% for MOZART-4x and CB05_GE, respectively. Both
400 MOZART-4x and CB05_GE largely overpredict the concentrations of SO₂ over CONUS
401 (with NMBs of 580.2% and 561.6%, respectively), East Asia (with NMBs of 47.0% and
402 35.5% %, respectively), and Europe (with NMBs of 100.9% and 94.1%, respectively),
403 likely due to the overestimation of SO₂ emissions, the uncertainties in the emission

404 injection heights as well as the vertical mixing scheme used. [For example, several](#)
405 [modeling studies over East Asia reported the underestimates of emissions of SO₂ and](#)
406 [NO_x are a main cause for poor model performance \(e.g., Liu et al., 2010; Zhang et al.,](#)
407 [2015a, b\).](#) The overpredictions of surface SO₂ concentrations result in the overpredictions
408 of the concentrations of SO₄²⁻ at the surface. [The overpredictions of surface SO₄²⁻](#)
409 [concentrations can also be attributed to the uncertainties in the OH predictions. The](#)
410 [air-mass weighted tropospheric mean OH concentrations predicted by MOZART-4x and](#)
411 [CB05_GE are both 13.1×10⁵ molec cm⁻³, which is slightly higher than the present-day](#)
412 [tropospheric mean OH levels of 11.1 ± 1.6 molec cm⁻³ of Naik et al. \(2013\).](#) The higher
413 [OH levels can result in higher oxidation of SO₂ to produce more SO₄²⁻.](#) Surface NH₃
414 concentrations from MOZART-4x and CB05_GE are overpredicted over Europe (with
415 NMBs of 112.4% and 104.3%, respectively), likely due to the overestimation of NH₃
416 emissions. The overpredictions of the NH₃ concentrations [can potentially](#) result in the
417 overpredictions of the NH₄⁺ concentrations at the surface. [On the other hand, the](#)
418 [overpredictions of the NH₄⁺ concentrations at the surface are also related to the](#)
419 [overpredictions of the concentrations of SO₄²⁻ at the surface.](#) The concentrations of NO₂
420 from MOZART-4x and CB05_GE are largely underpredicted over [CONUS \(with NMBs](#)
421 [of -51.4% and -52.2%, respectively\).](#) Europe (with NMBs of -61.4% and -62.1%,
422 respectively), and East Asia (with NMBs of -74.1% and -74.8%, respectively), which is
423 likely due to the uncertainties in estimating total NO_x emissions and emission injection

424 heights as well. As shown in Figure 1, the concentrations of O₃ from MOZART-4x and
425 CB05_GE are overpredicted over CONUS (with NMBs of 29.0% and 28.2% over the
426 CASTNET sites, respectively), Europe (with NMBs of 19.3% and 22.2% over the EMEP
427 sites, respectively) and East Asia (with NMBs of 68.8% and 65.7% over the KMOE sites,
428 respectively). This is likely due to ~~the~~ less O₃ titration resulted from the underpredictions
429 of NO_x, the dilution of NO_x emissions resulted from the use of a coarse grid resolution, as
430 well as possible underestimates in O₃ dry deposition. Martin et al. (2014) reported the
431 uncertainties in O₃ dry deposition associated with vegetation phenology in CAM-chem,
432 which led to positive biases of 16 ppb over eastern U.S. and 8 ppb over Europe,
433 respectively, for summertime surface O₃. The overpredictions of SO₄²⁻ result in the
434 underpredictions of NO₃⁻ and Cl⁻, through thermodynamic equilibrium, and therefore
435 overpredictions of HNO₃ over CONUS. As more NH₄⁺ are needed to neutralize SO₄²⁻,
436 less NH₄⁺ are available to neutralize NO₃⁻ and/or Cl⁻, driving total nitrate and total
437 chlorine to partition into the gas-phase to produce more HNO₃ and HCl. Yu et al. (2005)
438 also found that the model biases in total nitrate (TNO₃ = HNO₃ + NO₃⁻) predictions can be
439 attributed to measurement errors in SO₄²⁻ and total ammonium (TNH₄ = NH₃ + NH₄⁺) as
440 well as the inaccurate predictions in SO₄²⁻ and TNH₄. In addition, Reff et al. (2009)
441 suggested several sources for Cl⁻ (e.g., biomass burning and wildfires), which are not
442 included in this work. There are no anthropogenic Cl⁻ emissions included in this work
443 except from sea-salt emissions, which is calculated online in CESM/CAM5. Omission of

444 [additional chlorine emissions may also partly explain the underpredictions of Cl⁻ over](#)
445 [CONUS](#). HNO₃ is underpredicted over Europe, which is [mainly](#) due to the
446 underpredictions of NO_x. [The concentration of Cl⁻](#) is overpredicted over Europe, which is
447 likely due to the uncertainties for the gas/particle partitioning over coarse modes (He and
448 Zhang, 2014). [Unlike the performance of Cl⁻ over CONUS, which is only for fine Cl⁻ \(in](#)
449 [Aitken, accumulation, fine sea-salt, and fine dust modes\), the performance of Cl⁻ over](#)
450 [Europe is for fine and coarse Cl⁻ \(in all seven modes\). As the thermodynamic equilibrium](#)
451 [is not treated for coarse particles \(the irreversible condensation of HCl is assumed to](#)
452 [occur on the surface of coarse particles\), it is likely that the model overpredicts coarse Cl⁻,](#)
453 [but underpredicts fine Cl⁻ due to the missing sources.](#) Both MOZART-4x and CB05_GE
454 [over](#)predict PM_{2.5} over CONUS, however, they underpredict PM₁₀ over the AQS sites,
455 with NMBs of -38.6% and -38.9%, respectively. The underpredictions of PM₁₀ are
456 [mainly](#) due to the inaccurate predictions of coarse particles. Both MOZART-4x and
457 CB05_GE underpredict PM_{2.5} and PM₁₀ over Airbase and BDQA sites, however, they
458 overpredict PM₁₀ by 3.14 μg m⁻³ (or by 22.2%) and 3.43 μg m⁻³ (or by 24.2%) over the
459 EMEP sites, respectively, which is [mainly](#) due to the overpredictions of coarse particles
460 (e.g., Cl⁻) over these sites [and uncertainties in the sea-salt and dust emissions](#). Both
461 MOZART-4x and CB05_GE underpredict PM₁₀ by 33.61 μg m⁻³ (or by 33.4%) and 26.71
462 μg m⁻³ (or by 26.6%) over the MEPC sites in mainland China, respectively, which is
463 mainly due to the uncertainties in the emissions in primary gases (e.g., SO₂, NO_x, NH₃,

464 and VOCs) and particulate species (e.g., SO_4^{2-} , BC, and POA). Granier et al. (2011)
465 compared the regional emissions among different inventories and indicated large
466 uncertainties in the emissions over China. For example, the differences of BC biomass
467 burning emissions over China among different inventories can be as large as a factor of
468 2.1, and the differences of SO_2 anthropogenic emissions can be as large as a factor of 1.8.

469 4.1.2 VOCs and Organic Aerosols

470 VOCs species such as HCHO, ISOP, and TOL are underpredicted over CONUS,
471 likely due to the uncertainties in the biogenic emissions from MEGAN2.1, anthropogenic
472 emissions (e.g., HCHO and TOL) and the chemical reactions as well as a coarse
473 horizontal resolution used in this work. Both MOZART-4x and CB05_GE underpredict
474 BC with NMBs of -29.3% and -29.3%, respectively. The underpredictions of BC are
475 likely due to the underestimations of BC emissions, as well as uncertainties in the
476 transport and wet removal by convection (Ma et al., 2013; Wang et al., 2013; Tilmes et al.,
477 2015).

478 OC is slightly overpredicted with an NMB of 2.1% by MOZART-4x over
479 CONUS, whereas it is moderately underpredicted with an NMB of -20.7% by CB05_GE.
480 OC is evaluated against observations at the IMPROVE sites, and SOA dominates OC at
481 these sites for both simulations with MOZART4-x and CB05_GE, with SOA/OC ratios
482 of 83.0% and 59.6%, respectively. Although no SOA measurements are available from
483 IMPROVE for evaluation, the differences in OC predictions can be attributed to the

484 differences in SOA predictions because of dominances of SOA in total OC. Compared to
485 the SOA observations at the four sites in the U.S. from Lewandowski et al. (2013),
486 MOZART-4x underpredicts SOA by $0.03 \mu\text{g m}^{-3}$ (or by 1.9%), whereas CB05_GE
487 underpredicts SOA by $0.4 \mu\text{g m}^{-3}$ (or by 23.1%). Note that the SOA statistics are
488 calculated using only four pairs of seasonal mean values at four sites in the U.S. where
489 the observed SOA data are available during 2008-2010; they therefore may not be
490 representative because of limited data used for calculation. Figure 2 compares simulated
491 and observed SOA concentrations at the four sites. MOZART-4x predicts higher SOA
492 than CB05_GE at all four sites, which reduces underpredictions at Cleveland and Medina,
493 OH but increases overpredictions at Bakersfield and Pasadena, CA. This indicates a
494 better capability of MOZART-4x to simulate SOA at sites with relatively high SOA
495 concentrations ($\geq 1 \mu\text{g m}^{-3}$) compared to CB05_GE despite its tendency of
496 overpredictions at sites with lower SOA levels. The higher SOA concentrations predicted
497 by MOZART-4x can be attributed to the higher OH levels and higher biogenic emissions
498 in MOZART-4x. However, the concentration of OC is largely underpredicted by both
499 MOZART-4x and CB05_GE over Europe, with NMBs of -74.2% and -75.1%,
500 respectively, indicating the uncertainties in the emissions of SOA precursors and SOA
501 formation treatment. For example, the aqueous-phase oxidation of VOCs in clouds is not
502 taken into account in this work, which, however, can contribute several percentages of
503 SOA in some areas and seasons over Europe (Couvidat et al., 2013). The

504 hydrocarbon-like organic aerosol (HOA) predicted by MOZART-4x and CB05_GE
505 correlated well with the observations at 33 sites in the Northern Hemisphere (e.g., with
506 correlation coefficients of 0.93 for both simulations) but the amount is largely
507 underpredicted by both MOZART-4x and CB05_GE, with NMBs of -77.2% and -76.7%,
508 respectively, indicating that the POA may be too volatile with the implementation
509 currently in the model. Oxygenated organic aerosol (OOA), which is roughly equivalent
510 to the sum of SOA and SVOA, is also largely underpredicted at the 33 sites by both
511 MOZART-4x and CB05_GE, with NMBs of -56.5% and -62.3%, respectively. This is
512 mainly due to the uncertainties in the oxidation rate and fragmentation rates as well as
513 SOA formation treatment. The underpredictions of HOA and OOA result in an
514 underprediction of total organic aerosol (TOA) by both MOZART-4x and CB05_GE,
515 with NMBs of -67.8% and -71.2%, respectively.

516 **4.2 Chemical Column Evaluation**

517 Figure 3 shows the zonal mean of column concentrations of CO, HCHO, glyoxal,
518 NO₂, and TOR for June, July, and August during 2008-2010. In general, MOZART-4x
519 and CB05_GE predict similar zonal mean profiles of these species. Both MOZART-4x
520 and CB05_GE underpredict column CO, due to a significant underestimation of CO
521 emissions (Tilmes et al., 2015) and uncertainties in OH predictions. During summer,
522 column HCHO is overpredicted over middle latitudes (30-60° N) in the Northern
523 Hemisphere and tropical regions (0-10° S) in the Southern Hemisphere, while it is largely

524 underpredicted over the rest of regions. The underprediction of column HCHO is likely
525 due to the uncertainties in the emissions of HCHO and its precursors as well as pathways
526 for secondary HCHO formation. Both MOZART-4x and CB05_GE underpredict column
527 glyoxal, with more underpredictions in CB05_GE. The underpredictions of glyoxal are
528 mainly due to the uncertainties in the glyoxal chemical production and removal (Knote et
529 al., 2014b). Several studies indicate that aromatics, isoprene, and ethyne are the major
530 contributors to glyoxal formation (Washenfelder et al., 2011; Knote et al., 2014b). In
531 MOZART-4x, glyoxal can be produced from photolysis of the oxidation products of
532 toluene, and oxidation products of aromatics (e.g., benzene, toluene, and xylenes),
533 isoprene, and ethyne. CB05_GE does not include pathways for glyoxal production
534 through photolysis, but includes glyoxal production from oxidation of alkenes (e.g., OLE,
535 IOLE, ethene, and ISOP) and aromatics (e.g., toluene and xylenes). Uncertainties in the
536 emissions of these precursors and the production pathways can propagate into the
537 predicted glyoxal concentrations. MOZART-4x includes additional pathways for glyoxal
538 production through photolysis and improved treatments for glyoxal production from
539 additional oxidized VOCs (e.g., benzene) products (Knote et al., 2014b), which can result
540 in higher glyoxal than in CB05_GE. The major chemical loss of glyoxal includes
541 photochemical loss and oxidation by OH. The uncertainties in OH levels can propagate
542 into glyoxal predictions as well. In addition, CB05_GE includes an additional pathway
543 for glyoxal loss through its uptake by aerosols, which is not included in MOZART-4x.

544 This can explain in part the lower glyoxal concentrations predicted by CB05_GE than by
545 MOZART-4x. An advanced treatment for glyoxal formation should be therefore
546 developed in the future. Both MOZART-4x and CB05_GE overpredict column NO₂,
547 likely due to the uncertainties in the NO₂ aircraft emissions and overpredictions of
548 lightning NO_x, [as well as the satellite retrievals](#). The lightning NO_x emissions are
549 calculated online (i.e., 6.2 and 6.4 TgN yr⁻¹ in CB05_GE and MOZART-4x, respectively),
550 which is about 1.2-2.2 TgN yr⁻¹ higher than that in Lamarque et al. (2012) and Tilmes et
551 al. (2015). Tilmes et al. (2015) have shown that increased lightning NO_x emissions in
552 CAM-chem can lead to an increase in OH levels and therefore a decrease in the lifetime
553 of methane and an underestimation of CO in the model. [As discussed in Yarwood et al.](#)
554 [\(2012\), the errors in satellite NO₂ retrievals are dominated by atmospheric mass factor,](#)
555 [which has a large uncertainty due to errors in the specification of clouds, surface albedo,](#)
556 [a priori NO₂ profile shape, and aerosols. For example, Boersma et al. \(2004\) also reported](#)
557 [that the error in the tropospheric NO₂ retrievals is 35-60%, especially over polluted areas.](#)
558 [These can partly explain the overpredictions of column NO₂.](#) The higher zonal-mean
559 concentrations of NO₂ in CB05_GE than those in MOZART-4x are likely due to
560 additional NO₂ production from the reactions of VOCs with NO₃ radical in CB05_GE
561 (e.g., reactions of NO₃ with OLE, IOLE, and ethene). The zonal-mean distribution of
562 summer TOR from CB05_GE is similar to that from MOZART-4x. TOR is overpredicted
563 over 40° S-50° N, and underpredicted over 40° S-60° S. The higher TOR from CB05_GE

564 is mainly due to higher O₃ production from higher NO₂ and lower O₃ loss from lower OH
565 in CB05_GE than in MOZART-4x.

566 **4.3 Vertical Profile Evaluation**

567 Figure 4 compares the vertical profile of major gases against the aircraft
568 observations (i.e., ARCPAC, ARCTAS, START08, and CalNex). Compared with aircraft
569 measurements, MOZART-4x and CB05_GE predict similar O₃ and CO profiles, whereas
570 there are large differences in NO_x (above 9 km) and NO_y profiles (below 12 km). O₃
571 profiles from MOZART-4x and CB05_GE overall agree well with aircraft measurements,
572 although O₃ is slightly overpredicted near the surface. As discussed previously, the
573 significant underpredictions of CO profiles in both MOZART-4x and CB05_GE are
574 mainly due to the underestimations of CO biomass burning emissions and uncertainties in
575 OH predictions. Both MOZART-4x and CB05_GE underpredict the vertical
576 concentrations of NO_x at higher altitudes (e.g., above 9 km in ARCTAS and STRAT08),
577 with a slightly better agreement in CB05_GE than in MOZART-4x. The concentrations of
578 NO_x near the surface are slightly overpredicted by both simulations. The underpredictions
579 of the concentrations of NO_x at higher altitudes are likely due in part to the uncertainties
580 in the NO_x emissions, the chemical reactions of nitrogen cycles (e.g., heterogeneous
581 reactions of NO₂, NO₃, and N₂O₅ over the surface of aerosol particles), the convection
582 scheme, as well as the aircraft campaign data. Some field campaigns (e.g., ARCPAC)
583 focus on the polluted regions with a significant contribution from biomass burning and

584 local sources (Tilmes et al., 2015). The underestimations of emissions from these sources
585 and uncertainties in the vertical mixing scheme can result in the underpredictions of their
586 profiles. NO_y includes all the reactive nitrogen species. The simulated NO_y profiles from
587 CB05_GE agree better with those observed during APCPAC, ARCTAS, and CalNex than
588 those from MOZART-4x, whereas MOZART-4x predicts slightly better NO_y profile
589 against START08 in the lower troposphere than CB05_GE. OH concentrations are
590 underpredicted by both MOZART-4x and CB05_GE against ARCTAS observations,
591 whereas H₂O₂ mixing ratios are well predicted above 4 km but underpredicted below 4
592 km. Compared to CB05_GE, MOZART-4x predicts slightly higher H₂O₂ within 4-km
593 above the surface. However, the performance here only represents the local conditions,
594 instead of global conditions. Figure 5 compares the vertical profile of simulated CCN
595 against the aircraft observations from CCN_China. Both MOZART-4x and CB05_GE
596 slightly overpredict CCN (at supersaturation of 0.2%) profile over Beijing area, with less
597 overpredictions in MOZART-4x.

598 **4.4 Cloud/Radiative Evaluation**

599 Table [54](#) shows the statistical performance for major cloud/radiative variables for
600 MOZART-4x and CB05_GE simulations. Radiative variables such as OLR, FSDS, and
601 FLDS show excellent agreement with observations, with NMBs within $\pm 8\%$ for both
602 simulations. However, SWCF is overpredicted by both MOZART-4x and CB05_GE, with
603 NMBs of 26.4% and 27.7%, respectively, and LWCF is underpredicted by both

604 MOZART-4x and CB05_GE, with NMBs of -21.6% and -16.7%, respectively. All
605 predicted radiative variables show high correlation with observations, with correlation
606 coefficients of 0.9 to 0.99. CF is well predicted by MOZART-4x, with an NMB of 6.3%,
607 whereas CCN5, CDNC, COT, and LWP are moderately overpredicted or underpredicted,
608 with NMBs of -32.1%, 19.7%, -26.0%, and 2.8%, respectively. The performance of cloud
609 variables is similar in CB05_GE, with NMBs of 6.0%, -29.0%, 20.8%, -26.0%, and 1.7%
610 for CF, CCN5, CDNC, COT, and LWP, respectively. AOD is also underpredicted by both
611 MOZART-4x and CB05_GE, with NMBs of -23.9% and -24.6%, respectively.

612 Figure 86 shows the Taylor diagram (Taylor, 2001) comparing the model
613 performance of MOZART-4x with that of the CB05_GE for cloud and radiative
614 predictions. The similarity between the two patterns is quantified in terms of their
615 correlations (i.e., angle), their standard deviations (i.e., y axis), and the ratio of their
616 variances (i.e., x axis). In general, the performance of major cloud/radiative variables
617 between MOZART-4x and CB05_GE are similar. The major differences in the
618 performance of cloud/radiative variables between MOZART-4x and CB05_GE are the
619 variances of CCN5, CDNC, and SWCF, which is mainly due to the predicted aerosol
620 distributions (see Figure 6b). The larger deviation of COT and LWP from observations
621 (i.e., the two points located outside the diagram in Figure 86) suggests the uncertainties
622 both in the model treatments for cloud dynamics and thermodynamics as well as in the
623 satellite retrievals.

624 Due to the underpredictions of cloud variables (e.g., COT and CCN5), OLR is
625 slightly overpredicted by 7.8 W m^{-2} (or by 3.6%), and LWCF is underpredicted by 4.8 W
626 m^{-2} (or by 21.6%) in MOZART-4x. Similarly, OLR is slightly overpredicted by 6.7 W m^{-2}
627 (or by 3.1%) and LWCF is underpredicted by 3.7 W m^{-2} (or by 16.7%) in CB05_GE.

628 Figure 7 shows the comparisons of satellite observations with model predictions for AOD,
629 CCN5, CDNC, COT, and SWCF averaged during 2008-2010. The underpredictions of
630 AOD over oceanic areas can be attributed to the uncertainties in the sea-salt emissions
631 and inaccurate predictions of other PM components (e.g., marine organic aerosols) over
632 the ocean and overestimation of oceanic AOD in the MODIS collection 5.1 (Levy et al.,
633 2013). The underprediction of AOD over land (e.g., tropical islands) is mainly due to the
634 significant underestimation of biomass burning emissions in the model (Tilmes et al.,
635 2015). AOD is higher in MOZART-4x over most land areas (except East Asia and Europe)
636 than in CB05_GE. The higher AOD in MOZART-4x is mainly due to higher SOA (e.g.,
637 over most land areas) and higher NO_3^- (e.g., over CONUS) in MOZART-4x. The lower
638 AOD over East Asia and Europe in MOZART-4x is mainly due to the lower SO_4^{2-} as
639 there is an additional pathway of SO_2 (oxidized by O_3) included in CB05_GE but it is not
640 included in MOZART-4x and lower NH_4^+ to neutralize lower SO_4^{2-} through
641 thermodynamic equilibrium. This additional pathway also results in higher H_2SO_4
642 predictions in CB05_GE and higher aerosol number concentration through homogeneous
643 nucleation. Therefore, CCN5 is higher in CB05_GE than in MOZART-4x (see Figure 7).

644 CDNC is moderately overpredicted for both cases. Cloud droplet formation is sensitive to
645 both particle number concentrations and updraft velocity (Reutter et al., 2009). The
646 overprediction of CDNC is due partly to high activation fractions (e.g., inclusion of
647 adsorption activation from insoluble CCN and effective uptake coefficient of 0.06 used in
648 this work) (Gantt et al., 2014) as well as the uncertainties in the model treatments for
649 cloud microphysics (e.g., resolved clouds and subgrid-scale cumulus clouds) and satellite
650 retrievals (e.g., error propagation of the input variables to derive CDNC) (Bennartz,
651 2007). COT is largely overpredicted over Southeast Asia and South America and
652 underpredicted over polar regions for both simulations. Overpredictions in CDNC and
653 COT can increase cloud albedo and therefore, increase SWCF over the low and middle
654 latitudes. The large underpredictions of COT over polar regions can be attributed to the
655 uncertainties in plane-parallel visible-near-infrared retrievals with low solar zenith angle
656 (Seethala and Horváth, 2010) and the influence of radiatively active snow on overlying
657 cloud fraction (Kay et al., 2012). Due to the different gas-phase mechanisms, the
658 predicted SWCF (Figure 7) and LWCF (Figure not shown) are different, with a global
659 average difference of 0.5 W m^{-2} and 1.1 W m^{-2} , respectively. However, the absolute
660 differences in simulated SWCF can be as large as 13.6 W m^{-2} as shown in Figure 7. The
661 large differences of SWCF and LWCF between MOZART-4x and CB05_GE are mainly
662 over subtropical regions (e.g., $20^\circ\text{S} - 20^\circ\text{N}$), which is mainly due to lower COT in
663 MOZART-4x than in CB05_GE.

664

665 [5. Model-to-Model Comparisons](#)

666 [5.1 Column Comparisons](#)

667 [5.1.1 Column Gases](#)

668 Figures [5a-8a](#) and b compare the column mass abundance of major gaseous and
669 aerosol species simulated by MOZART-4x and CB05_GE. As shown in Figure [6a8a](#),
670 column CO predicted by MOZART-4x is about $2.4 \times 10^{20} \text{ m}^{-2}$ (or by 2.3%) lower than that
671 by CB05_GE in the global mean. The different column CO concentrations are due to
672 different pathways for chemical production and loss of CO between MOZART-4x and
673 CB05_GE, and different OH levels in MOZART-4x and CB05_GE. The chemical
674 production of CO is mainly from photolysis and oxidation of VOCs species, and the
675 chemical loss of CO is mainly from the oxidation by OH. Different concentrations of
676 VOCs species can result in different chemical production of CO. Meanwhile, the only
677 chemical loss of CO in CB05_GE is the oxidation of CO by OH, which produces HO₂
678 and CO₂. Higher OH levels in MOZART-4x can result in more CO loss. MOZART-4x
679 includes an additional loss pathway of CO oxidized by OH to produce CO₂ and H. As a
680 result, the combined rate constant for both pathways of CO oxidation by OH in
681 MOZART-4x is about 4% higher than in CB05_GE. All these differences result in 2301
682 and 2265 Tg yr⁻¹ chemical loss of CO in MOZART-4x and CB05_GE, respectively.

683 The global mean differences in the simulated column concentrations of SO₂ and

684 NH_3 between MOZART-4x and CB05_GE are $2.0 \times 10^{18} \text{ m}^{-2}$ (or by 12.5%) and 1.9×10^{17}
685 m^{-2} (or by 3.1%), respectively. The lower column abundance of SO_2 in CB05_GE is
686 mainly due the additional pathway for SO_2 loss through oxidation by O_3 over the surface
687 of dust particles, which is not included in MOZART-4x. This pathway can produce more
688 SO_4^{2-} and therefore, more NH_3 is partitioned into the particulate phase to form NH_4^+
689 which can neutralize additional SO_4^{2-} , resulting in lower column abundance of NH_3 in
690 CB05_GE. Both column concentrations of NO_x and NO_y from MOZART-4x are about
691 $9.4 \times 10^{17} \text{ m}^{-2}$ (or by 9.5%) and $3.6 \times 10^{19} \text{ m}^{-2}$ (or by 46.3%) lower than that from
692 CB05_GE. The higher NO_x in CB05_GE is mainly due to the lower OH available for the
693 chemical loss through the reaction of NO_2 with OH. NO_y in MOZART-4x includes NO_x ,
694 nitrate radical (NO_3), nitrogen pentoxide (N_2O_5), HNO_3 , peroxyacetic acid (HO_2NO_2),
695 chlorine nitrate (ClONO_2), bromine nitrate (BrONO_2), peroxyacetyl nitrate (PAN),
696 organic nitrate (ONIT), methacryloyl peroxyacetyl nitrate (MPAN), peroxy radical from the
697 reaction of NO_3 with ISOP (ISOPNO₃), and lumped isoprene nitrate (ONITR), whereas
698 NO_y in CB05_GE includes NO_x , NO_3 , N_2O_5 , HNO_3 , HO_2NO_2 , ClONO_2 , BrONO_2 , nitrous
699 acid (HONO), PAN, higher peroxyacetyl nitrates (PANX), and organic nitrate (NTR). The
700 reactions for reactive nitrogen species are different in MOZART-4x and CB05_GE,
701 resulting in different NO_y predictions. [Figure S1 in the supplementary material shows the](#)
702 [dominant species in \$\text{NO}_y\$ predicted by the simulations using both MOZART-4x and](#)
703 [CB05_GE. As shown in Figure S1, \$\text{NO}_x\$, \$\text{HNO}_3\$, and TPAN \(PAN+MPAN for](#)

704 MOZART-4x and PAN+PANX for CB05_GE) are the major components for NO_y
705 concentrations, with the ratios of 90.5% and 91.7%, respectively, for the sum of the
706 mixing ratios of top three species to that of NO_y. NO_x dominates over East Asia, eastern
707 U.S., and western Europe, whereas TPAN dominates over most oceanic area. Figure S2 in
708 the supplementary material shows the absolute and relative differences for major NO_y
709 species between MOZART-4x and CB05_GE. As shown in Figure S2, MOZART-4x
710 predicts lower column TPAN by 2.9×10¹⁹ molecules m⁻² (or by 63.4%), which dominates
711 the differences in NO_y predictions between the two simulations. The differences in TPAN
712 predictions can be attributed to the differences in the kinetic reactions. Table S2 in the
713 supplementary material lists the reactions involving TPAN. As shown in Table S2,
714 besides the differences in the reaction rate calculation, MOZART-4x includes one
715 additional reaction, i.e., PAN destruction by OH, which is not included in CB05_GE. In
716 addition, simulated OH levels are higher in MOZART-4x than those in CB05_GE, which
717 could result in more TPAN loss through oxidation by OH. These differences can explain
718 the lower TPAN mixing ratios in MOZART-4x than those in CB05_GE and thus lower
719 column NO_y mass abundances in MOZART-4x than those in CB05_GE. Table S3 in the
720 supplementary material lists the NO_y species used in the calculation for Figure 4 and
721 other NO_y related comparisons. Figure S3 in the supplementary material shows the
722 absolute differences in NO_y (with and without inclusion of aerosol nitrate) between
723 MOZART-4x and CB05_GE. If aerosol nitrate is accounted for in the NO_y definition, the

724 differences in NO_y between the two mechanisms decrease over East Asia, eastern U.S.,
725 Europe, and middle Africa as aerosol nitrate is higher in MOZART-4x over these regions
726 (see Figure 6b). For the rest of areas, the differences in NO_y between the two mechanisms
727 increase if aerosol nitrate is accounted for in the NO_y definition.

728 The tropospheric column O₃ from MOZART-4x is about 1.5 DU (or by 4.7%)
729 lower than that from CB05_GE. Table 5 shows the tropospheric O₃ budget from
730 MOZART-4x and CB05_GE. The burdens of tropospheric O₃ from MOZART-4x and
731 CB05_GE are 325 Tg and 333 Tg, respectively, which is comparable to the previous
732 studies using CAM (Lamarque et al., 2012; Young et al., 2013). The O₃ burden from
733 MOZART-4x in this work is about 12 Tg (or 3.8%) higher than that in Tilmes et al.
734 (2015), which is mainly due to the additional kinetic reactions included in this version of
735 MOZART-4x. The dry deposition flux of O₃ from MOZART-4x is 679 Tg yr⁻¹, which is
736 about 3.7% lower than that from CB05_GE (i.e., 705 Tg yr⁻¹). The lower O₃ dry
737 deposition flux is mainly due to the lower O₃ concentration simulated by MOZART-4x.
738 The O₃ chemical production and loss from CB05_GE and MOZART-4x are roughly
739 within the range of Young et al. (2013). The O₃ chemical production from MOZART-4x
740 is comparable to that of Lamarque et al. (2012), but the O₃ chemical production from
741 CB05_GE is about 12.8% higher than Lamarque et al. (2012). In this table, chemical
742 production is calculated mainly from reactions of NO with peroxy radicals and chemical
743 loss is calculated mainly from the oxygen radical in the reaction of excited oxygen atom

744 (O^1D) with water vapor (H_2O) and from the reactions of O_3 with the HO_2 , OH , and
745 alkenes. Different peroxy radicals and alkenes treated and different reaction rates used in
746 the two mechanisms can contribute to the different chemical production and chemical
747 loss of O_3 . The O_3 lifetime is calculated based on the ratio of O_3 burden to the total O_3
748 loss (dry deposition + chemical loss). The O_3 lifetime from CB05_GE is comparable to
749 those reported by Young et al. (2013), and the O_3 lifetime from MOZART-4x is
750 comparable to those reported by Lamarque et al. (2012) and Tilmes et al. (2015).

751 Column concentrations of OH , $HCHO$, and $ISOP$ from MOZART-4x are higher
752 than CB05_GE, with global mean values of $9.7 \times 10^{13} \text{ m}^{-2}$ (or by 0.8%), $3.5 \times 10^{17} \text{ m}^{-2}$ (or
753 by 1.3%), and $1.1 \times 10^{18} \text{ m}^{-2}$ (or by 25.6%), respectively. The higher column
754 concentrations of OH and $HCHO$ are likely due to the photolysis of more peroxide
755 species, better HO_x recycling, and higher precursors for secondary $HCHO$ (e.g., $ISOP$) in
756 MOZART-4x. MOZART-4x includes detailed organic peroxide species, whereas in
757 CB05_GE, all the organic peroxide species are lumped into one species (i.e., $ROOH$).
758 The uncertainties in HO_x recycling in CB05_GE can also result in uncertainties in OH
759 predictions. The higher $ISOP$ is mainly due to higher biogenic emissions and less
760 chemical loss in MOZART-4x than that in CB05_GE. In MOZART-4x, the chemical loss
761 of $ISOP$ is mainly from the oxidation of $ISOP$ by OH , O_3 , and NO_3 . However, in
762 CB05_GE, the chemical loss of $ISOP$ includes not only the oxidation of $ISOP$ by OH , O_3 ,
763 and NO_3 , but also the consumption of $ISOP$ by atomic oxygen (i.e., O), NO_2 , and Cl .

764 5.1.2 Column Aerosols

765 As shown in Figure [8b](#), the differences in the domain average column mass
766 abundances of most aerosol species (e.g., NH_4^+ , BC, Cl^- , and POA) between
767 MOZART-4x and CB05_GE are within $\pm 0.02 \text{ mg m}^{-2}$. The differences in the column
768 SO_4^{2-} vary from -25.2 to 0.4 mg m^{-2} , with the global mean of -0.2 mg m^{-2} . The simulated
769 column concentrations of SO_4^{2-} from MOZART-4x are much lower than those from
770 CB05_GE over East Asia, west Europe, and Middle Africa. SO_2 can be oxidized by O_3 to
771 form SO_4^{2-} on the surface of dust particles in CB05_GE, which explains additional
772 formation of SO_4^{2-} by CB05_GE over these regions. The differences of the spatial
773 distributions and magnitudes in the column concentrations of NH_4^+ are similar to those of
774 SO_4^{2-} over land areas, which is associated with thermodynamic equilibrium. The column
775 concentrations of NO_3^- simulated by MOZART-4x are higher over East Asia, India, and
776 Europe than those by CB05_GE, which is mainly due to its competition with SO_4^{2-} in
777 forming ammonium salts in the particulate phase in those regions where the column NH_3
778 concentrations are high (Figure [8a](#)). Dust emissions are very sensitive to the wind speed.
779 Slightly changes in wind speeds can result in significant change in dust emissions, thus,
780 dust concentrations.

781 The column concentrations of SOA predicted by MOZART-4x are about 0.18 mg
782 m^{-2} (or by 8.4%) higher than those predicted by CB05_GE. The higher SOA column
783 concentrations are mainly over most continental areas in the middle and low latitudes.

784 The SOA mainly includes biogenic SOA, anthropogenic SOA, and semi-volatile SOA.
785 The differences of SOA are mainly due to the higher BVOCs emissions and higher OH
786 levels in MOZART-4x than in CB05_GE. Different branching ratios used in
787 MOZART-4x and CB05_GE can also contribute to the different SOA predictions.
788 MOZART-4x includes explicit species and more types of precursors for alkylperoxy
789 radicals (RO_2), and different reaction rate constants for different reactions, whereas in
790 CB05_GE, all oxidized VOCs are lumped as one species (i.e., RO_2) and branching ratios
791 are estimated based on the only three reactions (i.e., reactions of RO_2 with NO, HO_2 , and
792 RO_2). These differences can contribute to the differences in the estimation of branching
793 ratios, and therefore, affect the partitioning between organic gas and aerosols through the
794 1.5 D VBS treatment implemented in CAM5-NCSU.

795

796 [5.2](#) SOA Comparisons

797 Figure 9 shows the contributions to total SOA (TSOA) concentrations from
798 anthropogenic sources (ASOA), biogenic sources (BSOA), glyoxal (GLSOA), and
799 semi-volatile organic aerosol (SVSOA) over Australia, Europe, North America, South
800 Africa, South America, and East Asia over 2008-2010. The contributions of ASOA to
801 TSOA predicted by MOZART-4x and CB05_GE are about 17-44%, and 10-47%,
802 respectively, with South America the least and East Asia the most. The contributions of
803 BSOA to TSOA predicted by MOZART-4x and CB05_GE are about 31-75%, and

804 26-76%, respectively, with East Asia the least and South America the most. The
805 contribution of GLSOA to TSOA predicted by CB05_GE is about 2-6%. CB05_GE used
806 in this work includes a simple conversion of glyoxal to condensable VOCs, which can be
807 uptaken by preexisting particles to form SOA. However, this conversion is not included
808 in MOZART-4x. Therefore, there is no GLSOA predicted by MOZART-4x despite it
809 predicts higher glyoxal as shown in Figure 3. The contributions of SVSOA to TSOA
810 predicted by MOZART-4x and CB05_GE are about 8-37%, and 8-41%, respectively, with
811 South America the least and South Africa the most. Among four types of SOA, both
812 MOZART-4x and CB05_GE predict BSOA as the main contributor over most regions
813 (e.g., Australia, North America, South Africa, and South America) and ASOA as the main
814 contributor over East Asia, which is mainly due to the much higher anthropogenic
815 emissions over East Asia. Europe is a different example. MOZART-4x predicts BSOA as
816 the top contributor (44%) and ASOA as the second largest contributor (40%), whereas
817 CB05_GE predicts ASOA as the top contributor (45%) and BSOA as the second largest
818 contributor (36%). Both MOZART-4x and CB05_GE predict ASOA as the top
819 contributor (46-59%) for spring, fall, and winter, and BSOA as the top contributor (57%
820 and 47%, respectively) for summer over Europe. Since MOZART-4x predicts higher
821 BSOA than CB05_GE, BSOA is dominant in MOZART-4x on the annual average. The
822 higher BSOA from MOZART-4x than CB05_GE is mainly due to the higher BVOCs
823 emissions in MOZART-4x and higher OH levels in MOZART-4x. The total BVOCs

824 emission in MOZART-4x is about $2.5 \times 10^{-3} \text{ kg m}^{-2} \text{ yr}^{-1}$, which is about $7.2 \times 10^{-5} \text{ kg m}^{-2}$
825 yr^{-1} (or 2.9%) higher than CB05_GE. The higher BVOCs emissions in MOZART-4x are
826 mainly due to the different species mapping for MEGAN emission calculations. The
827 differences of SOA from biogenic alkenes between MOZART-4x and CB05_GE are
828 MYRC and BCARY in MOZART-4x, and OCI, HUM, and TER in CB05_GE (as shown
829 in Table 1). In CAM-chem that uses MOZART, MEGAN calculates all of the individual
830 species and CAM-chem sums them up to map with the MOZART mechanism species.
831 For example, MYRC emissions consist of myrcene and ocimene, BCARY emissions
832 consist of beta-caryophyllene, alpha-bergamotene, beta-bisabolene, beta-farnescene, and
833 alpha-humulene, and LIMON emissions consist of limonene, phellandrene, and terpinene.
834 Therefore, the biogenic emissions for more types of VOCs in MOZART-4x are higher
835 than those in CB05_GE, resulting in higher BSOA in MOZART-4x. The differences in
836 SOA from aromatics between MOZART-4x and CB05_GE are BENZENE in
837 MOZART-4x and PAH in CB05_GE (as shown in Table 1). The emissions of PAH are
838 higher over Europe, East Asia, eastern U.S., and South Africa. The benzene emissions are
839 about 1 order of magnitude higher than the emissions of PAH, and the rate constant of the
840 oxidation of benzene by OH is temperature dependent whereas it is constant for oxidation
841 of PAH by OH. In addition, OH levels are higher in MOZART-4x than those in
842 CB05_GE. These differences could result in different ASOA between two simulations.
843 Both MOZART-4x and CB05_GE predict higher SVSOA contributions over South Africa

844 than other regions, which is mainly due to the higher POA emissions (e.g., biomass
845 burning) over this region.

846 Although the percentage contributions of different types of SOA predicted by
847 MOZART-4x and CB05_GE are similar over most regions, the absolute mass
848 concentrations of different types of SOA are different. For example, TSOA predicted by
849 MOZART-4x is about 0.02-2.0 mg m⁻² higher than by CB05_GE over these regions.
850 ASOA predicted by MOZART-4x is about 0.068-1.017 mg m⁻² higher than predicted by
851 CB05_GE over most regions except Europe (0.054 mg m⁻² lower) and East Asia (0.062
852 mg m⁻² lower). BSOA predicted by MOZART-4x is about 0.162-1.365 mg m⁻² higher
853 than predicted by CB05_GE over most regions except Australia (0.003 mg m⁻² lower).
854 MOZART-4x includes SOA formation from benzene, which can predict higher ASOA
855 formation. In addition, OH predicted by MOZART-4x is higher than CB05_GE (See
856 Figure 6a8a), which can produce more condensable SOA gaseous precursors through
857 oxidations of VOCs. The higher BVOCs emissions in MOZART-4x due to different
858 mapping for MEGAN species can also contribute to the higher BSOA formation in
859 MOZART-4x.

860 Both MOZART-4x and CB05_GE predict POA burdens of 0.36 Tg, which is
861 about 0.1 Tg lower than those by Shrivastava et al. (2015), indicating that POA may be
862 too volatile with the current implementation of VBS SOA in CESM/CAM5 and possible
863 lower POA emissions used in this work. MOZART-4x predicts SOA burden of 1.82 Tg.

864 which is slightly higher (by 0.05 Tg) than that predicted by Shrivastava et al. (2015). This
865 can be attributed to different emissions used in CESM/CAM5 and Shrivastava et al.
866 (2015), as well as differences in the model treatment for SOA formation in both work.
867 For example, nine volatility bins are used in this work to represent the aging and
868 gas-particle partitioning of POA, instead of five volatility bins used in Shrivastava et al.
869 (2015). In addition, compared to the reaction (3) in Shrivastava et al. (2015), ~~we simply~~
870 ~~assume~~ the remaining mass is assumed to be lost to a species with a volatility higher than
871 the volatility values in the VBS structure, instead of ~~to~~ being oxidized to form CO/CO₂.

872

873 **6. Conclusions**

874 In this work, MOZART-4x and CB05_GE are coupled with CAM5-NCSU.
875 MOZART-4x uses lumped species approach to represent organic chemistry whereas
876 CB05_GE uses lumped structure approach. MOZART-4x and CB05_GE include different
877 surrogates for SOA precursors, which can result in different SOA predictions.
878 MOZART-4x includes HO_x recycling associated with improved isoprene chemistry
879 whereas CB05_GE contains simpler isoprene chemistry, which can result in different OH
880 and isoprene predictions and thus, SOA predictions. CB05_GE includes additional
881 oxidation of SO₂ by O₃ over the surface of dust particles to produce additional SO₄²⁻,
882 which is not included in MOZART-4x. These differences can result in different secondary
883 gas and aerosols predictions.

884 The comparisons between the two gas-phase mechanisms are conducted in terms
885 of chemical and cloud/radiative predictions. Predictions of major gases and inorganic
886 aerosols predicted by MOZART-4x and CB05_GE are overall similar. Significant
887 differences in some species (e.g., NO_y, glyoxal, and SOA) predictions are mainly due to
888 the different reaction pathways treated in the two mechanisms. Large biases exist for
889 surface SO₂, CO, NH₃, [PM_{2.5} and PM₁₀](#) predictions against available observations, which
890 is likely due to the uncertainties in the emissions or emission injection heights. Several
891 studies indicate that the uncertainties in regional emissions (e.g., BC and SO₂) can be
892 expected to be as large as a factor of 2 or larger (Bond et al., 2007; Smith et al., 2011).
893 Large discrepancies still remain for major species such as SO₂, NO_x, BC, and CO among
894 different inventories (Granier et al., 2011). [Both surface CO mixing ratios and column](#)
895 [CO mass abundances are underpredicted, which is mainly due to underestimations in the](#)
896 [CO emissions from biomass burning and possible uncertainties in the OH production.](#)
897 [Surface SO₂ mixing ratio is overpredicted whereas column SO₂ abundance is](#)
898 [underpredicted, indicating the uncertainties in the vertical mixing scheme or emission](#)
899 [injection heights as reported in East Asia \(Zhang et al., 2015a, b\), as well as satellite](#)
900 [retrievals. For example, Lee et al. \(2009\) found that there is an overall error in the annual](#)
901 [SO₂ retrievals of 45-80% over polluted regions, especially over eastern China.](#)
902 [Uncertainties in online dust and sea-salt emissions can also result in inaccurate](#)
903 [predictions in PM_{2.5} and PM₁₀.](#) Both MOZART-4x and CB05_GE overpredict surface O₃

904 over CONUS, Europe, and East Asia, which is due in part to less O₃ titration resulted
905 from underpredictions of NO_x, [the dilution of NO_x emissions resulted from](#) the use of a
906 coarse grid resolution, as well as [uncertainties in the O₃ dry deposition simulated in the](#)
907 [model](#).

908 The concentration of OC over CONUS is well predicted by MOZART-4x, with an
909 NMB of 2.1%, whereas it is moderately underpredicted by CB05_GE, with an NMB of
910 -20.7%. Compared to the observations at the four sites in the U.S. from Lewandowski et
911 al. (2013), SOA is well predicted by MOZART-4x, with an NMB of -1.9%, whereas it is
912 moderately underpredicted by CB05_GE, with an NMB of -23.1%, indicating a better
913 capability to predict SOA over these sites by MOZART-4x despite its tendency to
914 overpredict SOA concentrations at sites with low SOA levels such as Bakersfield and
915 Pasadena, CA. However, the concentrations of OC over Europe [are](#) largely
916 underpredicted by both MOZART-4x and CB05_GE, with NMBs of -74.2% and -75.1%,
917 respectively, indicating the uncertainties in the emissions, chemical reactions, as well as
918 SOA formation treatment. The different AOD predictions between CB05_GE and
919 MOZART-4x are mainly due to ~~the~~ different predictions in SOA, SO₄²⁻, NH₄⁺, NO₃⁻, and
920 dust concentrations.

921 The cloud/radiative predictions from the two simulations are also similar, with
922 slightly better domain average performance of CCN5, LWP, and LWCF in CB05_GE.
923 But MOZART-4x predicts slightly better CCN profile over Beijing than CB05_GE

924 compared to aircraft measurements. The different gas-phase mechanisms result in
925 different predictions in aerosols and clouds, and therefore, a domain average difference of
926 0.5 W m^{-2} in simulated SWCF, which can be as large as 13.6 W m^{-2} over subtropical
927 regions.

928 In summary, MOZART-4x and CB05_GE differ in their approaches to represent
929 VOCs and surrogates for SOA precursors. MOZART-4x includes a more detailed
930 representation of isoprene chemistry compared to CB05_GE. Based on the above
931 comparisons of simulations using both mechanisms and evaluation against available
932 measurements in this study, MOZART-4x with the 1.5 D VBS SOA module in
933 CESM-NCSU generally gives a better agreement with observations for surface
934 concentrations of O_3 over Europe, HNO_3 , HCHO , ISOP over CONUS, SOA, SO_4^{2-} , NO_3^- ,
935 and NH_4^+ over CONUS and Europe, and column mass abundances of HCHO , $\text{C}_2\text{H}_2\text{O}_2$,
936 SO_2 , and O_3 , whereas CB05_GE generally gives a better agreement for surface
937 concentrations of SO_2 , NH_3 , O_3 over CONUS and East Asia, HNO_3 over Europe, $\text{PM}_{2.5}$
938 and PM_{10} over Europe, PM_{10} over East Asia, vertical profiles of NO_y , and column mass
939 abundances of CO . Both simulations give predictions of cloud/radiative variables with
940 slightly better domain average performance of CCN5, LWP, and LWCF in CB05_GE.

941 **7. Code and Data Availability**

942 [The presented results in our this paper are based on output from simulations](#)
943 [performed with the NCAR Community Earth System Model \(CESM\) version 1.2.2](#)

944 <https://www2.cesm.ucar.edu/models/current>) with additional model development and
945 modifications by ~~our group~~ the Air Quality Forecasting Laboratory, North Carolina State
946 University, Raleigh, NC, U.S.A. ~~Our~~ The added codes have been provided to NCAR for
947 potential future release to NCAR for community use. Upon request, we can provide the
948 inputs, the namelist file, a brief instruction, and sample output for a 1-day test case.

949

950 **Acknowledgments**

951 This work is sponsored by the U.S. National Science Foundation EaSM program
952 AGS-1049200 and NCAR Advanced Study Program. MODIS data and CERES data are
953 provided by NASA via <http://ladsweb.nascom.nasa.gov/data/search.html> and
954 http://ceres.larc.nasa.gov/order_data.php, respectively. CDNC data are provided by Ralf
955 Bennartz. Other surface network data were downloaded from their respective web sites.
956 ARCPAC and CalNex data are from NOAA, STRAT08 data are from NCAR, ARCTAS
957 data are from NASA, CCN_China are from Zhang et al. (2011), and SOA data of
958 Lewandowski et al. (2013) are provided by Tadeusz Kleindienst, U.S. EPA. We would like
959 to acknowledge high-performance computing support from Yellowstone
960 (<ark:/85065/d7wd3xhc>) provided by NCAR's Computational and Information Systems
961 Laboratory, sponsored by the U.S. National Science Foundation. The National Center for
962 Atmospheric Research is operated by the University Corporation for Atmospheric
963 Research with funding from the National Science Foundation.

964

965 **References**

- 966 Aghedo, A. M., Bowman, K. W., Worden, H. M., Kulawik, S. S., Shindell, D. T.,
967 Lamarque, J.-F., Faluvegi, G., Parrington, M., Jones, D. B. A., and Rast, S.: The
968 vertical distribution of ozone instantaneous radiative forcing from satellite and
969 chemistry climate models, *J. Geophys. Res.*, 116, D01305,
970 doi:10.1029/2010JD014243, 2011.
- 971 Barahona, D., West, R. E. L., Stier, P., Romakkaniemi, S., Kokkola, H., and Nenes, A.:
972 Comprehensively accounting for the effect of giant CCN in cloud activation
973 parameterizations, *Atmos. Chem. Phys.*, 10(5), 2467-2473,
974 doi:10.5194/acp-10-2467-2010, 2010.
- 975 Bennartz, R.: Global assessment of marine boundary layer cloud droplet number
976 concentration from satellite, *J. Geophys. Res.*, 112, D02201, doi:
977 10.1029/2006JD007547, 2007.
- 978 [Boersma, K. F., Eskes, H. J., and Brinksma E. J.: Error analysis for tropospheric NO₂](#)
979 [retrieval from space, *J. Geophys. Res.*, 109, D04311, doi:10.1029/2003JD003962,](#)
980 [2004.](#)
- 981 Bond, T. C., Bhardwaj, E., Dong, R., Jogani, R., Jung, S., Roden, C., Streets, D. G., and
982 Trautmann, N. M.: Historical emissions of black and organic carbon aerosol from
983 energy-related combustion, 1850-2000, *Global Biogeochem. Cy.*, 21, GB2018,
984 doi:10.1029/2006GB002840, 2007.
- 985 Brock, C. A., Cozic, J., Bahreini, R., Froyd, K. D., Middlebrook, A. M., McComiskey, A.,
986 Brioude, J., Cooper, O. R., Stohl, A., Aikin, K. C., de Gouw, J. A., Fahey, D. W.,
987 Ferrare, R. A., Gao, R.-S., Gore, W., Holloway, J. S., Hübler, G., Jefferson, A., Lack,
988 D. A., Lance, S., Moore, R. H., Murphy, D. M., Nenes, A., Novelli, P. C., Nowak, J.
989 B., Ogren, J. A., Peischl, J., Pierce, R. B., Pilewskie, P., Quinn, P. K., Ryerson, T. B.,
990 Schmidt, K. S., Schwarz, J. P., Sodemann, H., Spackman, J. R., Stark, H., Thomson,
991 D. S., Thornberry, T., Veres, P., Watts, L. A., Warneke, C., and Wollny, A. G.:
992 Characteristics, sources, and transport of aerosols measured in spring 2008 during the
993 aerosol, radiation, and cloud processes affecting Arctic Climate (ARCPAC) Project,
994 *Atmos. Chem. Phys.*, 11, 2423-2453, doi:10.5194/acp-11-2423-2011, 2011.
- 995 Cappa, C. D. and Jimenez, J. L.: Quantitative estimates of the volatility of ambient
996 organic aerosol, *Atmos. Chem. Phys.*, 10, 5409-5424, doi:10.5194/acp-10-5409-2010,
997 2010.

- 998 Chan, A. W. H., Kautzman, K. E., Chhabra, P. S., Surratt, J. D., Chan, M. N., Crouse, J.
999 D., Kürten, A., Wennberg, P. O., Flagan, R. C., and Seinfeld, J. H.: Secondary
1000 organic aerosol formation from photooxidation of naphthalene and alkylnaphthalens:
1001 implications for oxidation of intermediate volatility organic compounds (IVOCs),
1002 *Atmos. Chem. Phys.*, 9, 3049-3060, 2009.
- 1003 Couvidat, F., Kim, Y., Sartelet, K., Seigneur, C., Marchand, N., and Sciare, J.: Modeling
1004 secondary organic aerosol in an urban area: application to Paris, France, *Atmos.*
1005 *Chem. Phys.*, 13, 983-996, 2013.
- 1006 Emmons, L. K., Walters, S., Hess, P. G., Lamarque, J.-F., Pfister, G. G., Fillmore, D.,
1007 Granier, C., Guenther, A., Kinnison, D., Laepple, T., Orlando, J., Tie, X., Tyndall, G.,
1008 Wiedinmyer, C., Baughcum, S. L., and Kloster, S.: Description and evaluation of the
1009 Model for Ozone and Related chemical Tracers, version 4 (MOZART-4), *Geosci.*
1010 *Model Dev.*, 3, 43-67, doi:10.5194/gmd-3-43-2010, 2010.
- 1011 Fountoukis, C. and Nenes, A.: Continued Development of a Cloud Droplet Formation
1012 Parameterization for Global Climate Models, *J. Geoph. Res.*, 110, D11212,
1013 doi:10.1029/2004JD005591, 2005.
- 1014 Fountoukis, C and Nenes, A.: ISORROPIA II: a computationally efficient
1015 thermodynamic equilibrium model for K^+ - Ca^{2+} - Mg^{2+} - NH_4^+
1016 $-Na^+$ - SO_4^{2-} - NO_3^- - Cl^- - H_2O aerosols, *Atmos. Chem. Phys.*, 7, 4639-4659,
1017 doi:10.5194/acp-7-4639-2007, 2007.
- 1018 Gantt, B., He, J., Zhang, X., Zhang, Y., and Nenes, A.: Incorporation of advanced aerosol
1019 activation treatments into CESM/CAM5: model evaluation and impacts on aerosol
1020 indirect effects, *Atmos. Chem. Phys.*, 14, 7485-7497, doi:10.5194/acp-14-7485-2014.
- 1021 Gery, M. W., Whitten, G. Z., Killus, J. P., and Dodge, M. C.: A photochemical kinetics
1022 mechanism for urban and regional scale computer modeling, *J. Geophys. Res.*,
1023 94(D10), 12,925-12,956, doi:10.1029/JD094iD10p12925, 1989.
- 1024 Glotfelty, T., He, J., and Zhang, Y.: Updated organic aerosol treatments in CESM/CAM5:
1025 development and initial application, in preparation, 2015.
- 1026 Granier, C., Bessagnet, B., Bond, T., D'Angiola, A., Denier van der Gon, H., Frost, G. J.,
1027 Heil, A., Kaiser, J. W., Kinne, S., Klimont, Z., Kloster, S., Lamarque, J.-F., Liousse,
1028 C., Masui, T., Meleux, F., Mieville, A., Ohara, T., Raut, J.-C., Riahi, K., Schultz, M.
1029 G., Smith, S. J., Thompson, A., van Aardenne, J., van der Werf, G. R., and van
1030 Vuuren, D. P.: Evolution of anthropogenic and biomass burning emissions of air

1031 pollutants at global and regional scales during the 1980-2010 period, *Climatic*
1032 *Change*, 109, 163-190, doi:10.1007/s10584-011-0154-1, 2011.

1033 Guenther, A. B., Jiang, X., Heald, C. L., Sakulyanontvittaya, T., Duhl, T., Emmons, L. K.,
1034 and Wang, X.: The Model of Emissions of Gases and Aerosols from Nature version
1035 2.1 (MEGAN2.1): an extended and updated framework for modeling biogenic
1036 emissions, *Geosci. Model Dev.*, 5, 1471-1492, doi:10.5194/gmd-5-1471-2012, 2012.

1037 He, J. and Zhang, Y.: Improvement and further development in CESM/CAM5: gas-phase
1038 chemistry and inorganic aerosol treatments, *Atmos. Chem. Phys.*, 14, 9171-9200,
1039 doi:10.5194/acp-14-9171-2014, 2014.

1040 He, J., Zhang, Y., Glotfelty, T., He, R., Bennartz, R., Rausch, J., and Sartelet, K.: Decadal
1041 simulation and comprehensive evaluation of CESM/CAM5.1 and advanced
1042 chemistry, aerosol microphysics, and aerosol-cloud interactions, *J. Adv. Model. Earth*
1043 *Syst.*, 7, 110-141, doi: 10.1002/2014MS000360, 2015.

1044 Hodzic, A., Jimenez, J. L., Madronich, S., Canagaratna, M. R., DeCarlo, P. F., Kleinman,
1045 L., and Fast, J.: Modeling organic aerosols in a mega-city: Potential contribution of
1046 semi-volatile and intermediate volatility primary organic compounds to secondary
1047 organic aerosol formation, *Atmos. Chem. Phys.*, 10(12), 5491-5514,
1048 doi:10.5194/acp-10-5491-2010, 2010.

1049 [IPCC: Climate Change 2013: The Physical Science Basis. Contribution of Working](#)
1050 [Group I to the Fifth Assessment Report of the Intergovernmental Panel on Climate](#)
1051 [Change \[Stocker, T.F., D. Qin, G.-K. Plattner, M. Tignor, S.K. Allen, J. Boschung, A.](#)
1052 [Nauels, Y. Xia, V. Bex and P.M. Midgley \(eds.\)\]. Cambridge University Press,](#)
1053 [Cambridge, United Kingdom and New York, NY, USA, 1535 pp.](#)
1054 [doi:10.1017/CBO9781107415324, 2013.](#)

1055 Jacob, D. J., Crawford, J. H., Maring, H., Clarke, A. D., Dibb, J. E., Emmons, L. K.,
1056 Ferrare, R. A., Hostetler, C. A., Russell, P. B., Singh, H. B., Thompson, A. M., Shaw,
1057 G. E., McCauley, E., Pederson, J. R., and Fisher, J. A.: The Arctic Research of the
1058 Composition of the Troposphere from Aircraft and Satellites (ARCTAS) mission:
1059 design, execution, and first results, *Atmos. Chem. Phys.*, 10, 5191-5212,
1060 doi:10.5194/acp-10-5191-2010, 2010.

1061 Jacob, D. J. and Winner, D. A.: Effect of climate change on air quality, *Atmos. Environ.*,
1062 43, 51-63, 2009.

1063 Jathar, S. H., Farina, S. C., Robinson, A. L., and Adams, P. J.: The influence of
1064 semi-volatile and reactive primary emissions on the abundance and properties of

1065 global organic aerosol, *Atmos. Chem. Phys.*, 11, 7727-7746,
1066 doi:10.5194/acp-11-7727-2011, 2011.

1067 Jimenez, J. L., Canagaratna, M. R., Donahue, N. M., Prevot, A. S. H., Zhang, Q., Kroll, J.
1068 H., DeCarlo, P. F., Allan, J. D., Coe, H., Ng, N. L., Aiken, A. C., Docherty, K. S.,
1069 Ulbrich, I. M., Grieshop, A. P., Robinson, A. L., Duplissy, J., Smith, J. D., Wilson, K.
1070 R., Lanz, V. A., Hueglin, C., Sunn, Y. L., Tian, J., Laaksonen, A., Raatikainen, T.,
1071 Rautiainen, J., Vaattovaara, P., Ehn, M., Kulmala, M., Tomlinson, J. M., Collins, D.
1072 R., Cubison, M. J., Dunlea, E., J., Huffman, J. A., Onasch, T. B., Alfarra, M. R.,
1073 Williams, P. I., Bower, K., Kondo, Y., Schneider, J., Drewnick, F., Borrmann, S.,
1074 Weimer, S., Demerjian, K., Salcedo, D., Cottrell, L., Griffin, R., Takami, A., Miyoshi,
1075 T., Hatakeyama, S., Shimono, A., Sun, J. Y., Zhang, Y. M., Dzepina, K., Kimmel, J.
1076 R., Sueper, D., Jayne, J. T., Herndon, S. C., Trimborn, A. M., Williams, L. R., Wood,
1077 E. C., Middlebrook, A. M., Kolb, C. E., Baltensperger, U., Worsnop, D. R.: Evolution
1078 of organic aerosols in the atmosphere, *Science*, 326, 1525-1529,
1079 doi:10.1126/science.1180353, 2009.

1080 Karamchandani, P., Zhang, Y., Chen, S.-Y., and Balmori-Bronson, R.: Development of an
1081 extended chemical mechanism for global-through-urban applications, *Atmospheric
1082 Pollution Research*, 3, 1-24, 2012.

1083 Kay, J. E., Hillman, B. R., Klein, S. A., Zhang, Y., Medeiros, B., Pincus, R., Gettelman,
1084 A., Eaton, B., Boyle, J., Marchand, R., and Ackerman, T. P.: Exposing global cloud
1085 biases in the Community Atmosphere Model (CAM) using satellite observations and
1086 their corresponding instrument simulators, *J. Climate*, 25, 5190-5207,
1087 doi:10.1175/JCLI-D-11-00469.1, 2012.

1088 Kim Y., Sartelet, K., and Seigneur C.: Comparison of two gas-phase chemical kinetic
1089 mechanisms of ozone formation over Europe, *J. Atmo. Chem.*, 62, 89-119,
1090 DOI10.1007/s10874-009-9142-5, 2009.

1091 Kim, Y., Sartelet, K., and Seigneur, C.: Formation of secondary aerosols: impact of the
1092 gas-phase chemical mechanism, *Atmos. Chem. Phys.* 11, 583-598,
1093 doi:10.5194/acp-11-583-2011, 2011a.

1094 Kim, Y., Couvidat, F., Sartelet, K., and Seigneur, C.: Comparison of Different Gas-Phase
1095 Mechanisms and Aerosol Modules for Simulating Particulate Matter Formation, *J. of
1096 Air & Waste Management Association*, 61, 1218-1226,
1097 doi:10.1080/10473289.2011.603999, 2011b.

1098 Kinnison, D. E., Brasseur, G. P., Walters, S., Garcia, R. R., Marsh, D. A., Sassi, F.,
1099 Boville, B. A., Harvey, L., Randall, C., Emmons, L., Lamarque, J.-F., Hess, P.,

- 1100 Orlando, J., Tyndall, G., Tie, X. X., Randel, W., Pan, L., Gettelman, A., Granier, C.,
1101 Diehl, T., Niemeier, U., and Simmons, A. J.: Sensitivity of chemical tracers to
1102 meteorological parameters in the MOZART-3 chemical transport model, *J. Geophys.*
1103 *Res.*, 112, D20302, doi:10.1029/2006JD007879, 2007.
- 1104 Knote, C., Tuccella, P., Curci, G., Emmons, L., Orlando, J. J., Madronich, S., Baró, R.,
1105 Jiménez-Guerrero, P., Luecken, D., Hogrefe, C., Forkel, R., Werhahn, J., Hirtl, M.,
1106 Pérez, J. L., San José, R., Giordano, L., Brunner, D., Khairunnisa, Y., and Zhang, Y.:
1107 Influence of the choice of gas-phase mechanism on predictions of key gaseous
1108 pollutants during the AQMEII phase-2 intercomparison, *Atmos. Environ.*,
1109 <http://dx.doi.org/10.1016/j.atmosenv.2014.11.066>, 2014a.
- 1110 Knote, C., Hodzic, A., Jimenez, J. L., Volkamer, R., Orlando, J. J., Baidar, S., Brioude, J.,
1111 Fast, J. Gentner, D. R., Goldstein, A. H., Hayes, P. L., Knighton, W. B., Oetjen, H.,
1112 Setyan, A., Stark, H., Thalman, R., Tyndall, G., Washenfelder, R., Waxman, E., and
1113 Zhang, Q.: Simulation of semi-explicit mechanisms of SOA formation from glyoxal
1114 in aerosol in a 3-D model, *Atmos. Chem. Phys.*, 14, 6213-6239,
1115 doi:10.5194/acp-14-6213-2014, 2014b.
- 1116 Kumar, P., Sokolik, I. N., and Nenes, A.: Parameterization of cloud droplet formation for
1117 global and regional models: including adsorption activation from insoluble CCN,
1118 *Atmos. Chem. Phys.*, 9, 2517-2532, doi:10.5194/acp-9-2517-2009, 2009.
- 1119 Lamarque, J.-F., Bond, T. C., Eyring, V., Granier, C., Heil, A., Klimont, Z., Lee, D.,
1120 Liousse, C., Mieville, A., Owen, B., Schultz, M. G., Shindell, D., Smith, S. J.,
1121 Stehfest, E., Van Aardenne, J., Cooper, O. R., Kainuma, M., Mahowald, N., Mc-
1122 Connell, J. R., Naik, V., Riahi, K., and van Vuuren, D. P.: Historical (1850-2000)
1123 gridded anthropogenic and biomass burning emissions of reactive gases and aerosols:
1124 methodology and application, *Atmos. Chem. Phys.*, 10, 7017-7039, doi:10.5194/acp-
1125 10-7017-2010, 2010.
- 1126 Lamarque, J. F., Emmons, L. K., Hess, P. G., Kinnison, D. E., Tilmes, S., Vitt, F., Heald,
1127 C. L., Holland, E. A., Lauritzen, P. H., Neu, J., Orlando, J. J., Rasch, P. J., and
1128 Tyndall, G. K.:CAM-chem: description and evaluation of interactive atmospheric
1129 chemistry in CESM, *Geosci. Model Dev.*, 5, 369-411, doi:10.5194/gmd-5-369-2012,
1130 2012.
- 1131 Lamarque, J.-F., McConnell, J. R., Shindell, D. T., Orlando, J. J., and Tyndall, G. S.:
1132 Understanding the drivers for the 20th century change of hydrogen peroxide in
1133 Antarctic ice-cores, *Geophys. Res. Lett.*, 38, L04810, doi:10.1029/2010GL045992,
1134 2011a.

- 1135 Lamarque, J.-F., Kyle, G. P., Meinshausen, M., Riahi, K., Smith, S. J., van Vuuren, D. P.,
1136 Conley, A., and Vitt, F.: Global and regional evolution of short-lived
1137 radiatively-active gases and aerosols in the Representative Concentration Pathways,
1138 *Climatic Change*, 109, 191-212, 2011b.
- 1139 Lamarque, J.-F., Kinnison, D. E., Hess, P. G., and Vitt, F.: Simulated lower stratospheric
1140 trends between 1970 and 2005: identifying the role of climate and composition
1141 changes, *J. Geophys. Res.*, 113, D12301, doi:10.1029/2007JD009277, 2008.
- 1142 Lamarque, J. F., Shinedell, D. T., Josse, B., Young, P. J., Cionni, I., Eyring, V.,
1143 Bergmann, D., Cameron-Smith, P., Collins, W. J., Doherty, R., Dalsoren, S.,
1144 Faluvegi, G., Folberth, G., Ghan, S. J., Hiriwutz, L. W., Lee, Y. H., MacKenzie, I. A.,
1145 Nagashima, T., Naik, V., Plummer, D., Righi, M., Rumbold, S. T., Schulz, M., Skeie,
1146 R. B., Stevenson, D. S., Strode, S., Sudo, K., Szopa, S., Voulgarakis, A., and Zeng,
1147 G.: The atmospheric chemistry and climate model intercomparison project: overview
1148 and description of models, simulations and climate diagnostics, *Geosci. Model Dev.*,
1149 6, 179-206, doi:10.5194/gmd-6-179-2013, 2013.
- 1150 Lamarque, J.-F. and Solomon, S.: Impact of Changes in Climate and Halocarbons on
1151 Recent Lower Stratosphere Ozone and Temperature Trends, *J. Climate*, 23,
1152 2599-2611, 2010.
- 1153 [Lee, C., Martin, R. V., Donkelaar, A. van, O'Byrne, G., Krotkov, N., Richter, A., Huey, L.](#)
1154 [G., and Holloway, J. S.: Retrieval of vertical columns of sulfur dioxide from](#)
1155 [SCIAMACHY and OMI: Air mass factor algorithm development, validation, and](#)
1156 [error analysis, *J. Geophys. Res.*, 114, D22303, doi:10.1029/2009JD012123, 2009.](#)
- 1157 Levy, R. C., Mattoo, S., Munchak, L. A., Remer, L. A., Sayer, A. M., Patadia, F., and Hsu,
1158 N. C.: The Collection 6 MODIS aerosol products over land and ocean, *Atmos. Meas.*
1159 *Tech.*, 6, 2989–3034, doi:10.5194/amt-6-2989-2013, 2013.
- 1160 Lewandowski, M., Piletic, I. R., Kleindienst, T. E., Offenber, J. H., Beaver, M. R., Jaoui,
1161 M., Docherty, K. S., and Edney, E. O.: Secondary organic aerosol characterization at
1162 field sites across the United States during the spring-summer period, *Int. J. Environ.*
1163 *An. Ch.*, 93, 1084-1103, 2013.
- 1164 Liu, X., Easter, R. C., Ghan, S. J., Zaveri, R., Rasch, P., Shi, X., Lamarque, J.-F.,
1165 Gettleman, A., Morrison, H., Vitt, F., Conley, A., Park, S., Neale, R., Hannay, C.,
1166 Ekman, A. M. L., Hess, P., Mahowald, N., Collins, W., Iacono, M.J., Bretherton, C.
1167 S., Flanner, M. G., and Mitchell, D.L.: Toward a minimal representation of aerosols
1168 in climate models: description and evaluation in the Community Atmosphere Model
1169 CAM5, *Geosci. Model Dev.*, 5, 709-739, 2012.

- 1170 [Liu, X., Zhang, Y., Cheng, S.-H., Xing, J., Zhang, Q., Streets, D. G., Jang, C., Wang,](#)
1171 [W.-X., and Hao, J.-M.: Understanding of regional air pollution over China using](#)
1172 [CMAQ, partI: performance evaluation and seasonal variation, Atmos. Environ., 44](#)
1173 [\(2010\), pp. 2415-2426, <http://dx.doi.org/10.1016/j.atmosenv.2010.03.035>.](#)
- 1174 Luecken, D. J., Phillips, S., Sarwar, G., and Jang, C.: Effects of using the CB05 vs.
1175 SAPRC99 vs. CB4 chemical mechanism on model predictions: Ozone and gas-phase
1176 photochemical precursor concentrations, Atmos. Environ., 42, 5805-5820,
1177 doi:10.1016/j.atmosenv.2007.08.056, 2008.
- 1178 Ma, P.-L., Rasch, P. J., Wang, H., Zhang, K., Easter, R. C., Tilmes, S., Fast, J. D., Liu, X.,
1179 Yoon, J.-H., and Lamarque, J.-F.: The role of circulation features on black carbon
1180 transport into the Arctic in the Community Atmosphere Model version 5 (CAM5), J.
1181 Geophys. Res. Atmos., 118, 4657-4669, doi:10.1002/jgrd.50411, 2013.
- 1182 Martensson, E. M., Nilsson, E. D., deLeeuw, G., Cohen, L. H., and Hansson, H. C.:
1183 Laboratory simulations and parameterization of the primary marine aerosol
1184 production, J. Geophys. Res., 108(D9), 4297, doi:10.1029/2002JD002263, 2003.
- 1185 [Martin, M. V., Heald, C. L., and Arnold, S. R.: Coupling dry deposition to vegetation](#)
1186 [phenology in the Community Earth System Model: Implications for the simulation of](#)
1187 [surface O₃, Geophys. Res. Lett., 41, 2988-2996, doi:10.1002/2014GL059651, 2014.](#)
- 1188 May, A. A., Presto, A. A., Hennigan, C. J., Nguyen, N. T., Gordon, T. D., and Robinson,
1189 A. I.: Gas-particle partitioning of primary organic aerosol emissions: (1), gasoline
1190 vehicle exhaust, Atmos. Environ., 77, 128-139, doi:10.1016/j.atmosenv.2013.04.060,
1191 2013a.
- 1192 May, A. A., Levin, E. J. T., Hennigan, C. J., Riipinen, I., Lee, T., Collett Jr., J. L., Jimenez,
1193 J. L., Kreidenweis, S. M., and Robinson, A. L.: Gas-particle partitioning of primary
1194 organic aerosol emissions: 3. Biomass burning, J. Geophys. Res. Atmos., 118,
1195 11,327-11,338, doi:10.1002/jgrd.50828, 2013b.
- 1196 [Meinshausen, M., Smith, S. J., Calvin, K., Daniel, J. S., Kainuma, M. L. T., Lamarque,](#)
1197 [J.-F., Matsumoto, K., Montzka, S., Raper, S., Riahi, K., Thomson, A., Velders, G. J.](#)
1198 [M., and van Vuuren, D. P.: The RCP Greenhouse gas concentrations and their](#)
1199 [extensions from 1765 to 2300, Climatic Change, 109, 213-241, 2011.](#)
- 1200 Merikanto, J., Napari, I., Vehkamäki, H., Anttila, T., and Kulmala, M.: New
1201 parameterization of sulfuric acid-ammonia-water ternary nucleation rates at
1202 tropospheric conditions, J. Geophys. Res., 112, D15207, doi: 10.1029/2006JD007977,
1203 2007.

1204 [Naik, V., Voulgarakis, A., Fiore, A. M., Horowitz, L. W., Lamarque, J.-F., Lin, M.,](#)
1205 [Prather, M. J., Young, P. J., Bergmann, D., Cameron-Smith, P. J., Cionni, I., Collins,](#)
1206 [W. J., Dalsøren, S. B., Doherty, R., Eyring, V., Faluvegi, G., Folberth, G. A., Josse,](#)
1207 [B., Lee, Y. H., MacKenzie, I. A., Nagashima, T., van Noije, T. P. C., Plummer, D. A.,](#)
1208 [Righi, M., Rumbold, S. T., Skeie, R., Shindell, D. T., Stevenson, D. S., Strode, S.,](#)
1209 [Sudo, K., Szopa, S., and Zeng, G.: Preindustrial to present-day changes in](#)
1210 [tropospheric hydroxyl radical and methane lifetime from the Atmospheric Chemistry](#)
1211 [and Climate Model Intercomparison Project \(ACCMIP\), Atmos. Chem. Phys., 13,](#)
1212 [5277-5298, doi:10.5194/acp-13-5277-2013, 2013.](#)

1213 Pan, L. L., Bowman, K. P., Atlas, E. L., Wofsy, S. C., Zhang, F., Bresch, J. F., Ridley, B.
1214 A., Pittman, J. V., Homeyer, C. R., Romashkin, P., and Cooper, W. A.: The
1215 stratosphere-troposphere analyses of regional transport 2008 (START08) experiment,
1216 Bull. Am. Meteorol. Soc., 91, 327-342, 2010.

1217 Price, C. and Rind, D.: A simple lightning parameterization for calculating global
1218 lightning distributions, J. Geophys. Res., 97, 9919-9933, doi:10.1029/92JD00719,
1219 1992.

1220 Price, C., Penner, J., and Prather, M.: NO_x from lightning 1, Global distribution based on
1221 lightning physics, J. Geophys. Res., 102, 5929-5941, 1997.

1222 Reutter, P., Su, H., Trentmann, J., Simmel, M., Rose, D., Gunthe, S. S., Wernli, H.,
1223 Andreae, M. O., and Pöschl, U.: Aerosol- and updraft-limited regimes of cloud
1224 droplet formation: influence of particle number, size and hygroscopicity on the
1225 activation of cloud condensation nuclei (CCN), Atmos. Chem. Phys., 9, 7067-7080,
1226 doi:10.5194/acp-9-7067-2009, 2009.

1227 Robinson, A. L., Donahue, N. M., Shrivastava, M. K., Weitkamp, E. A., Sage, A. M.,
1228 Grieshop, A. P., Lane, T. E., Pierce, J. R., and Pandis, S. N.: Rethinking organic
1229 aerosols: Semivolatile emissions and photochemical aging, Science, 315, 1259-1262,
1230 doi:10.1126/science.1133061, 2007.

1231 Ryerson, T. B., Andrews, A. E., Angevine, W. M., Bates, T. S., Brock, C. A., Cairns, B.,
1232 Cohen, R. C., Cooper, O. R., de Gouw, J. A., Fehsenfeld, F. C., Ferrare, R. A.,
1233 Fischer, M. L., Flagan, R. C., Goldstein, A. H., Hair, J. W., Hardesty, R. M.,
1234 Hostetler, C. A., Jimenez, J. L., Langford, A. O., McCauley, E., McKeen, S. A.,
1235 Molina, L. T., Nenes, A., Oltmans, S. J., Parrish, D. D., Pederson, J. R., Pierce, R. B.,
1236 Prather, K., Quinn, P. K., Seinfeld, J. H., Senff, C. J., Sorooshian, A., Stutz, J.,
1237 Surratt, J. D., Trainer, M., Volkamer, R., Williams, E. J., and Wofsy, S. C.: The 2010
1238 California Research at the Nexus of Air Quality and Climate Change (CalNex) field
1239 study, J. Geophys. Res., 118, 5830-5866, doi:10.1002/jgrd.50331, 2013.

- 1240 Sarwar, G., Luecken, D., Yarwood, G., Whitten, G., and Carter, W. P. L.: Impact of an
1241 updated carbon bond mechanism on predictions from the Community Multiscale Air
1242 Quality Model, *J. Appl. Meteorol. Climatol.*, 47, 3-14,
1243 doi:10.1175/2007JAMC1393.1, 2008.
- 1244 Seethala, C. and Horvath, Á.: Global assessment of AMSR-E and MODIS cloud liquid
1245 water path retrievals in warm oceanic clouds, *J. Geophys. Res.*, 115, D13202,
1246 doi:10.1029/2009JD012662, 2010.
- 1247 Shrivastava, M. K., Lane, T. E., Donahue, N. M., Pandis, S. N., and Robinson, A. L.:
1248 Effects of gas particle partitioning and aging of primary emissions on urban and
1249 regional organic aerosol concentrations, *J. Geophys. Res.*, 113, D18301,
1250 doi:10.1029/2007JD009735, 2008.
- 1251 [Shrivastava, M., Easter, R., Liu, X., Zelenyuk, A., Singh, B., Zhang, K., Ma, P-L, Chand,](#)
1252 [D., Ghan, S., Jimenez, J.L., Zhang, Q., Fast, J., Rasch, P. and Tiitta, P.: Global](#)
1253 [transformation and fate of SOA: Implications of low volatility SOA and gas-phase](#)
1254 [fragmentation reactions, *J. Geophys. Res. Atmos.*, 120, 4169-4195,](#)
1255 [doi:10.1002/2014JD022563, 2015.](#)
- 1256 Shrivastava, M., Zelenyuk, A., Imre, D., Easter, R., Beranek, J., Zaveri, R. A., and Fast, J.:
1257 Implications of low volatility SOA and gas-phase fragmentation reactions on SOA
1258 loadings and their spatial and temporal evolution in the atmosphere, *J. Geophys. Res.*,
1259 118, 3328-3342, doi:10.1029/jgrd.50160, 2013.
- 1260 Smith S. J., van Aardenne, J., Klimont, Z., Andres, R., Volke, A., Delgado Arias, S.:
1261 Anthropogenic sulfur dioxide emissions: 1850-2005. *Atmos Chem Phys.*, 11,
1262 1101-1116. doi:10.5194/acp-11-1101-2011, 2011.
- 1263 Stainer, C. O., Donahue, N., and Pandis, S. N.: Parameterization of secondary organic
1264 aerosol mass fractions from smog chamber data, *Atmos. Environ.*, 42, 2276-2299,
1265 doi:10.1016/j.atmosenv.2007.12.042, 2008.
- 1266 Taylor, K. E: Summarizing multiple aspects of model performance in a single diagram, *J.*
1267 *Geophys. Res.*, 106, 7183-7192, 2001.
- 1268 Tilmes, S., Lamarque, J.-F., Emmons, L. K., Kinnison, D. E., Ma, P.-L., Liu, X., Ghan, S.,
1269 Bardeen, C., Arnold, S., Deeter, M., Vitt, F., Ryerson, T., Elkins, J. W., Moore, F.,
1270 Spackman, R., and Martin, M. V.: Description and evaluation of tropospheric
1271 chemistry and aerosols in the Community Earth System Model (CESM1.2), *Geosci.*
1272 *Model Dev.*, 8, 1395-1426, doi:10.5194/gmd-8-1395-2015, 2015.

- 1273 Tsimpidi, A. P., Karydis, V. A., Zavala, M., Lei, W., Molina, L., Ulbrich, I. M., Jimenez,
1274 J. L., and Pandis, S. N.: Evaluation of the volatility basis-set approach for the
1275 simulation of organic aerosol formation in the Mexico City metropolitan area, *Atmos.*
1276 *Chem. Phys.*, 10, 525-546, doi:10.5194/acp-10-525-2010, 2010.
- 1277 Vehkamäki, H., Kulmala, M., Napari, I., Lehtinen, K. E. J., Timmreck, C., Noppel, M.,
1278 and Laaksonen, A.: an improved parameterization for sulfuric acid-water nucleation
1279 rates for tropospheric and stratospheric conditions, *Journal of Geophysical*
1280 *Research-Atmospheres*, 107(D22), 4622, doi:10.1029/2002JD002184, 2002.
- 1281 Wang, M. and Penner, J. E.: Aerosol indirect forcing in a global model with particle
1282 nucleation, *Atmos. Chem. Phys.*, 9, 239-260, 2009.
- 1283 Wang, K., Yahya, K., Zhang, Y., Wu, S.-Y., and Grell G.: Implementation and initial
1284 application of a new chemistry-aerosol option in WRF/Chem for simulation of
1285 secondary organic aerosols and aerosol indirect effects, *Atmos. Environ.*, [115](https://doi.org/10.1016/j.atmosenv.2014.12.007),
1286 [doi:10.1016/j.atmosenv.2014.12.007](https://doi.org/10.1016/j.atmosenv.2014.12.007), 2014.
- 1287 Wang, H., Easter, R. C., Rasch, P. J., Wang, M., Liu, X., Ghan, S. J., Qian, Y., Yoon, J.-H.,
1288 Ma, P.-L., and Vиноj, V.: Sensitivity of remote aerosol distributions to representation
1289 of cloud-aerosol interactions in a global climate model, *Geosci. Model Dev.*, 6,
1290 765-782, doi:10.5194/gmd-6-765-2013, 2013.
- 1291 Washenfelder, R., Young, C., Brown, S., Angevine, W., Atlas, E., Blake, D., Bon, D.,
1292 Cubison, M., De Gouw, J., Dusanter, S., Flynn, J., Gilman, J. B., Graus, M., Griffith,
1293 S., Grossberg, N., Hayes, P. L., Jimenez, J., Kuster, W., Lefer, B. L., Pollack, I.,
1294 Ryerson, T., Stark, H., Stevens, P. S., and Trainer, M.: The glyoxal budget and its
1295 contribution to organic aerosol for Los Angeles, California, during CalNex 2010, *J.*
1296 *Geophys. Res.*, 116, D00V02, doi:10.1029/2011JD016314, 2011.
- 1297 Young, P. J., Archibald, A. T., Bowman, K. W., Lamarque, J.-F., Naik, V., Stevenson, D.
1298 S., Tilmes, S., Voulgarakis, A., Wild, O., Bergmann, D., Cameron-Smith, P., Cionni,
1299 I., Collins, W. J., Dalsøren, S. B., Doherty, R. M., Eyring, V., Faluvegi, G., Horowitz,
1300 L. W., Josse, B., Lee, Y. H., MacKenzie, I. A., Nagashima, T., Plummer, D. A., Righi,
1301 M., Rumbold, S. T., Skeie, R. B., Shindell, D. T., Strode, S. A., Sudo, K., Szopa, S.,
1302 and Zeng, G.: Pre-industrial to end 21st century projections of tropospheric ozone
1303 from the Atmospheric Chemistry and Climate Model Intercomparison Project
1304 (ACCMIP), *Atmos. Chem. Phys.*, 13, 2063-2090, doi:10.5194/acp-13-2063-2013,
1305 2013.
- 1306 [Yarwood, G., Kemball-Cook, S., Johnson, J., Wilson, G., Dornblaser, B., and Estes, M:](#)
1307 [Evaluating NOx Emission Inventories for Air Quality Modeling Using Satellite.](#)

1308 [Model and SEARCH NO₂ Data, 11th Annual CMAS Conference, Chapel Hill, NC,](#)
1309 [October 16, 2012.](#)

1310 Yarwood, G., Rao, S., Yocke, M., and Whitten, G. Z.: Updates to the carbon bond
1311 mechanism: CB05, Report to the U.S. Environmental Protection Agency,
1312 RT-04-00675, 2005.

1313 Yu, F.: Ion-mediated nucleation in the atmosphere: Key controlling parameters,
1314 implications, and look-up table, *J. Geophys. Res.*, 115, D03206, doi:
1315 10.1029/2009JD012630, 2010.

1316 [Yu, S.-C., Mathur, R., Sarwar, G., Kang, D., Tong, D., Pouliot, G., and Pleim, J.:](#)
1317 [Eta-CMAQ air quality forecasts for O₃ and related species using three different](#)
1318 [photochemical mechanisms \(CB4, CB05, SAPRC-99\): comparisons with](#)
1319 [measurements during the 2004 ICARTT study, *Atmos. Chem. Phys.*, 10, 3001-3025,](#)
1320 [2010.](#)

1321 [Yu, S.-C., Dennis, R., Roselle, S., Nenes, A., Walker, J., Eder, B., Schere, K., Swall, J.,](#)
1322 [Robarge, W.: An assessment of the ability of 3-D air quality models with current](#)
1323 [thermodynamic equilibrium models to predict aerosol NO₃⁻, *J. Geophys. Res.*, 110,](#)
1324 [D07S13, doi:10.1029/2004JD004718, 2005.](#)

1325 [Yu, S.-C., Eder, B., Dennis, R., Chu, S.-H., Schwartz, S.: New unbiased symmetric](#)
1326 [metrics for evaluation of air quality models, *Atmos. Sci. Lett.*, 7, 26-34, 2006.](#)

1327 Zender, C. S., Bian, H., and Newman, D.: The mineral Dust Entrainment And Deposition
1328 (DEAD) model: Description and 1990s dust climatology, *J. Geophys. Res.*, 108(D14),
1329 4416, doi: 10.1029/2002JD002775, 2003.

1330 Zhang, Q., Jimenez, J. L., Canagaratna, M. R., Allan, J. D., Coe, H., Ulbrich, I., Alfarra,
1331 M. R., Takami, A., Middlebrook, A. M., Sun, Y. L., Dzepina, K., Dunlea, E.,
1332 Docherty, K., DeCarlo, P. F., Salcedo, D., Onasch, T., Jayne, J. T., Miyoshi, T.,
1333 Shimono, A., Hatakeyama, S., Takegawa, N., Kondo, Y., Schneider, J., Drewnick, F.,
1334 Borrmann, S., Weimer, S., Demerjian, K., Williams, P., Bower, K., Bahreini, R.,
1335 Cottrell, L., Griffin, R. J., Rautiainen, J., Sun, J. Y., Zhang, Y. M., and Worsnop, D.
1336 R.: Ubiquity and dominance of oxygenated species in organic aerosols in
1337 anthropogenically-influenced Northern Hemisphere midlatitudes, *Geophys. Res.*
1338 *Lett.*, 34, L13801, doi:10.1029/2007GL029979, 2007.

1339 Zhang, Q., Quan, J., Tie, X., Huang, M., and Ma, X.: Impacts of aerosol particles on
1340 cloud formation: Aircraft measurements in China, *Atmospheric Environment*, 45,
1341 665-672, 2011.

- 1342 [Zhang, Y., Liu, P., Pun, B., and Seigneur, C.: A comprehensive performance evaluation](#)
1343 [of MM5-CMAQ for summer 1999 Southern Oxidants Study episode, Part I.](#)
1344 [Evaluation protocols, databases, and meteorological predictions, Atmos. Environ., 40,](#)
1345 [4825-4838, 2006.](#)
- 1346 Zhang, Y., Pun, B., Vijayaraghavan, K., Wu, S.-Y., Seigneur, C., Pandis, S., Jacobson,
1347 M., Nenes A., and Seinfeld, J. H.: Development and Application of the Model of
1348 Aerosol Dynamics, Reaction, Ionization and Dissolution (MADRID), Journal of
1349 Geophysical Research, 109, D01202, doi:10.1029/2003JD003501, 2004.
- 1350 Zhang, Y., Karamchandani, P., Glotfelty, T., Street, D. G., Grell, G., Nenes, A., Yu, F., and
1351 Bennartz, R.: Development and initial application of the global-through-urban
1352 weather research and forecasting model with chemistry (GU-WRF/Chem), J.
1353 Geophys. Res., 117, D20206, doi:10.1029/2012JD017966, 2012a.
- 1354 Zhang, Y., Chen, Y., Sarwar, G., and Schere, K.: Impacts of gas-phase mechanisms on
1355 weather research forecasting model with chemistry (WRF/Chem) predictions:
1356 Mechanism implementation and comparative evaluation, J. Geophys. Res., 117,
1357 D01301, doi: 10.1029/2011JD015775, 2012b.
- 1358 Zhang, Y., Zhang, X., Wang, L.-T., Zhang, Q., Duan, F.-K., and He, K.-B.: Application of
1359 WRF/Chem over East Asia: Part I. Model Evaluation and Intercomparison with
1360 MM5/CMAQ, Atmospheric Environment, in press,
1361 [doi:10.1016/j.atmosenv.2015.07.022](#), 2015a.
- 1362 Zhang, Y., Zhang, X., Wang, K., Zhang, Q., Duan, F.-K., and He, K.-B.: Application of
1363 WRF/Chem over East Asia: Part II. Model Improvement and Sensitivity Simulations,
1364 Atmospheric Environment, in press, [doi:10.1016/j.atmosenv.2015.07.023](#), 2015b.

Table 1. Gas-phase organic aerosol precursors in the two mechanisms

Precursors	MOZART-4x ¹	CB05_GE ²
Aromatics	TOLUENE, BENZENE , XYLENES, CRESOL	TOL, XYL, CRES, PAH
Alkanes	BIGALK	ALKH
Anthropogenic alkenes	C3H6, BIGENE	OLE, IOLE
Biogenic alkenes	APIN, BPIN, LIMON, MYRC, BCARY, ISOP	APIN, BPIN, LIM, OCI, HUM, TER, ISOP

¹ BIGALK: lumped alkanes C > 3; C₃H₆: propene; BIGENE: lumped alkenes C > 3; APIN: α -pinene + others; BPIN: β -pinene+others; LIMON: limonene + others; MYRC: myrcene + others; BCARY: beta-caryophyllene + other sesquiterpenes; ISOP: isoprene.

² TOL: toluene and other monoalkyl aromatics; XYL: xylene and other polyalkyl aromatics; CRES: cresol and higher molecular weight phenols; PAH: polycyclic aromatic hydrocarbons; ALKH: long-chain alkanes, C >6; OLE: terminal olefin carbon bond (R-C=C); IOLE: internal olefin carbon bond (R-C=C-R); APIN: α -pinene; BPIN: β -pinene; LIM: limonene; OCI: ocimene; HUM: humulene; TER: terpinene; ISOP: isoprene.

Table 2. Datasets for model evaluation

Species/Variables	Dataset (Number of sites)
Cloud fraction (CF)	MODIS
Cloud optical thickness (COT)	
Cloud liquid water path (LWP)	
Precipitating water vapor (PWV)	
Aerosol optical depth (AOD)	
Column cloud condensation nuclei (ocean) at S = 0.5% (CCN5)	
Cloud droplet number concentration (CDNC), LWP	Bennartz (2007)
Shortwave cloud radiative forcing (SWCF)	CERES- EBAF
Longwave cloud radiative forcing (LWCF)	
Downwelling longwave radiation at surface (FLDS)	
Downwelling shortwave radiation at surface (FSDS)	
Outgoing longwave radiation (OLR)	NOAA/CDC
Carbon monoxide (CO)	East Asia: NIESJ (2133), TAQMN (70), KMOE (258)
Ozone (O ₃)	CONUS: CASTNET (141)
	Europe: Airbase (3846), BDQA (490), EMEP (317)
	East Asia: TAQMN (70), KMOE (258)
Sulfur dioxide (SO ₂)	CONUS: CASTNET (141) Europe: Airbase (3846), BDQA (490), EMEP (317) East Asia: MEPC (84), NIESJ (2133), KMOE (258), TAQMN (70)
Nitric acid (HNO ₃)	CONUS: CASTNET (141); Europe: EMEP (317)
Ammonia (NH ₃)	Europe: Airbase (3846), EMEP (317)
Nitrogen dioxide (NO ₂)	CONUS: ARS (25877)
	Europe: Airbase (3846), BDQA (490), EMEP (317) East Asia: NIESJ, TAQMN, KMOE
Sulfate (SO ₄ ²⁻), Ammonium (NH ₄ ⁺), Nitrate (NO ₃ ⁻)	CONUS: CASTNET (141), IMPROVE (199), STN (18129); Europe: Airbase (3846), EMEP (317)
Chloride (Cl ⁻)	CONUS: IMPROVE (199)
	Europe: Airbase (3846), EMEP (317)
Organic carbon (OC)	CONUS: IMPROVE (199); Europe: EMEP (317)
Black carbon (BC), Total carbon (TC)	CONUS: IMPROVE (199), STN(18129)
Formaldehyde (HCHO), Isoprene (ISOP), and Toluene (TOL)	CONUS: AQS (25877)
Hydrocarbon-like organic aerosol (HOA), Oxygenated organic aerosol (OOA), Total organic aerosol (TOA)	Northern Hemisphere: Zhang et al. (2007) and Jimenez et al. (2009) (Z07 & J09) (33)
Secondary organic aerosol (SOA)	CONUS: Ohio (2) and California (2) (Lewandowski et al., 2013)
Particulate matter with diameter less than and equal to 2.5 μm (PM _{2.5})	CONUS: IMPROVE (199), STN (18129)
	Europe: BDQA (490), EMEP (317)
Particulate matter with diameter less than and equal to 10 μm (PM ₁₀)	CONUS: AQS (25877)
	Europe: Airbase (3846), BDQA (490), EMEP (317) East Asia: MEPC (84), NIESJ (2133), KMOE (258), TAQMN (70)
Column CO	Globe: MOPITT
Column NO ₂ , Column SO ₂ , Column HCHO, Column glyoxal (C ₂ H ₂ O ₂)	Globe: SCIAMACHY
Tropospheric ozone residual (TOR)	Globe: OMI/MLS
O ₃ , CO, NO _x , and NO _y profiles	ARCPAC (Mar.-Apr., 2008), ARCTAS (Apr.-Jun., 2008), START08 (Apr.-Jun., 2008), and CalNex (May.-Jun., 2010)
CCN_China	Beijing: Zhang et al. (2011) (Jul.-Sep., 2008)

NOAA/CDC: National Oceanic and Atmospheric Administration Climate Diagnostics Center; MODIS: Moderate Resolution Imaging Spectroradiometer; CERES-[EBAF](#): Clouds and Earth's Radiant Energy System-[Energy Balanced and Filled product](#); MOPITT: the Measurements Of Pollution In The Troposphere; OMI/MLS: the Aura Ozone Monitoring Instrument in combination with Aura Microwave Limb Sounder; SCIAMACHY: the SCanning Imaging Absorption spectroMeter for Atmospheric CHartographY; CASTNET: Clean Air Status and Trends Network; IMPROVE: Interagency Monitoring of Protected Visual Environments; STN: Speciation Trends Network; AQS: Air Quality System; EMEP: European Monitoring and Evaluation Program; BDQA: Base de Données sur la Qualité de l'Air; AirBase: European air quality database; MEPC: Ministry of Environmental Protection of China; TAQMN: Taiwan Air Quality Monitoring Network; NIESJ: National Institute for Environmental Studies of Japan; KMOE: Korean Ministry of Environment; ARCPAC: Aerosol, Radiation, and Cloud Processes affecting Arctic Climate in 2008 (Brock et al., 2011); ARCTAS: Arctic Research of the Composition of the Troposphere from Aircraft and Satellites (Jacob et al., 2010), START08: Stratosphere-Troposphere Analyses of Regional Transport in 2008 (Pan et al., 2010); CalNex: California Nexus 2010 (Ryerson et al., 2013)..

Table 3. Performance statistics of chemical species

Species	Domain	Obs	MOZART-4x			CB05_GE		
			Sim	NMB (%) ⁶	NME (%) ⁶	Sim	NMB (%) ⁶	NME (%) ⁶
CO (ppb)	East Asia	438.7	150.9	-65.6	65.7	150.4	-65.7	65.8
SO ₂ ¹	CONUS	1.7	11.6	580.2	580.2	11.2	561.6	561.6
	Europe	4.7	9.5	100.9	121.2	9.2	94.1	115.4
	East Asia	2.9	4.3	47.0	70.6	3.9	35.5	64.0
NH ₃ (μg m ⁻³)	Europe	1.2	2.5	112.4	146.0	2.4	104.3	139.8
NO ₂ ²	CONUS	8.3	4.0	-51.4	55.9	4.0	-52.2	56.4
	Europe	17.4	6.7	-61.4	65.5	6.6	-62.1	66.0
	East Asia	11.7	3.0	-74.1	75.2	3.0	-74.8	75.8
O ₃ ³	CONUS	34.7	44.7	29.0	29.5	44.4	28.2	28.5
	Europe	56.2	78.6	39.9	40.8	80.6	43.5	44.2
	East Asia	29.8	48.3	62.4	62.4	47.7	60.3	60.3
HNO ₃ (μg m ⁻³)	CONUS	0.9	2.1	145.0	145.2	2.2	154.7	154.7
	Europe	0.8	0.7	-15.6	65.4	0.8	-10.9	64.9
HCHO (ppb)	CONUS	2.3	1.6	-30.1	48.4	1.5	-36.3	49.0
ISOP (ppb)	CONUS	0.3	0.2	-27.3	63.2	0.2	-29.0	64.7
Toluene (ppb)	CONUS	0.5	0.2	-65.3	69.2	0.2	-65.1	69.1
Col. CO (molec.cm ⁻²)	Globe	1.6×10 ¹⁸	1.2×10 ¹⁸	-25.8	27.5	1.2×10 ¹⁸	-24.4	26.1
Col. NO ₂ (molec.cm ⁻²)	Globe	5.5×10 ¹⁴	8.5×10 ¹⁴	56.0	71.0	9.3×10 ¹⁴	70.2	83.3
Col. HCHO (molec.cm ⁻²)	Globe	4.6×10 ¹⁵	3.1×10 ¹⁵	-31.2	39.2	3.1×10 ¹⁵	-32.7	40.4
Col. C ₂ H ₂ O ₂ (molec.cm ⁻²)	Globe	2.8×10 ¹⁴	3.9×10 ¹³	-86.0	86.0	5.9×10 ¹²	-97.9	-97.9
Col. SO ₂ (DU)	Globe	1.2	0.3	-70.1	90.1	0.3	-73.5	88.7
TOR (DU)	Globe	28.6	30.3	6.0	15.0	31.8	11.3	16.5
SO ₄ ²⁻ (μg m ⁻³)	CONUS	1.8	3.0	72.9	72.9	3.3	89.7	89.7
	Europe	1.8	2.9	62.1	70.1	3.2	79.7	85.2
NH ₄ ⁺ (μg m ⁻³)	CONUS	0.9	1.3	37.8	49.9	1.3	44.3	55.6
	Europe	0.9	1.3	51.5	63.1	1.4	63.4	72.8
NO ₃ ⁻ (μg m ⁻³)	CONUS	0.9	0.9	-6.0	44.4	0.7	-21.2	40.2
	Europe	1.7	1.2	-28.9	54.2	1.2	-30.5	53.4
Cl ⁻ (μg m ⁻³)	CONUS	0.1	0.02	-78.1	84.3	0.02	-78.3	84.5
	Europe	1.1	4.1	273.4	274.7	4.2	273.7	274.8
BC (μg m ⁻³)	CONUS	0.3	0.2	-29.3	44.6	0.2	-29.3	44.6
OC (μg m ⁻³)	CONUS	0.9	1.0	2.1	33.2	0.7	-20.7	32.8
	Europe	2.9	0.7	-74.2	77.3	0.7	-75.1	78.0
TC (μg m ⁻³)	CONUS	1.8	1.3	-29.6	39.3	1.1	-42.1	45.8
SOA ⁴	CONUS	1.8	1.8	-1.9	29.3	1.4	-23.1	35.8
HOA ⁴	N.H. ⁵	2.1	0.5	-77.2	81.5	0.5	-76.7	81.3
OOA ⁴	N.H. ⁵	4.8	2.1	-56.5	56.6	1.8	-62.3	62.3
TOA ⁴	N.H. ⁵	7.9	2.5	-67.8	68.2	2.3	-71.2	72.0
PM _{2.5} (μg m ⁻³)	CONUS	7.4	10.3	38.9	58.1	10.3	37.7	58.6
	Europe	14.4	11.5	-20.4	48.4	11.8	-18.3	47.0
PM ₁₀ (μg m ⁻³)	CONUS	20.6	12.6	-38.6	50.2	12.6	-38.9	50.7
	Europe	22.1	18.8	-14.9	39.9	19.2	-13.1	38.9
	East Asia	88.0	59.0	-32.9	41.1	64.8	-26.4	37.2

¹ The unit is μg m⁻³ for CONUS and ppb for East Asia. ² The unit is μg m⁻³ for Europe and ppb for CONUS and East Asia. ³ The unit is ppb for CONUS and East Asia, and μg m⁻³ for Europe. ⁴ SOA: secondary organic aerosol; HOA: hydrocarbon-like organic aerosol; OOA: oxygenated organic aerosol; TOA: total organic aerosol; ⁵ N.H.: northern hemisphere; ⁶ MB: mean bias; NMB: normalized mean bias (%); NME: normalized mean error (%); RMSE: root mean squared error; Corr.: correlation coefficient.

Table 4. Performance statistics of cloud/radiative variables

<u>Variables¹</u>	<u>Networks</u>	<u>Obs</u>	<u>MOZART-4x</u>					<u>CB05 GE</u>				
			<u>Sim</u>	<u>NMB</u> <u>(%)²</u>	<u>NME</u> <u>(%)²</u>	<u>RMSE²</u>	<u>Corr²</u>	<u>Sim</u>	<u>NMB</u> <u>(%)²</u>	<u>NME</u> <u>(%)²</u>	<u>RMSE²</u>	<u>Corr²</u>
<u>OLR</u> <u>(W m⁻²)</u>	<u>NOAA/</u> <u>CDC</u>	<u>217.0</u>	<u>224.8</u>	<u>3.6</u>	<u>4.1</u>	<u>10.0</u>	<u>0.99</u>	<u>223.7</u>	<u>3.1</u>	<u>3.9</u>	<u>9.6</u>	<u>0.98</u>
<u>FLDS</u> <u>(W m⁻²)</u>	<u>CERES</u>	<u>306.7</u>	<u>307.3</u>	<u>0.2</u>	<u>3.1</u>	<u>11.6</u>	<u>0.99</u>	<u>307.3</u>	<u>0.2</u>	<u>3.1</u>	<u>11.5</u>	<u>0.99</u>
<u>FSDS</u> <u>(W m⁻²)</u>	<u>CERES</u>	<u>163.4</u>	<u>150.9</u>	<u>-7.6</u>	<u>10.2</u>	<u>22.6</u>	<u>0.9</u>	<u>150.8</u>	<u>-7.7</u>	<u>10.2</u>	<u>22.7</u>	<u>0.9</u>
<u>SWCF</u> <u>(W m⁻²)</u>	<u>CERES</u>	<u>-40.7</u>	<u>-51.5</u>	<u>26.4</u>	<u>33.4</u>	<u>19.0</u>	<u>0.9</u>	<u>-52.0</u>	<u>27.7</u>	<u>-34.4</u>	<u>19.6</u>	<u>0.9</u>
<u>LWCF</u> <u>(W m⁻²)</u>	<u>CERES</u>	<u>22.4</u>	<u>17.6</u>	<u>-21.6</u>	<u>25.1</u>	<u>6.8</u>	<u>0.9</u>	<u>18.7</u>	<u>-16.7</u>	<u>23.8</u>	<u>6.6</u>	<u>0.9</u>
<u>CCN5</u> <u>(# cm⁻²)</u>	<u>MODIS</u>	<u>2.2×10⁸</u>	<u>1.5×10⁸</u>	<u>-32.1</u>	<u>46.4</u>	<u>1.7×10⁸</u>	<u>0.4</u>	<u>1.6×10⁸</u>	<u>-29.0</u>	<u>46.6</u>	<u>1.7×10⁸</u>	<u>0.4</u>
<u>CF (%)</u>	<u>MODIS</u>	<u>67.3</u>	<u>71.5</u>	<u>6.3</u>	<u>12.7</u>	<u>12.5</u>	<u>0.8</u>	<u>71.3</u>	<u>6.0</u>	<u>12.7</u>	<u>12.5</u>	<u>0.8</u>
<u>COT</u>	<u>MODIS</u>	<u>16.5</u>	<u>12.2</u>	<u>-26.0</u>	<u>61.6</u>	<u>14.0</u>	<u>-0.3</u>	<u>12.2</u>	<u>-26.0</u>	<u>61.3</u>	<u>14.0</u>	<u>-0.3</u>
<u>AOD</u>	<u>MODIS</u>	<u>0.15</u>	<u>0.11</u>	<u>-23.9</u>	<u>40.5</u>	<u>0.08</u>	<u>0.7</u>	<u>0.11</u>	<u>-24.6</u>	<u>40.5</u>	<u>0.08</u>	<u>0.7</u>
<u>PWV</u> <u>(cm)</u>	<u>MODIS</u>	<u>1.9</u>	<u>2.0</u>	<u>5.6</u>	<u>11.4</u>	<u>0.3</u>	<u>0.99</u>	<u>2.0</u>	<u>5.5</u>	<u>11.4</u>	<u>0.3</u>	<u>0.99</u>
<u>CDNC</u> <u>(# cm⁻³)</u>	<u>Bennartz</u> <u>(2007)</u>	<u>105.8</u>	<u>126.6</u>	<u>19.7</u>	<u>38.7</u>	<u>56.5</u>	<u>0.5</u>	<u>127.8</u>	<u>20.8</u>	<u>39.1</u>	<u>58.1</u>	<u>0.6</u>
<u>LWP</u> <u>(g m⁻²)</u>	<u>MODIS</u>	<u>142.0</u>	<u>65.2</u>	<u>-54.1</u>	<u>65.4</u>	<u>143.3</u>	<u>-0.4</u>	<u>64.7</u>	<u>-54.4</u>	<u>65.3</u>	<u>143.3</u>	<u>-0.4</u>
	<u>Bennartz</u> <u>(2007)</u>	<u>84.6</u>	<u>87.0</u>	<u>2.8</u>	<u>38.3</u>	<u>42.3</u>	<u>0.4</u>	<u>86.0</u>	<u>1.7</u>	<u>37.7</u>	<u>41.7</u>	<u>0.4</u>

¹ OLR: outgoing long wave radiation; FLDS: downwelling longwave radiation at the surface; FSDS: downwelling shortwave radiation at the surface; SWCF: shortwave cloud radiative forcing; LWCF: longwave cloud radiative forcing; CCN5: column CCN (ocean) at supersaturation of 0.5%; CF: cloud fraction; COT: cloud optical thickness; AOD: aerosol optical depth; PWV: precipitable water vapor; CDNC: cloud droplet number concentration; LWP: liquid water path.

² NMB: normalized mean bias (%); NME: normalized mean error (%); RMSE: root mean squared error; Corr.: correlation coefficient.

Table 5. Tropospheric Ozone Budget

Ozone	MOZART-4x	CB05_GE	Lamarque et al. (2012)	Young et al. (2013)
Burden (Tg)	325	333	328	337 ± 23
Dry Deposition (Tg yr ⁻¹)	679	705	705	1003 ± 200
^a Chemical Production (Tg yr ⁻¹)	4974	5743	4897	5110 ± 606
^b Chemical Loss (Tg yr ⁻¹)	4259	5194	4604	4668 ± 727
Lifetime (days)	24	21	26	22.3 ± 2.0

^a Chemical production is mainly contributed by reactions of NO with peroxy radicals.

^b Chemical loss is mainly contributed by the oxygen radical in the O(¹D) + water (H₂O) reaction and by the reactions of ozone with the hydroperoxyl radical (HO₂), OH, and alkenes.

Figure captions

Figure 1. Scatter plots of O₃, PM, organic carbon (OC), [secondary organic aerosol \(SOA\)](#), hydrocarbon-like organic aerosol (HOA), oxygenated organic aerosol (OOA), total organic aerosol (TOA) over various sites during 2008-2010.

Figure 2. Comparisons of simulated and observed SOA concentrations at the four field study sites during 2009-2010. The observations are based on Lewandowski et al. (2013).

Figure 3. Zonal-mean profiles of HCHO, glyoxal, CO, NO₂, and TOR from CB05_GE and MOZART-4x simulations for June, July, and August during 2008-2010.

Figure 4. Simulated vertical profiles of O₃, CO, NO_x, and NO_y, against aircraft measurements. The black solid line represents observations from aircraft measurements (Pan et al., 2010; Brock et al., 2011; Ryerson et al., 2011; Jacob et al., 2010). The red solid and blue solid lines represent model output from MOZART-4x and CB05_GE, respectively.

Figure 5. Simulated vertical profiles of CCN against aircraft measurements. The black solid line represents observations from aircraft measurements of Zhang et al. (2011). The red solid and blue solid lines represent model output from MOZART-4x and CB05_GE, respectively.

Figure [6](#). Taylor diagram of comparison of cloud and radiative predictions between MOZART-4x and CB05_GE.

Figure [7](#). Comparison of satellite observations with predictions of AOD, CCN5, CDNC, COT, and SWCF by MOZART-4x and CB05_GE.

Figure [8a](#). Absolute differences averaged during 2008-2010 in tropospheric column concentrations of major gaseous species between MOZART-4x and CB05_GE.

Figure [8b](#). Absolute differences averaged during 2008-2010 in tropospheric column concentrations of major aerosol species between MOZART-4x and CB05_GE.

Figure [9](#). Column abundances (mg m⁻²) averaged during 2008-2010 of secondary organic aerosols (SOA) from anthropogenic sources (ASOA), biogenic sources (BSOA), and glyoxal (GLSOA), and semi-volatile organic aerosol (SVSOA) over Australia, Europe, North America, South Africa, South America, and East Asia.

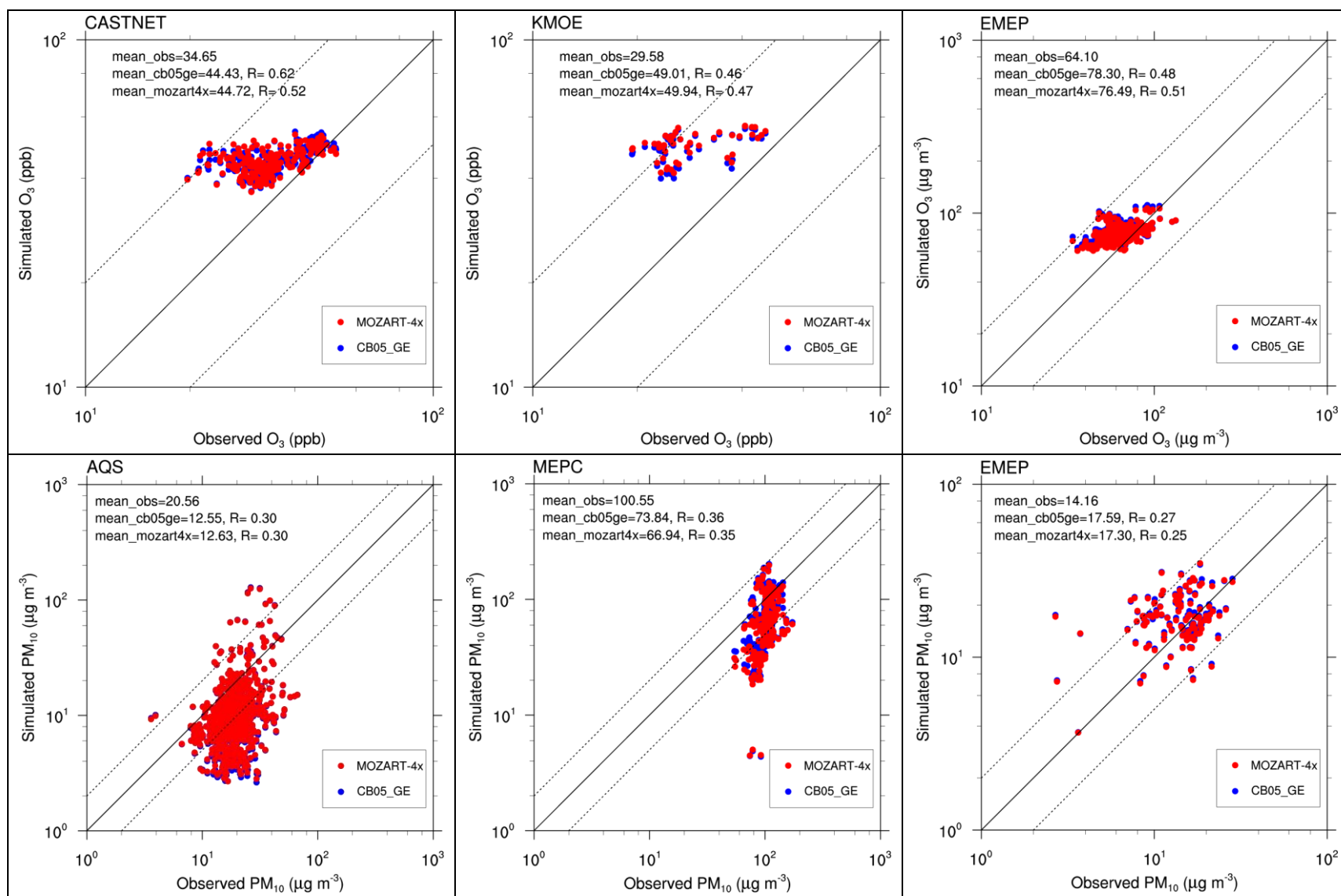


Figure 1. Scatter plots of O₃, PM, organic carbon (OC), [secondary organic aerosol \(SOA\)](#), hydrocarbon-like organic aerosol (HOA), oxygenated organic aerosol (OOA), total organic aerosol (TOA) over various sites during 2008-2010. The X (observations) and Y (simulations) axes are in log scale. Red dots represent MOZART-4x and blue dots represent CB05_GE. R is the correlation coefficient between simulated results and observational data. Z07: Zhang et al. (2007); J09: Jimenez et al. (2009); L13: Lewandowski et al. (2013).

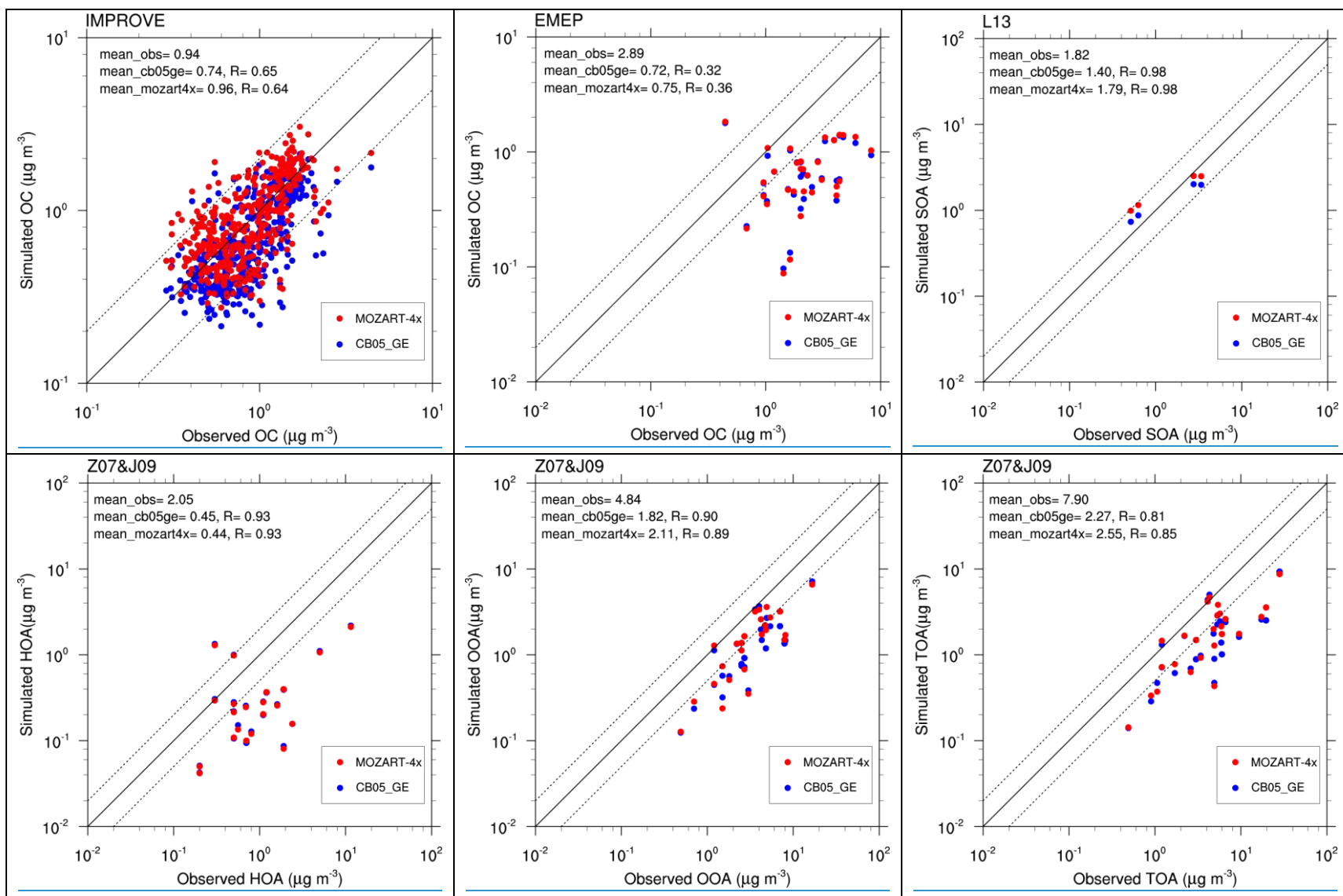


Figure 1. Continued.

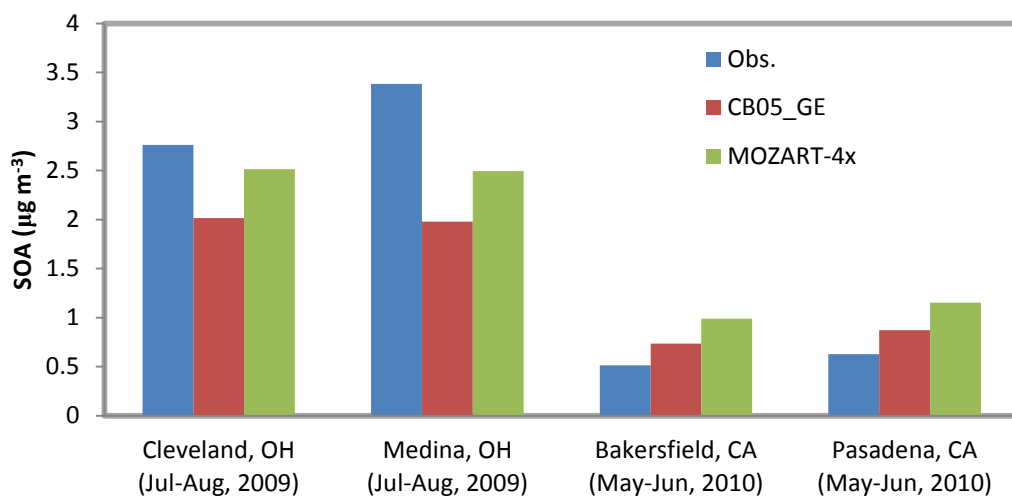


Figure 2. Comparisons of simulated and observed SOA concentrations at the four field study sites during 2009-2010. The observations are based on Lewandowski et al. (2013).

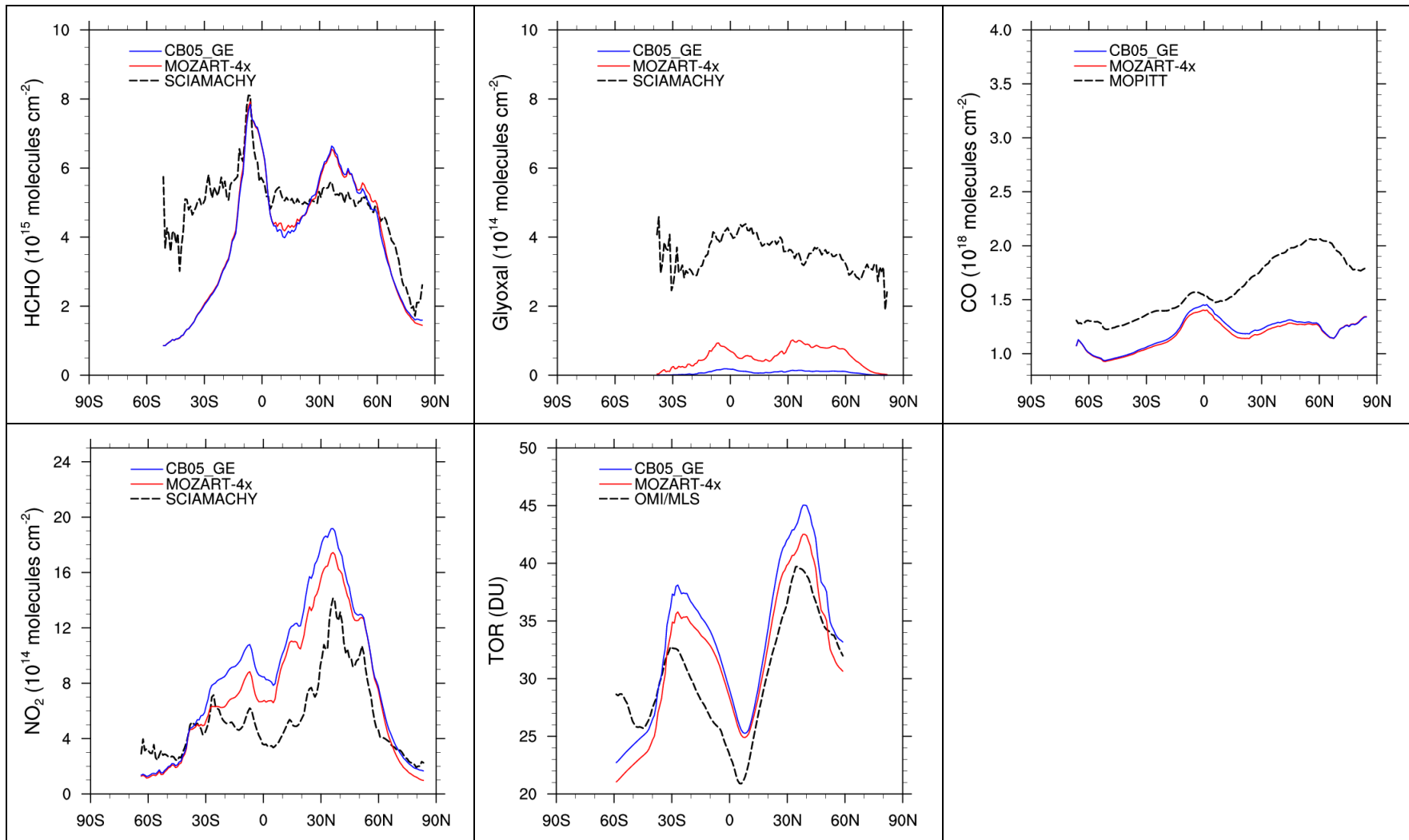


Figure 3. Zonal-mean profiles of HCHO, glyoxal, CO, NO_2 , and TOR from CB05_GE and MOZART-4x simulations for June, July, and August during 2008-2010.

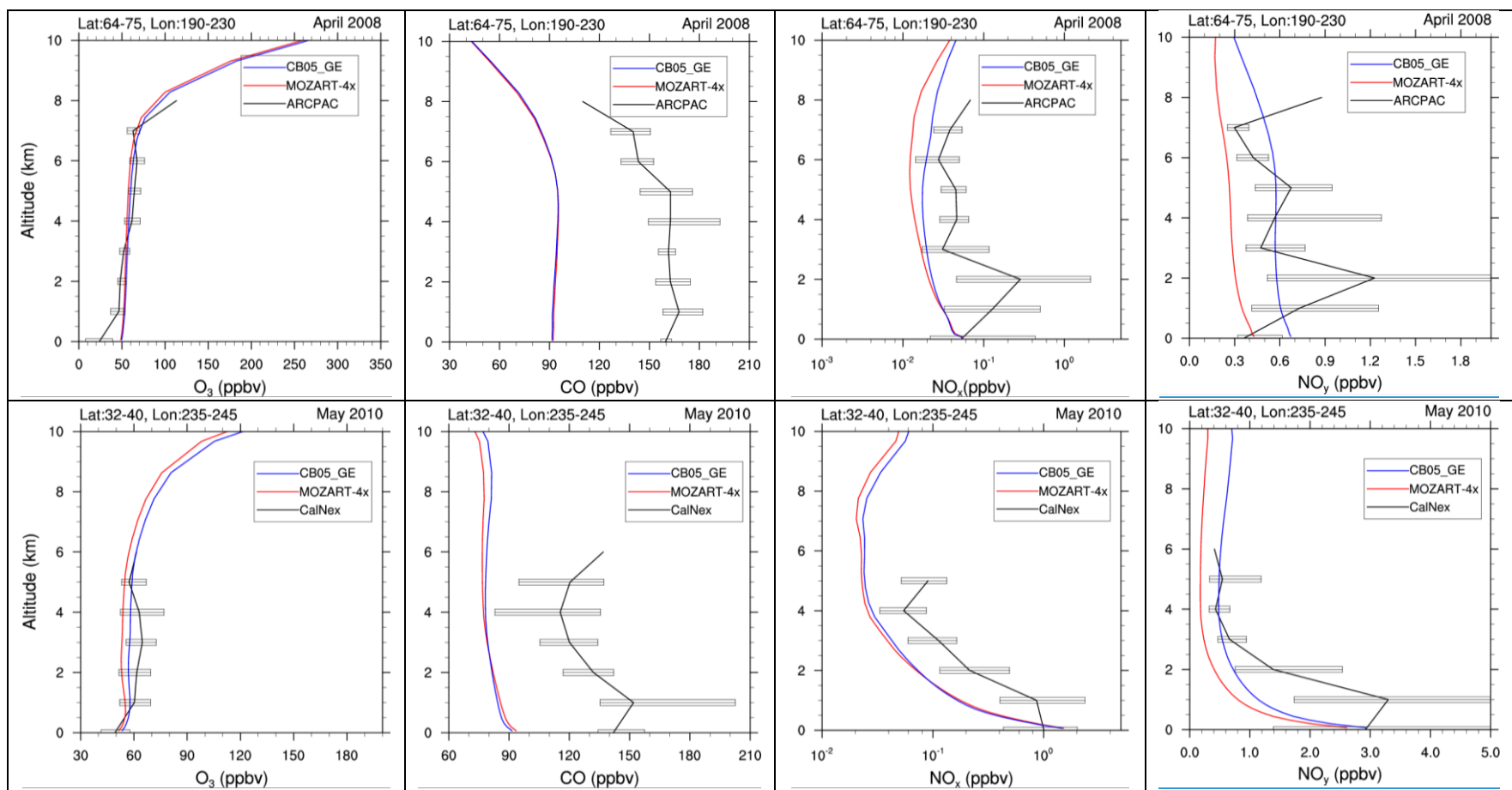


Figure 4. Simulated vertical profiles of O₃, CO, NO_x, NO_y (including aerosol nitrate), OH and H₂O₂, against aircraft measurements. The black solid line represents observations from aircraft measurements (Pan et al., 2010; Brock et al., 2011; Ryerson et al., 2011; Jacob et al., 2010). The red solid and blue solid lines represent model output from MOZART-4x and CB05_GE, respectively.

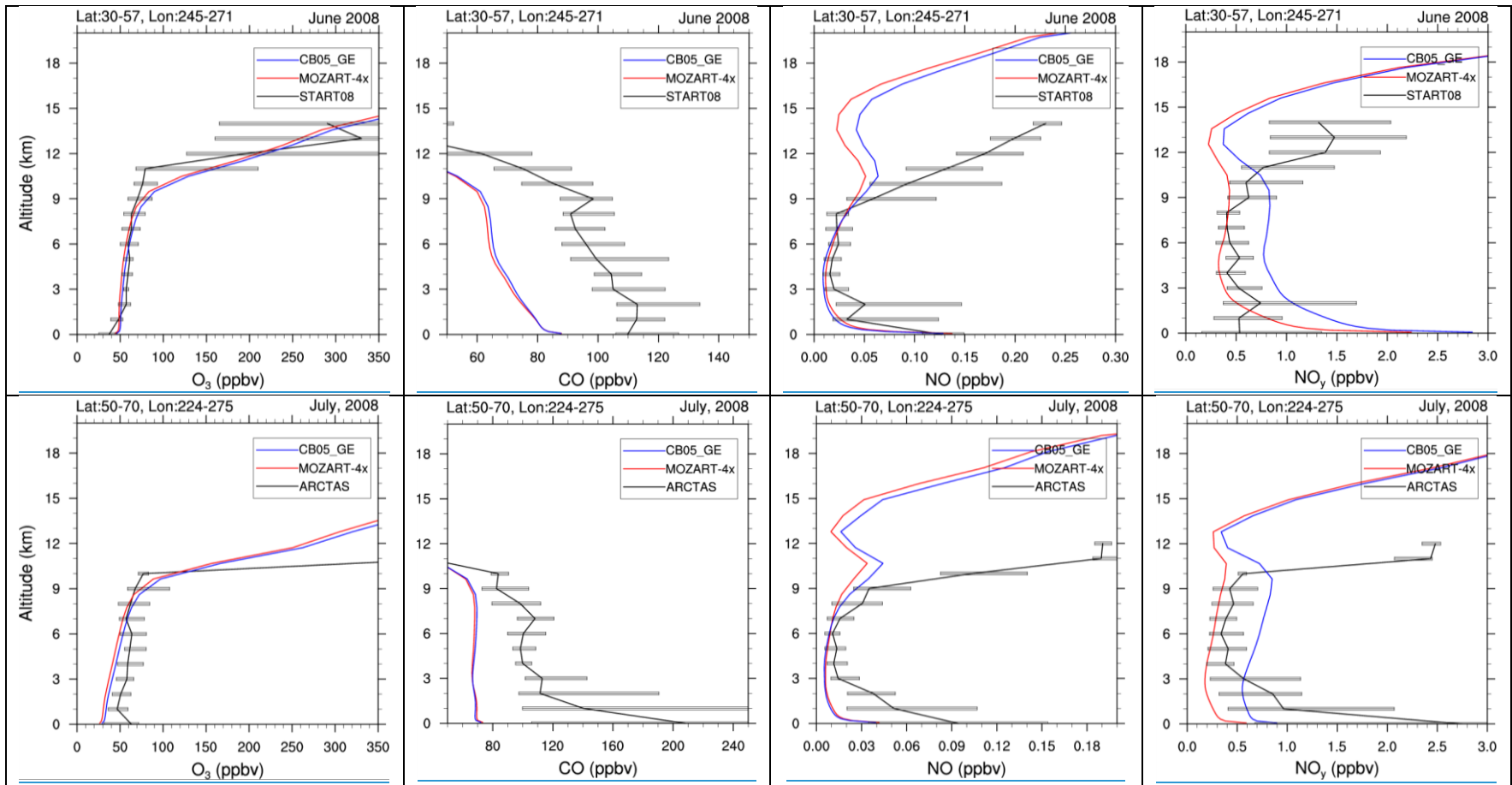


Figure 4. Continued.

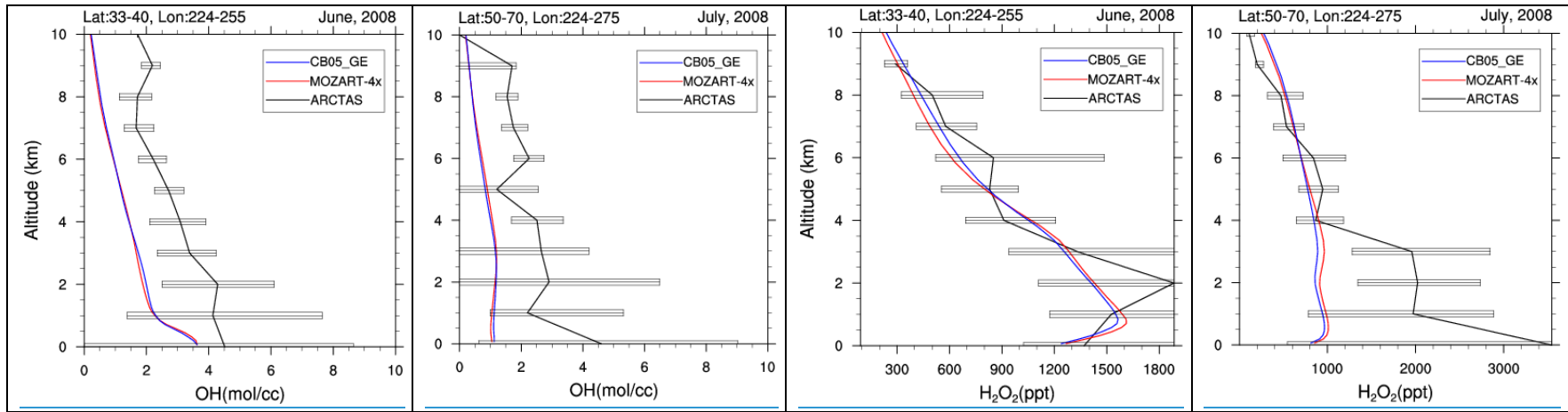


Figure 4. Continued.

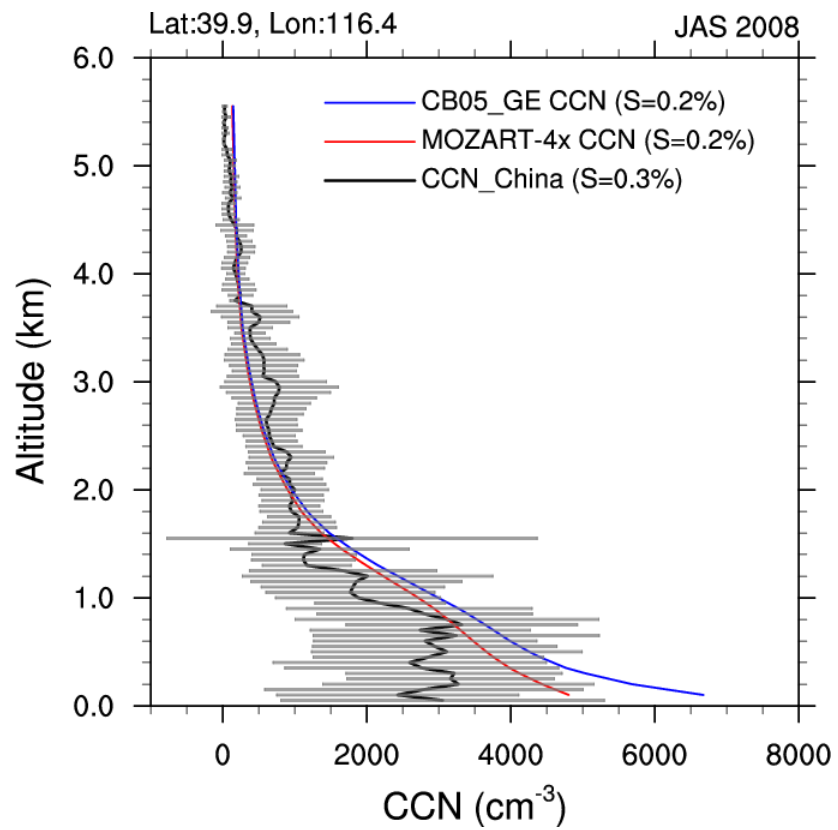


Figure 5. Simulated vertical profiles of CCN against aircraft measurements. The black solid line represents observations from aircraft measurements of Zhang et al. (2011). The red solid and blue solid lines represent model output from MOZART-4x and CB05_GE, respectively.

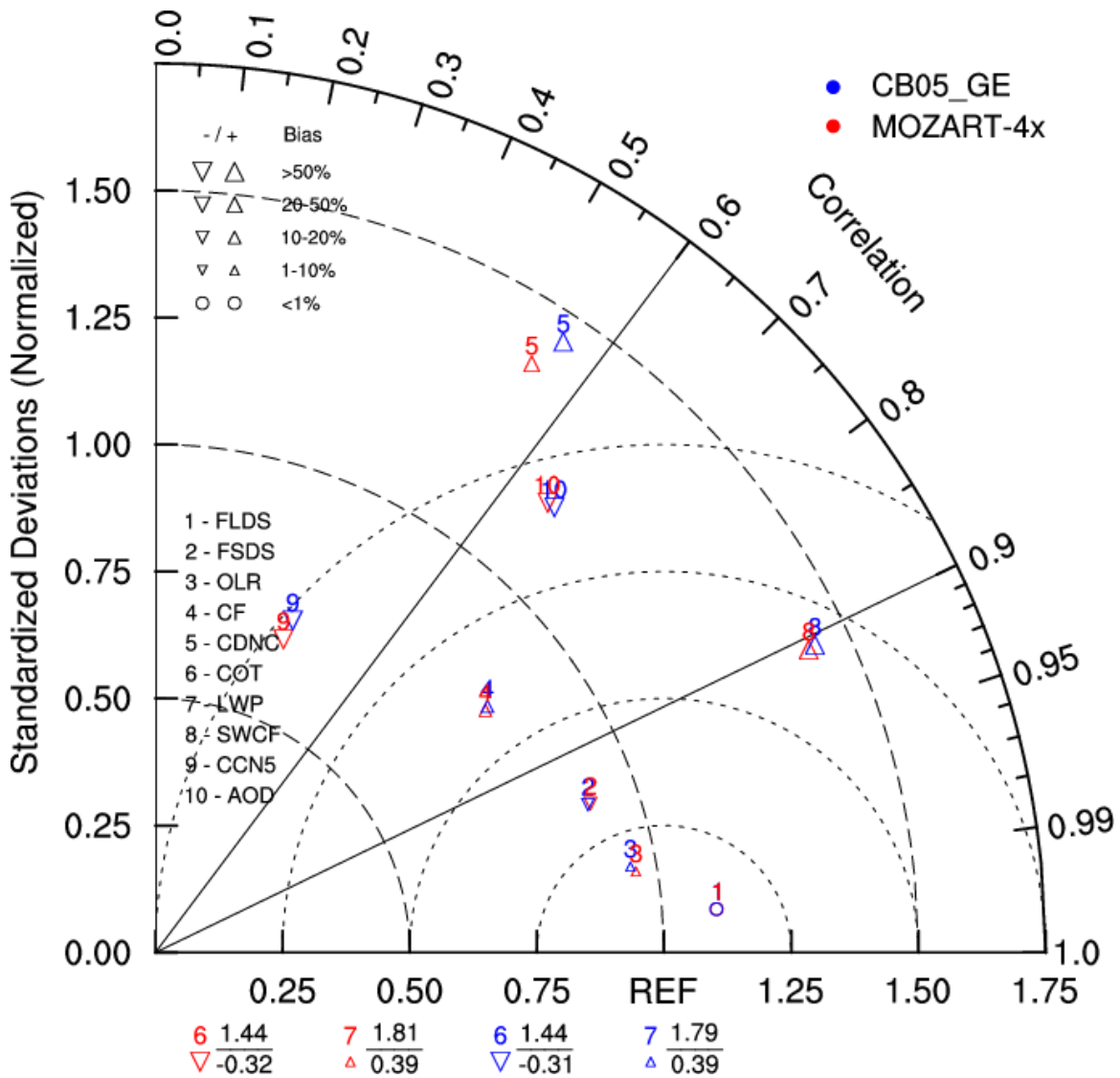


Figure 6. Taylor diagram of comparison of cloud and radiative predictions between MOZART-4x and CB05_GE. The results are based on 3-year average. This diagram represents the similarity between MOZART-4x and CB05_GE. X-axis represents the ratio of variances between observations and simulations (proportional to the reference point identified as “REF”), and Y-axis represents the normalized standard deviation between the two patterns (proportional to the radial distance from the origin). Two variables, COT and LWP, are located outside the diagram because the ratios of variance between simulated results and observations (the values of 1.81 from MOZART-4x and 1.79 from CB05_GE in the top) are larger than 1.75 for LWP and the correlation coefficients (the values of -0.32 from MOZART-4x and -0.31 from CB05_GE in the bottom) for COT are negative.

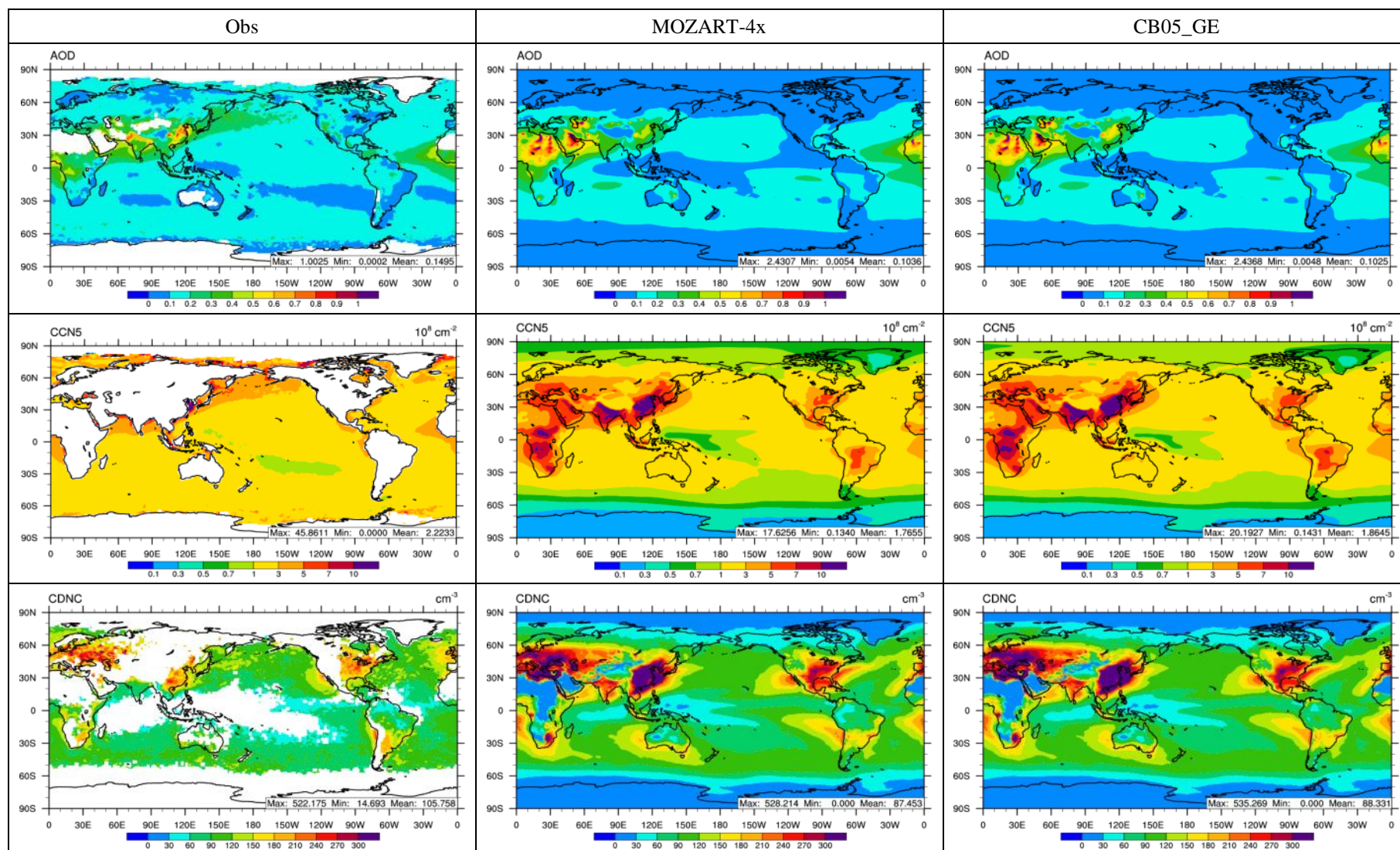


Figure 7. Comparison of satellite observations with predictions of for AOD, CCN5, CDNC, COT, and SWCF by MOZART-4x and CB05_GE.

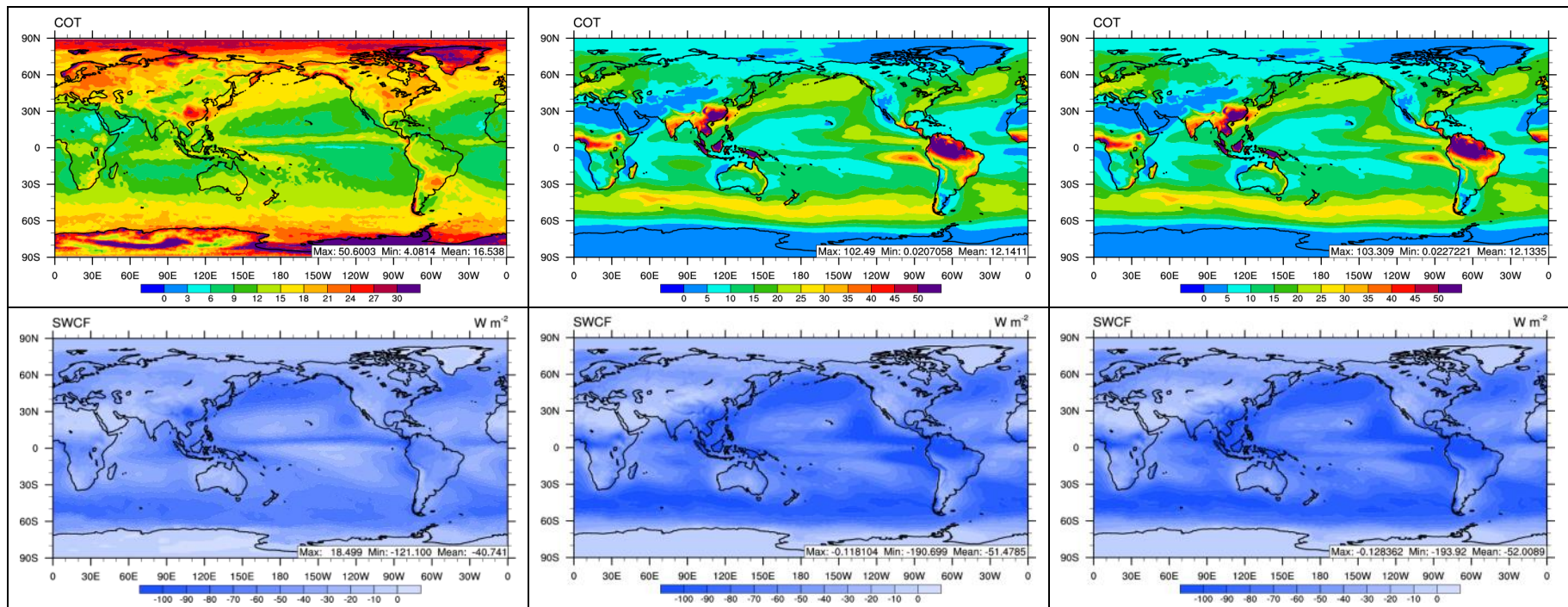


Figure 7. [Continued.](#)

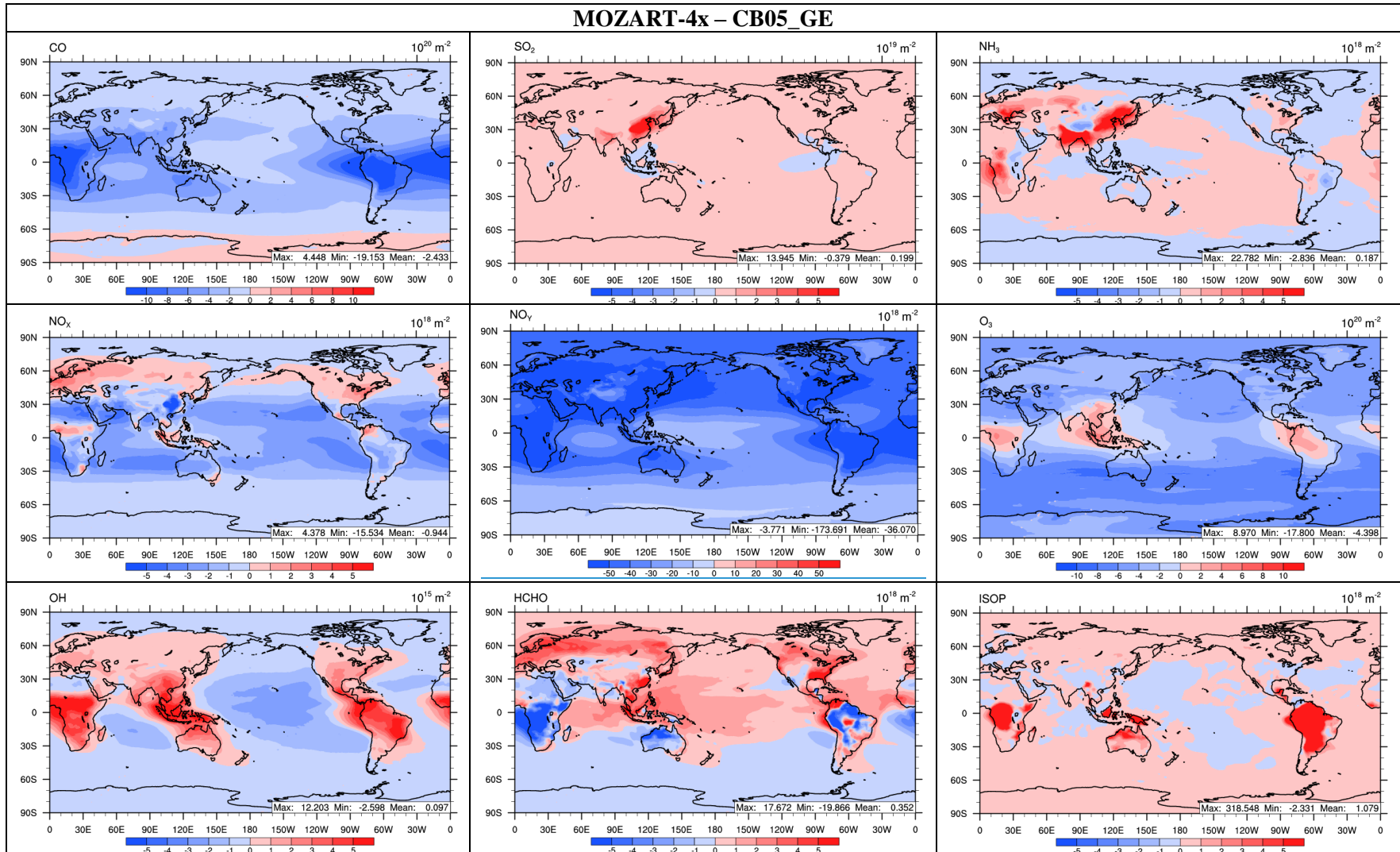


Figure 8a. Absolute differences averaged during 2008-2010 in tropospheric column concentrations of major gaseous species between MOZART-4x and CB05_GE.

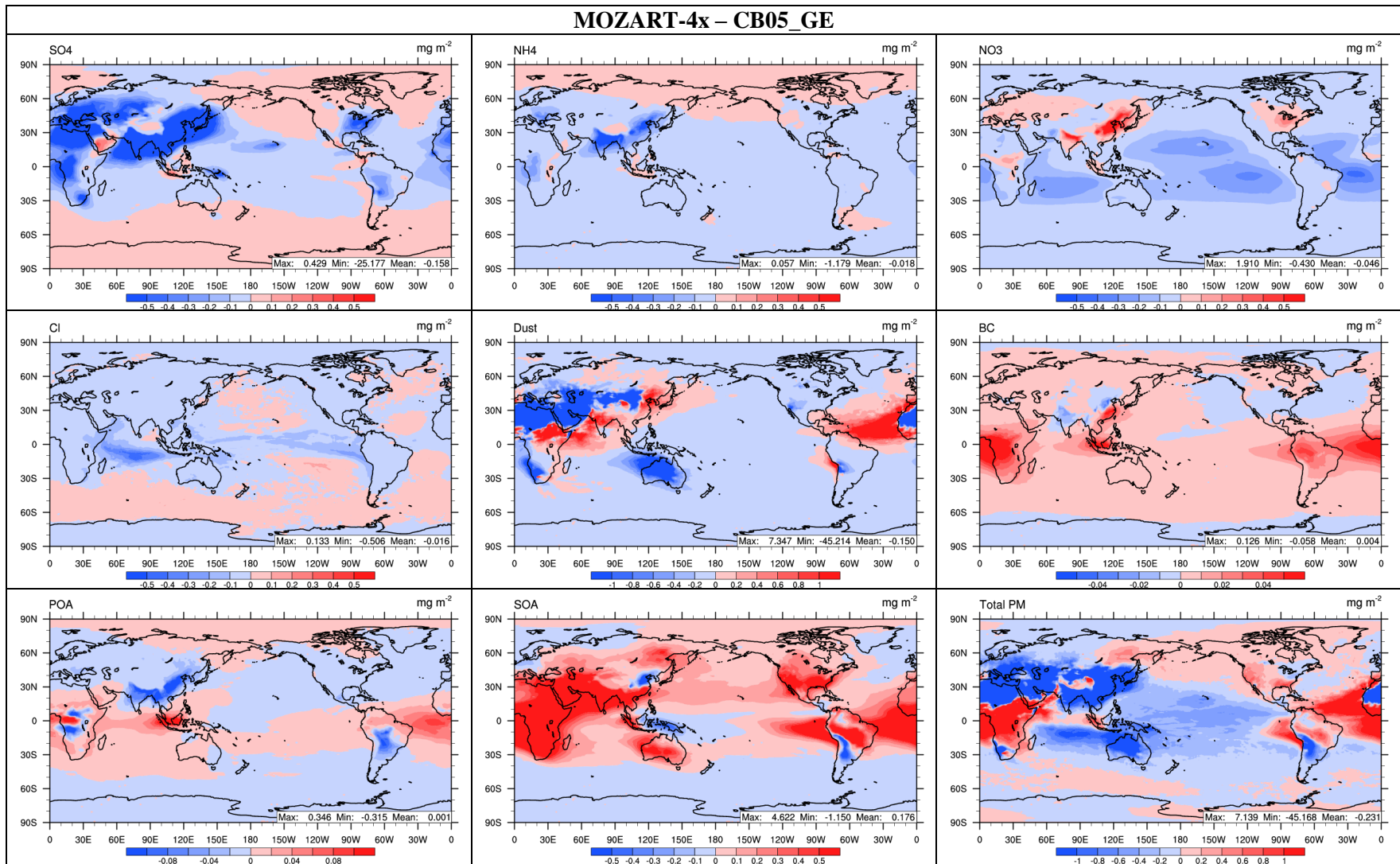


Figure 8b. Absolute differences averaged during 2008-2010 in tropospheric column concentrations of major aerosol species between MOZART-4x and CB05_GE.

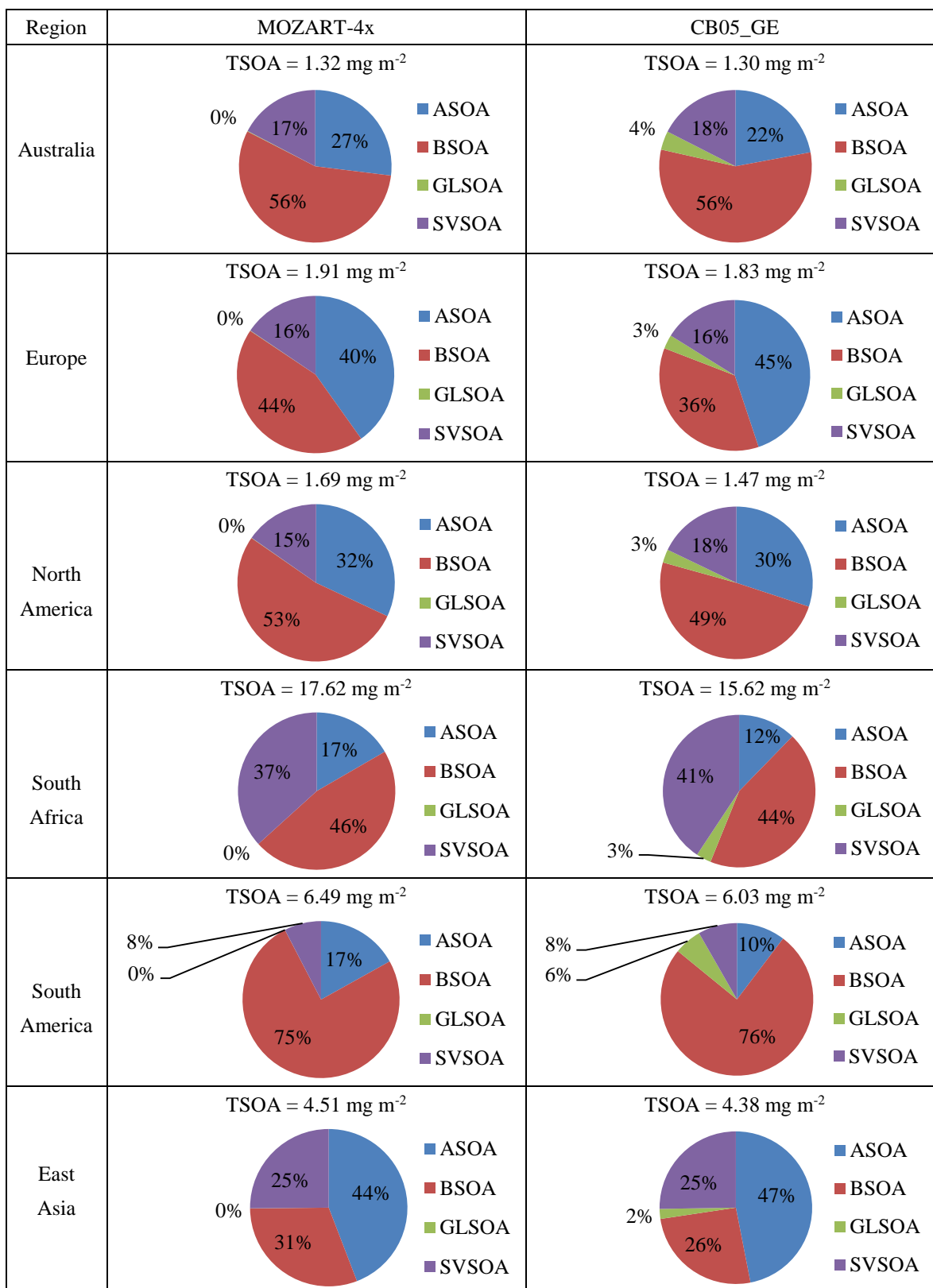


Figure 9. Column abundances (mg m⁻²) averaged during 2008-2010 of secondary organic aerosols (SOA) from anthropogenic sources (ASOA), biogenic sources (BSOA), and glyoxal (GLSOA), and semi-volatile organic aerosol (SVSOA) over Australia, Europe, North America, South Africa, South America, and East Asia.